

In this document, the authors provide answers to the two reviews of paper tc-2018-127.

Lavergne, T., Sørensen, A. M., Kern, S., Tonboe, R., Notz, D., Aaboe, S., Bell, L., Dybkjær, G., Eastwood, S., Gabarro, C., Heygster, G., Killie, M. A., Kreiner, M. B., Lavelle, J., Saldo, R., Sandven, S., and Pedersen, L. T.: Version 2 of the EUMETSAT OSI SAF and ESA CCI Sea Ice Concentration Climate Data Records, The Cryosphere Discuss., <https://doi.org/10.5194/tc-2018-127, in review, 2018>.

We thank the two anonymous reviewers for thorough comments on our manuscript, and many suggestions to improve both the content and the language.

Anonymous Referee #1

Summary:

This paper describes a new version of the OSISAF sea ice concentration product and the ESA sea ice CDR. The products are derived from passive microwave data. The new version includes several enhancements from the Version 1 OSISAF product. Comparisons with independent estimates show good agreement. The new version provides a consistent record of sea ice concentrations for the scientific community.

General Comment:

The manuscript provides a thorough introduction of the new versions. The description of the algorithm and processing, including enhancements from Version 1 is clear and detailed. The initial evaluation results look reasonable and given that it builds on the previous version and thorough earlier validation, they are quite sufficient to provide high confidence in the quality of the product. The Level 4 filtered product is particularly beneficial for users who wish to have a “clean” concentration estimate and this is an excellent improvement from Version 1. I have only a few minor comments that the authors should address before publication.

Thank you for your positive appreciation of our manuscript. Your comments are very valuable and are addressed below.

(One further general comment: it would be helpful for readability to either indent new paragraphs and/or skip a line between paragraphs.)

This is done in the revised manuscript.

Specific Comments (by page and line number):

P2, L9: while the albedo specifically depends on concentration, it is not only concentration: snow melt state and particularly melt ponds substantially affect albedo even for 100% concentration.

We agree and have changed the wording to now read “For example, the albedo of the polar oceans is strongly influenced by sea-ice concentration”

P4, L24-25: I find the (resp. XXXX) style awkward to read and somewhat confusing. I would just write out each in sequence rather than using parenthesis, but this may just be a preference by me.

We changed this sentence to read: “Although not identical, the spatial resolution of the channels needed for the SIC algorithms is similar for the three coarse resolution sensor series (SMMR, SSM/I, and SSMIS) with about 70x45 km instantaneous Field-of-View (iFoV) diameters for the 19 GHz frequency channels, and 38x30 km for the 37 GHz ones (Table 2)”.

P6, L1: “daily composited fields of SIC” – how is the compositing done? Is it simply drop-in-the-bucket?

We use a weighted average with Gaussian spatial weights, and equal weights in the temporal domain. This is added to section 3.6 where gridding and daily compositing was briefly covered.

P10, L12-20: What are the uncertainties in the NWP fields and the RTM? While the dynamical tiepoints and the double-difference approach may negate much of the influence, I do wonder how effective the correction is if the NWP data and/or the RTM have high uncertainties? This feeds into my next comment below.

The quality of RTMs and NWP fields indeed play a role in the effectiveness of the T_B correction. In our experience however, the T_B correction always yields more accurate SIC fields over open water when correcting for wind speed, and water vapour. As others we do not correct for Cloud Liquid Vapour (L) which is not reliable in NWP data (see next comment).

P10, L28: the use of the NWP fields is novel and I like the physical approach. However, L is not reliable from NWP. Isn't L one of the largest if not generally the largest source of emission, at least over open water. So not being able to correct for that really limits the effectiveness of the NWP correction, doesn't it? The use of weather filters in the Level 4 fields eliminates this, which is good, but the quality of the Level 3 fields must be limited, right?

The use of NWP fields and RTM-based correction schemes is one of the specificities of the OSI SAF approach, and was introduced in Andersen et al. (2007). So far, Cloud Liquid Water (CLW, symbol L in the paper) in global NWP field has rarely been found to be reliable enough for correcting T_B . One factor is probably that the modelled fields are not at the same temporal and spatial scales as the satellite data.

Although CLW is not used, the correction based only on 10m wind speed and water vapour is still quite efficient (see for example the offset of 1% to 1.5% standard deviation in Figure 8). Correcting T_B for WS and WV leads to a 35% reduction in T_B variance at 18/19 GHz and 22% reduction in T_B variance at 37 GHz. This subsequently leads to a 35-45% reduction of SIC variance for standard algorithms (ESA SICCI PVASR p151-159). The noise associated to CLW is rather localized on small geographical domains, and is indeed taken care of by the weather filter (and maximum extent climatology) at Level-4. As in previous version of the CDR (Tonboe et al. 2016), the Level-3 product files indeed present some remaining noise, more pronounced in the case of high CLW. Noticeably: the statistics of the remaining noise is integrated in the uncertainty fields: not correcting for CLW leads to higher product uncertainties.

P13, L17: It might be worth considering showing an example of the “ice curve”. I can generally visualize, but a figure would perhaps better illustrate it.

Yes, this is added to Figure 3, and discussed in section 3.4.3.

P13, L20-26: I’m not sure I understand Figure 5. It appears to show an increase in open water concentration near the ice edge due to the correction (e.g., in Barents Sea and Davis Strait regions). Is that correct? Wouldn’t that reduce the quality if the correction essentially added ice to open water regions?

You are referring to the “open water” region of Figure 5 left panel (outside the 15% SIC contour). This part of the plot was actually not described nor discussed in the text, something that was clearly missing and triggers your comment (also from Reviewer #2).

Figure 5 (left and center panels) shows the effect of the total correction, including both the correction due to the ice curve (described in this section 3.4.3), and the effect of the RTM-based atmospheric correction (section 3.4.1). The ice curve correction has most of its impact in high-concentration regions (inside the 70% SIC contour) while the atmospheric correction has most of its impact over open water regions (outside the 15% SIC contour). Outside the 15% SIC contour, it is correct that Figure 5 (left) shows increase in SIC after correction. This was confirmed by plotting similar maps for other months. This is because the SIC before correction SICucorr is mostly slightly negative there, and the correction step brings it closer to 0%. This is linked to the way our OW tie-point is tuned. As explained in section 3.4, the OW tie-point is tuned dynamically against open ocean cases that are outside a maximum ice extent climatology, thus potentially more representative of “open ocean” Tie-point than the conditions closer to the edge. Prior to atmospheric correction, the open-water tie-point is thus “warmer” than the T_B conditions closer to the edge, thus the uncorrected SICs are slightly negative there. After correction, our OW tie-point is re-tuned and is more representative of T_B close to the ice edge, hence the increase (reds in Figure 5). The net effect is a reduction in variability over ocean (blues on Figure 5, center panel) which indicates that the atmospheric

correction step on average does a good job reducing weather-induced noise over the open ocean.

Your comment prompted several edits: in section 3.4.1 we added that the effect of the RTM-based correction is largest over open water, and very limited over sea-ice. in section 3.4.3, we stated the “ice curve” correction has most impact over consolidated ice, and little effect over open water. Then we started that Figure 5 shows the combined effects of both correction. We also reworked the description of Figure 5 to first address the “ice curve” correction (including the discussion with ice-age on right panel), before addressing the atmospheric correction (including addressing your specific comment above). This results mostly in a re-arranging of text for improved readability. Thank you for this comment.

P16, L3: This should be discussed further – why is the gridded land-spillover correction still needed after the swath correction? How much coastal contamination remains after the swath correction. If the swath correction is not sufficient on its own, is it worth doing – i.e., would the Cavalieri correction work just as well without the swath correction? I guess the basic question is whether there is a benefit to doing both corrections or is the Cavalieri correction just as good? If so, then why do the swath correction?

We believe there is a benefit of combining the two approaches: first perform a physically based correction, then a statistical-based correction/filtering. We have however not studied in details if the statistical method alone could have done a good enough job alone, and cannot answer your (very valid) questions above. We added the following text in section 5.2 “Outlooks” when discussing algorithm improvements.

Other steps in the processing chain can further be improved upon, e.g. the land spill-over correction schemes. In section 3.6 we described how land spill-over was corrected in two steps, first through a physically-based algorithm on swath T_B data (adapted from Maass and Kaleschke, 2010), followed by a statistically-based correction of gridded SICs (adapted from Cavalieri et al. 1999). Several reasons can have led to the swath-based correction to not be enough. For example, the method relies heavily on accurate geolocation of the T_B measurements, however its uncertainty for the SSM/I and SSMIS instrument is known to be large (Poe et al. 2008), and is not corrected for in the current version of the FCDR (R3) we used (Fennig et al. 2017). We used approximated iFoVs weighting functions instead of eFoVs (see section 2.1) when convolving antenna pattern with the land mask, thus neglecting the effect of the measurements integration period. Finally, strategies to avoid gridding land-contaminated FoVs when building Level 3 maps might help in the future. It will also be beneficial to use high-resolution SIC maps from coastal regions (e.g. from navigational ice charts) to tune the various thresholds embedded in the statistically-based correction. To improve further on the land spill-over correction will be an objective for upcoming versions of the CDRs.

P16, L31: “basic isotropic schemes” is not very specific. Is it a bi-linear interpolation?
It is a interpolation with gaussian weights of the distance. This is now specified in the text.

P19, L17-23: I can understand that the ERA-Interim fields are not as good earlier in the record and thus the correction for SMMR is not as good. However, there is a noticeable step-change between SMMR and SSMI in Figure 8. Did ERA-Interim undergo a step change in terms of data sources or other processing quality at the same time? If not, then it seems like it’s not ERA-Interim (or at least not only), but rather something else causing the step change. Perhaps it’s related to the change in frequency from 18 GHz for SMMR to 19.3 GHz for SSMI?

This is a very good point, also made by Reviewer #2. We added a sentence discussing the impact of 18.0 GHz Ku-band.

Concerning the quality of ERA-Interim in the SMMR era: the main ERA-Interim reference is Dee et al. 2011, but it only describes the “1st production stream” of ERA-Interim (post 1989). A second stream covering 1979-1989 was added at a later stage, but there are no publications. We contacted the ECMWF team, and obtained a personal communication that can give some insight. We modified the manuscript P19 to read: “Another plausible explanation would be that the re-analysed fields for wind speed and water vapour from ERA-Interim are less accurate in the SMMR era than in the SSM/I and SSMIS era. We note that clear-sky radiances from SSM/I and SSMIS were directly assimilated in ERA-Interim over the ocean (Dee et al. 2011), but not SMMR radiances (Paul Poli, personal communication). This can especially have an impact in the SH, where other sources of conventional observations are scarcer”.

P21, L4: One thing not discussed is the potential impact of satellite crossing times on the retrievals. I assume the dynamic tiepoints should handle these discrepancies, but it might be worth mentioning.

The dynamic tuning of tiepoints and OWF threshold work with samples gathered at an hemispheric scale, and over a [-7:+7d] sliding time window. This technique can thus not handle intra-daily differences -arising from one region to the next- that are due to not observing the surface at the same time. It can however mitigate the potential impacts due to different missions observing at different times (if any). We added the following sentence when describing how OWFs are tuned and applied at Level-2 (P12): “To compute OWFs at Level 2 can also help mitigate the potential impacts of changes in satellite crossing time between different missions”.

P25, L12: Why not produce a 12.5 km or 10 km resolution AMSR-E and/or AMSR2 product, i.e., using the same channels (19, 37 GHz) as for SMMR-SSMI-SSMIS, but obtaining a higher spatial resolution for the period of 2002-present? It seems like this

would be more beneficial than at least the 25 km SICCI. I can see a benefit of using the 6V channel for the 50 km product, but that isn't in the 25 km SICCI.

This is an excellent question. The channels we use for AMSR-E and AMSR2 have the following iFoVs (reproduced from Table 2).

IFoV	18.7GHz	36.5GHz
AMSR-E	16x27 km	9x14 km
AMSR2	14x22 km	7x12 km

They all have a 10x10 km spacing. The diameters given here are those of the 3dB ellipses of the main lobe of the antenna pattern. Considering in addition that eFoVs are larger (mostly in the across track direction), we approximate that the eFoV diameter for the 18.7GHz channels are about 25km, while the eFoVs of 36.5GHz are about 15km. These two resolution are then merged into a SIC algorithm (that uses one 18.7GHz channel, and two 36.5GHz channels). What is the spatial resolution (eFoV) of the computed SIC? Probably somewhere between 15km and 25km, but in any case larger than 10km (the spacing) or 12.5km (half the grid spacing used for OSI-450).

The choice of a grid spacing for SIC products is very much based on “feelings” and historical reasons. Because the SSM/I brightness temperature daily maps were originally provided on a polar stereographic 25km grid, the NOAA/NSIDC SIC CDR is also on a 25km grid, and OSI-450 as well. This is probably too fine a spacing as we discuss in our section 4.3. The choice of 25km grid for the SICCI product based on 19 and 37 GHz channels from AMSR-E and AMSR2 is potentially too conservative (not by much), but this choice was made to ease uptake by users (only one spacing to refer to).

Your comment prompted the following revision:

A sentence was added section 4.3: “The true resolution of the SICCI-25km CDR might be slightly better than 25x25 km, but this grid spacing was retained to ease uptake by users, and comparison with OSI-450.”

A sentence was added section 5.2 (Outlooks) when discussing needs for further research efforts: “Finally, research is needed to assign a true spatial resolution to SIC fields computed from combinations of n T_B channels, themselves at different spatial resolutions. Some knowledge is embedded in our parametrization of smear, but it is currently not enough to e.g. choose and fully justify a grid spacing for SIC data records.”

Minor Comments (by page and line number):

P3, L17: use “in” instead of “entering”

P3, L26: use “share” or “provide” instead of “keep”

P16, L26: use “contrasts with” instead of “is conversely to”

P24, L3: “aiming at most complete” to “aiming to produce the most complete daily maps possible”

P25, L11: use “allowed, e.g., consistent processing of SIC CDRs. . .”

P26, L18: use “on the order of. . .”

P27, L1-2: use “the impact that melting and melt-ponds have. . .”

P27, L10: use “could be investigated if selecting. . .”

P28, L24: use “aim to have the best temporal consistency. . .”

Thank you, all your suggestions were implemented.

Anonymous Referee #2

This paper gives a thorough, informative and detailed description of three important new climate data records of sea ice concentration. The science in the paper is comprehensive. I therefore only have suggestions for minor improvements (though there are quite a few) - mostly for clarifications to the text. The paper is clear and easy to read, despite a number of minor grammatical errors which are detailed below.

Thank you for your positive evaluation of our manuscript. Your “quite a few” suggestions for minor improvements were processed thoroughly and led to an improvement of our text and figures. Thank you for having taken the time.

Minor comments

Page 2 line 1: Is this the observation uncertainty in assimilation for models? Unclear, need to elaborate

We have added a sentence to clarify this statement: “This is because both the bias correction of large-scale climate models and the extrapolation of observed relationships between forcing and sea-ice coverage can only be carried out robustly if observational uncertainty is sufficiently small.”

line 32: quantify what you mean by “coarse resolution”

Done: “coarse resolution (30-60 km)”.

Page 3 line 4: quantify what you mean by “medium resolution” line 19/20 & 22 (and throughout): Why only an “initial evaluation”. Reading on shows that you have done

more than just a cursory evaluation which is what this wording implies. Suggest reword.

Done: “medium resolution (15-25 km)”.

“initial” is here meant as “a first set of evaluation results”. More evaluation is underway, that will be published at a later stage. Since both reviewers estimate that the evaluation presented in this manuscript is enough for a publication, we will remove “initial”. That more evaluation will come in later publications is already announced in our Outlooks section.

Page 4 line 2: Suggest mentioning data gap in AMSR data earlier, perhaps when introducing Table 1. line 4: Suggest “documented in Table 2” should be “documented in the comments in Table 2”. Would also be useful to have a full list of outages, perhaps a link to this in another document? Line 10 (and Table 2): “width of the polar observation hole” is not given, it’s the bit that’s viewed rather than the hole, also not a width as it’s an angle, suggest rename this column line 23: Not sure that spatial resolution of SMMR is “somewhat similar” to SSM/I and SSMIS, suggest reword line 26: Clarify difference between sampling and resolution line 32: Consider showing eFoV in Table 2.

P4L2: this would require discussing acronyms earlier, we feel it is not worth the rewriting since the information comes shortly after. L4 done, we refer to the Product User Guides (PUGs) for extensive list of missing dates. L10&T2: done. L23 done (removed “somewhat”). L26: done (add sentence “The dimensions of the iFoV and eFoV are referred to as the resolution of the channels. The sampling is how close in space the FoVs are acquired. Most channels are thus oversampled.”). L32: unfortunately there is no authoritative source for eFoVs across all the instruments. iFoVs is what is generally documented (e.g. at WMO OSCAR database).

Page 5 line 4/5: Clarify if L1 data for SMMR, SSMI/S, SSMIS line 5: Add a line on what is an FCDR and what reprocessing has it undergone. Overlaps? Calibration? QC? line 6: add what period AMSR-E data covers line 9: more information needed on “resolution-matched”

P5L4: done. L5: done (add sentence “In the FCDR, the T_B are re-computed from Antenna Temperatures (TA), screened and corrected for known artefacts like solar intrusion, and intercalibrated between missions.”) L6: done, L9: done. The sentence is edited to read : “For both AMSR-E and AMSR2, the T_B are available both at their nominal resolution (documented in Table 2), and post-processed at lower resolution matching those of other channels (e.g. the 36.5GHz T_B at the resolution of the 6.9GHz channel). We use the nominal resolution of the T_B channels, not the resolution-matched ones.”

Page 6 line 1: what type of grid? EASE? Line 2: what are the necessary steps? Can reference later on in paper if necessary lines 5-8: suggest moving these lines to page 5 line 32, after "flags". Would flow better. Line 18: clarify these numbers are sea ice fraction line 23: needs citation for BRI more accurate than BPM at high concentrations line 28: Figure 3 illustrates for AMSR-E data, example from Comiso (1986) is for SMMR. Need to clarify that these can be applied to other instruments.

P6L1: Yes. The type and definition of grids is covered later in the text. L2: the sentence was simplified to "The Level 4 (L4) chain fills the gaps, apply extra corrections, and format the data files that will appear in the CDR.". L5-8: done, L18: done, L23: same references as the sentence before, so we merged the two sentences. L28: the reference to SMMR was not needed and was removed.

Page 7 lines 4/5: show ice signatures on plot (mentions in text to left and right but not that clear) line 8: text says D-A, use A-D for consistency. Also A,D in figure 3 and D,A in figure 4, make consistent.

Well spotted. We made this consistent.

Page 8 line 4: What is the magnitude of the ice concentration change between algorithms for this example? Line 10: show theta = 90 on figure

The improvement is only few tens of %s RMSE, but can be more significant in other conditions. We specified the [-90;90] range for Figure 4.

Page 9 line 5: Have you also used a sliding window? Wording implies not, if it is suggest adding "similarly" before sliding. Why was the window changed from +-15 to +-7 days? Line 13: Why can this be assumed? Expand. Line 15: and SMMR, SSM/I, SSMIS? Also remove "than". Line 15/16: suggest moving sentence beginning "Recent investigations..." to line 13, before "It is assumed..."

P9L5. Done. We add a sentence: "Our sliding window is made shorter so that tie-points react more rapidly to seasonal cycles, e.g. onset of melting." L13, L15, L15/16: all done by a refactoring: "As in Tonboe et al. (2016), the CI training sample is based on the results of the NASA Team (NT) algorithm (Cavalieri et al., 1984): locations for which the NT value is greater than 95% are used as a representation of 100 % ice. Recent investigations, e.g. during the ESA CCI Sea Ice projects confirmed that NT was an acceptable choice for the purpose of selecting closed-ice samples."

Page 11 First paragraph: This is confusing as it sounds like different RTMs for each instrument but is it actually different optimisations? Rework. Line 10: quantify what is meant by "rather large" line 27: Is there a citation for the ATBD document itself? From line 20: As not using GR2219v suggest editing this section as don't need to describe in detail or give previous examples.

P11: we re-worded to avoid confusion of different RTMs. L10 done (“sometimes up to 50%”) L27: we are not aware of a citation for the ATBD. L20: we kept the text as-is.

Page 12 line 1: Would be helpful to use a different symbol other than T to avoid confusion with temperature line 26: Implies that <10% will be removed anyway, even if GR3719v < T. If so need to clarify this in text. Note also in this section that GR3719v is also used for AMSR despite different channels. Also in this section, it is not really clear how the threshold values for the Gradient Ratios are selected, needs clarification.

P12, L1. In retrospect we agree that another symbol could have been chosen, but T is also ok as a symbol for Threshold. We kept T. L26: your observation is correct, and we added a justification for adding a test to SIC<10% (“In addition, GR3719v contains information on sea-ice type (Cavalieri et al. 1984) and it is desirable the filter should work equally for first-year and multiyear sea ice.”). Concerning the need for clarification, the dynamical tuning of the OWF is described with several sentences already, we made the link to Figure 3 clearer. We changed one of them to be better described by Figure 3: “First, the coordinates for the point J are computed: J falls where the SIC=10% isoline (thick blue line) crosses the (blue, dotted) line between the OW signature point H and a point at the right-most end of the line A-D. Then, the GR3719v value corresponding to J is computed, and used as a threshold T”.

Page 13 line 1: If you say it’s visible, need to show on a figure line 12: Would be useful to show in a figure for visualisation line 13: “u” in italics is given as “U” on figure 4, needs to be consistent line 26: Why is there an increase in concentration due to the atmospheric correction (with reduced standard deviation) in figure 5? line 29: Are the contours specifically for 2015? Need to elaborate.

P13L1: We show it on Figure 5 introduced in the next paragraph., L12: Yes. The need for visualization is expressed by both reviewers and we agree. We added such a visualization on Figure 3 (black curve). L13: U is a direction sustained by unit vector u. We made this clear in the caption for Figure 4. L26: Both reviewer asked the same question. We added an explanation in section 3.4.3.

See also our answer to a similar point made by Reviewer #1: “Outside the 15% SIC contour, it is correct that Figure 5 (left) shows increase in SIC after correction. This was confirmed by plotting similar plots for other months. This is because the SIC before correction SICucorr is mostly slightly negative there, and the correction step brings it closer to 0%. This is linked to the way our OW tie-point is tuned. As explained in section 3.4, the OW tie-point is tuned dynamically against open ocean cases that are outside a maximum ice extent climatology, thus potentially more representative of “open ocean” Tie-point than the conditions closer to the edge. Prior to atmospheric correction, the open-water tie-point is thus “warmer” than the T_B

conditions closer to the edge, thus the uncorrected SICs are slightly negative there. After correction, our OW tie-point is re-tuned and is more representative of T_B close to the ice edge, hence the increase (reds in Figure 5). The net effect is a reduction in variability over ocean (blues on Figure 5, center panel) which indicates that the atmospheric correction step on average does a good job reducing weather-induced noise over the open ocean.”

L29: yes, the contour are for january 2015, this was added in the text.

Page 14 line 2: confirm if this is the standard deviation of the differences, or the standard deviation over January for each pixel, then the difference of these (latter is as worded) line 8: Would be useful to see impact of ice curve correction and atmospheric correction separately on figures line 26: clarify footprint mismatch is between different channels

P14L2: This is indeed the second option: “the standard deviation over January for each pixel, then the difference of these”. L8: we cannot show the impact of the two separately. However, and as now clearly noted in the manuscript as a response to Reviewer #1 comments: the RTM-based correction has most effect at low concentration (outside the 15% contour in Figure 5), and the ice curve correction at high concentration values (inside the 70% contour). Thus, although we cannot have separate figures, the effect of the two corrections are clearly separated in space. L26: done: changed “footprints mismatch” to “the mismatch between footprints at different channels”.

Page 15 lines 1&3: need to explain “3 dB footprint” or remove lines 2/3: also mention AMSR products line 10 and paragraph: Needs more information on how K was calculated line 21: land spill-over effects are critical for users in that missing data around coasts causes problems and has to be dealt with. Where you have removed data, have you done any filling?

P15L1&3: removed “3dB” as unnecessary. L10: the following text was added: “The MODIS images are first classified as water/ice at full resolution. Two sets of coarser resolution SIC fields are then prepared: 1) the foot-print simulator is applied to prepare a synthetic sea-ice concentration field at the resolution of the PMR channels, and 2) the high-resolution classified pixels are binned into regular grid cells, e.g. at the target resolution of the CDR (e.g. 25x25 km). The mismatch between the two fields is what we call the smearing uncertainty, and is parametrized against proxies such as (MAX-MIN)3x3.” L21: contrarily to the operational SIC product by OSISAF, we do not have a stripe of missing data along the coastline. We rather correct the coastal SICs for land spill-over. For this version of the datasets, we combine a swath-based correction scheme, with a statistically-based one. The land spill-over is much reduced with respect to earlier versions, but more work is needed (and planned) on these aspects.

Page 16 line 3: Does this improve things compared to Cavalieri et al. (1999) alone? line 6: Year for Donlon paper should be 2012. Also, not to change in the paper but note that I believe the mask has been updated for the SST CCI v2 processing. Line 15: "New Scotland" should be "Nova Scotia", no need to translate as still same in English lines 15&16: State whether you have done anything different in processing to get ice over inland regions and fresh water, either here or elsewhere in paper line 29&30: Clarify that you are not filling in missing days, e.g. in the SMMR period etc. Are you filling around coasts?

P16L3: It does improve wrt to Cavalieri et al. (1999) alone, we added a paragraph in the Discussion section (5.2): "Other steps in the processing chain can further be improved upon, e.g. the land spill-over correction schemes. In section 3.6 we described how land spill-over was corrected in two steps, first through a physically-based algorithm on swath T_B data (adapted from Maass and Kaleschke, 2010), followed by a statistically-based correction of gridded SICs (adapted from Cavalieri et al. 1999). Several reasons can have led to the swath-based correction to not be enough. For example, the method relies heavily on accurate geolocation of the T_B measurements, however its uncertainty for the SSM/I and SSMIS instrument is known to be large (Poe et al. 2008), and is not corrected for in the current version of the FCDR (R3) we used (Fennig et al. 2017). We used approximated iFoVs weighting functions instead of eFoVs (see section 2.1) when convolving antenna pattern with the land mask, thus neglecting the effect of the measurements integration period. Finally, strategies to avoid gridding land-contaminated FoVs when building Level 3 maps might help in the future. It will also be beneficial to use objective high-resolution SIC maps from coastal regions (e.g. from navigational ice charts) to tune the various thresholds embedded in the statistically-based correction. To improve further on the land spill-over correction will be an objective for upcoming versions of the CDRs."

Donlon paper: done. Thank you for the update on the SST CCI land mask, we will act upon this for next version. L15&16: We added this information at the end of section 4.3: ("Ice resulting from freezing of fresh and brackish waters does not have the same emissivity as that from sea water. The retrieval of ice area fraction in these conditions would call for dedicated tie-points (e.g. Ghaffari et al. 2011), which we did not implement here. In addition to the difficulty of computing dynamic tie-points over such small areas, it is unclear if such dedicated tie-points would make a large difference in the end, because of the combination of many error sources in these close water bodies (land spill-over, thin sea-ice, larger atmospheric influence, etc...). A layer in the status_flag variable indicates fresh and brackish water bodies.")

Fully missing days: we added the sentence "Days with fully missing input data (e.g. every other day in the SMMR period) are not created by interpolation, and the files are missing."

Page 17 Evaluation of the data: Have you simply looked through the data? Issues where processing has gone wrong, or the data looks strange have previously been an issue for OSI SAF CDRs. It would be very helpful for users not to have to do this QC. Line 7: add what the ERA-Interim data is used for in the processing line 28: colour scale is blue-red, not blue-yellow-red line 29: Is noise just characterised as below 10%? line 33: suggest move “as nominally returned by the SIC algorithm” to line 27 after “raw_ice_conc_values”

P17: The data was thoroughly looked at. We hope no artefacts are left. The situation should also be improved wrt OSISAF v1 thanks to using QCed FCDR as input (instead of an archive of operational data stream). L7 ERA-Interim: Done. L28: done, L29: no, “noise” characterises that the true SIC is 0% (unless close to the edge), before the OWF is applied. L33: done.

Page 18 line 16: what about summer?

Good question. The following sentence was added: “During summer, sigma_algo is larger by few percents, and the increased variability inside the ice pack yields higher sigma_smear, leading to larger sigma_tot.”

Page 19 line 23: SMMR uncorrected is also better than for SSM/I and SSMIS, particularly in the NH. Why? Line 30: in winter? Line 31: need to give seasonal figures

P19, L23: Indeed, SMMR uncorrected is also better than SSM/I and SSMIS. This is due to the center frequency of the Ku-band channel (18GHz) being farther away from the water vapour absorption line (22GHz) than the SSM/I channel (19.3GHz). 18GHz is less influenced by water vapour. This explanation was added in the manuscript.

L30 and L31: the offset between SICCI-50km and the others is mostly constant in all seasons.

Page 20 line 4: “internally consistent” - do you mean consistent over time? Line 5: Can’t tell from figure 8 that it’s the smallest possible. Suggest reword “and smallest possible retrieval noise” to “and a small retrieval noise” line 14: change “thus after the OWF is applied” to “thus after all the filters including the OWF are applied” for clarification line 17&18: as the range changes are they stable with time? Also need to give separate summer and winter values and incorporate line 20 in the discussion. Also separate summer and winter values line 21. line 27: might be worth adding that this is addressed as future work later in the paper line 33: Need to elaborate on how this could cause an increase over time

P20L4&5: clarified as suggested. L14: done as suggested. L17&18 We added a values for summer and winter. L33: this is an hypothesis, and is now clearly marked as such. The mechanism would go via improving atmospheric correction via better

re-analysis field, that would lead to stronger separation of the projection plane in (19v,37v,37h) and the (19v,37v) OWF plane. We changed the sentence to: "The departure of the optimal SIC data plane from the OWF plane (by convention at theta=0°, see right-hand side panel in Figure 4) could be the cause for the slight increase of the 1%-percentile curves of OSI-450 during the time period (via an improvement of the reanalysis data entering the atmosphere correction step over time), and the different value obtained with SICCI-25km".

Page 21 lines 17&18: Why 2 months in summer and 3 months in winter?

The motivation doing so is the temporal duration of sea-ice conditions being close to the annual sea-ice extent minimum and maximum. This period lasts longer in winter than summer. We also chose to limit the comparison to these months because the climatological ocean mask varies least during these time periods and allows us to put the locations of the reference 0% sea-ice concentration as close as possible to the maximum extent of sea ice. This way we make sure to perform the evaluation in "polar"-type waters and atmospheric conditions.

line 23: Give the T2m threshold (if not mentioned elsewhere?)

The T2m threshold is +5C, this is now added in the text.

line 25: "skewed a bit" – could quantify the skewness, or reword to "slight negative skew" or similar, and elsewhere.

Reworded.

Line 27,28,29: should refer to Figure 12, not Figure 10.

To refer to Figure 12 instead of 10 is correct. Done.

Values given are not the same as on Figure 10, unclear. Line 33: In winter it looks fairly similar though.

This was a rounding issue in the figure text. Figure 10 (and 12) are now revised to show the same values as in the text.

Page 22 line 3: reference "(Figure 12)" after "100%"

The reference to Figure 11 at the end of the sentence is actually covering quite well the information given on this sentence, not changed.

line 4: should be Figure 12, not Figure 11

Indeed, this was changed.

line 7: Suggest replace "less good" with something like "poorer, but still acceptable". Suggest cut the last sentence of this paragraph as is a repetition.

We replaced "less good accuracy" by "slightly larger bias", and removed last sentence.

Line 12: The total uncertainty is described as "standard error" on Figure 12, need to reword this.

This is now better captured in the caption of Figure 12: black error bars are for plus/minus one standard deviation of the standard error, while blue error bars are for plus/minus one standard deviation of the total uncertainties.

Paragraph around line 20: Elaborate on why uncertainties for SICCI-50km are smaller than for the other two datasets.

The following sentence was added: “These results are in agreement with those introduced in section 4.2.1 and are mainly explained by the frequency channels used in the three CDRs: 18.7 GHz for SICCI-25km, instead of 19.3 GHz for OSI-450 (less noise contribution from atmospheric water vapour content), and 6.9 GHz for SICCI-50km (smaller sensitivity to atmosphere and surface snow and sea-ice property variations).”

Line 25: For high sea-ice concentration range they are slightly underestimated, especially for OSI-450.

Indeed. We reworded the sentence to: “Thus, the results summarized in Figure 12 indicate that the uncertainty tot provided with the three CDRs are slightly underestimated, especially for OSI-450, for the high sea-ice concentration range (SIC = 100%), and are slightly overestimated for the low sea-ice concentration range (SIC = 0%).”

Page 23 line 1: Confusing wording. Ground truth locations are not outside expanded maximum ice climatology?

This was reworded as: “For SIC = 0%, the ground-truth open water locations are selected just outside the maximum sea-ice climatology, while we used an expanded version of this climatology for the selection of the open water training data samples (sections 3.3 and 3.6)”

Line 17: Reword “it is also designed to remove” as “it also has the effect of removing”, as this is a side-effect of the filter, rather than a planned part of the design. Line 24: replace “these wavelengths” with “the wavelengths of the PMR channels” for clarity.

P23L17: done as suggested. L24: done as suggested.

Page 24 line 3: Unclear what is meant by “at most” in this context line 13: add “AMSR-E and AMSR2” before “channels” for clarity. Line 21: add “variable” after “raw_ice_conc_values” for clarity. Line 29: Expand “ECV” acronym here

P24L3: reworded. L13: done. L21: done, L29: done.

Page 25 line 5: change “two components” to “two algorithm components” for clarity line 10: add section number after “Outlook” line 16: add “data” after “AMSR2” line 23: add “channel” before “frequencies” for clarity. Lines 26&31: add “closed” before “sea ice”

P25L5: done, L10: done, L16: done L23: done, L26&31: done

Page 26 lines 18-19: The level itself is not stable, though always remains below 15% - needs rewording. Also not accurate to say “well below 15% SIC threshold” for SICCI50km. Lines 23&24: Confusing wording: “maximum 1%” and then “a couple of percent” - needs rewording.

P26L18/19: we rewored but still find that this is quite stable over >30 years.
L23&24: fixed (kept couple of percent).

Page 27 line 20: expand SIE acronym line 24: Add some more information on plans to implement improvements for CDRs into operational processing chains (a few lines).

P27L20: done. L24: done, but on the page after (when discussing ICDR).

Page 28 line 6: expand EO acronym (and use acronym on line 7) line 23: URL for CMEMS is “marine.copernicus.eu” (there is a typo)

P28L6: done. L23: done (thanks!)

Page 29 lines 2&3: Confusing wording – is it the first satellite or the first satellite with MWI? Reword. Line 14: Add “channel” before frequencies for clarity. Line 15: This implies users should combine the products (which they shouldn’t if they want a consistent product). Clarify that different products are available for different user needs. Lines 25-27: how can this be used? Users will treat uncertainties provided with data as the observation uncertainty

P29L2&3: We rewored: “The first satellite of the European Polar System Second Generation (EPS-SG) series to carry a Microwave Imager (MWI) is scheduled for launch in 2023.” L15: interesting question. Users can combine information they retrieve separately from the three datasets. They can also attempt the combination of the products, but have to take into account the difference in spatial resolutions, which requires more advanced techniques that we could use here. We did not modify the text. L25/27: based on our evaluation of the observation uncertainties, users 1) are confident that our uncertainties mostly correspond to the statistical observed error, and 2) our uncertainties are slightly too large over open water, and users can thus decide to shrink them a bit if relevant for their application.

Page 30 Line 7: Would be useful to provide URLs for the data archives. Line 18: Update this, says “[Indicate subset used]” References in general: Provide URLs if available for Technical Reports etc. Some DOIs have come out as links and others not.

P30L7: Rather than the URLs, we provide the DOIs (when available) that allow link to documentation. The list of references was thoroughly checked.

Figures and tables: Some acronyms are in figure and table captions before being introduced in the text. Suggest defining in captions.

Figure 1: Add section number for Outlook.

Done

Figure 2: Add that L2 SIC is also swath, L3 is a single daily averaged file. Define acronyms used in figure in caption

Done

Figure 3: Title should be “AMSR-E” (currently “AMSR”). Labels in the figure need to be closer to the points (or colour coding would help). In figure caption, give section numbers where BFM and OWF are described in the text. “mean water signature” should be “mean open water signature”

Done

Figure 4: Left plot: Label “BRI”, “BPM” and “BFM” on plot. Add theta label on plot. “u” in caption is labelled “U” on plot, make consistent. Axis labels should also match convention in caption, e.g. “37H” rather than “h37”. Right plot: “Freq. Mode” should be “BFM”, “Bristol” should be “BRI”. Add “theta” symbol to “Rotation angle” axis label. As noted in the text and figure caption, the original figure is from Smith et al. (1996), so that we cannot change the labels on the arrows. The other suggestions are implemented as text in the caption to Figure 4.

Figure 5: Centre panel: Difficult to see any detail using this scale, needs to be shortened. Doesn’t have to be the same as left panel as showing different variables

Done.

Figure 6: a) Need to show 0% as white (or similar) for SIC plots so can see detail around ice edge. b) Would also be helpful to plot ice_conc minus raw_ice_conc_values.

- a) We tried your suggestion, but it gives the impression that the SIC fields have missing value (instead of 0% SIC). We did not observe it added much information in the ice edge region. Readers interested in such details would probably open the netCDF files and inspect this more closely, while we aim here at a high-level feel of what is in the variables. We did not change figure 6.
- b) raw_ice_conc_values holds non-masked values iif ice_conc = 0% (in places the OWF was triggered) and ice_conc = 100% (in places ice_conc_raw_values is larger than 100%). Thus, a plot of “ice_conc minus raw_ice_conc_values” would be very similar to our plot of “raw_ice_conc_values”. Because it is the first time users are presented with

such “raw” ice concentration values, we feel it is more important to illustrate them what they find in the file. We did not add or change on Figure 6.

Figure 7: Need to show 0% as white (or similar) so can see detail at low uncertainties.

There are no grid cells with exactly 0% in sigma_algo (left) and thus sigma_tot (right). There are some 0% values in sigma_smear (center) but as in Figure 6, using white for them gives the impression that the sigma_smear field has missing values. Readers interested in such details would probably open the netCDF files and inspect this more closely, while we aim here at a high-level feel of what is in the variables. We did not change Figure 6.

Figure 8: Figure legend - datasets should be capitalised for consistency
Done.

Figure 9: Figure legend - datasets should be capitalised for consistency. If SICCI-25km and OSI-450 lines were thinner (like SICCI-50km) it would be easier to see the lines for both hemispheres.

Capitalization done. We did not change the line width as NH lines were too difficult to read. As per your suggestion, we added some description of the NH and SH curves in the text with discussing Figure 9.

Figures 10, 11: Specify that the sea ice concentration is uncorrected. Numbers in parentheses are in front of the season, not behind. Unclear - “Numbers below the season denote the mean SIC plus/minus one standard deviation” - there’s only one number so how can this be plus/minus? Also Figure 11: The SH plots are “bumpier” than the NH plots – add comments on this.

The sea-ice concentration are corrected but not filtered (the OWF and 100% thresholding are not applied). This is now specified in the legend to both Figures. The description of the numbers appearing in the plot area was revised. The SH plots are “bumpier” simply because of the reduced number of data pairs, as indicated in the plot area.

Figure 12: Standard error is not mentioned in the text.
This is now done.

Table 1: Give months in the time period. Worth adding that grid is EASE grid.
Caption: “entering” should be “entered in”.

Done

Table 2: Start date for DMSP SSM/I has an error (“090”), check table for other errors
Done, thank you.

Technical corrections

General comments: Throughout, need to ensure there is a space between numbers and their units.

Done.

Throughout have used “...” or “etc...”, should probably just be “etc.” or sometimes “e.g.” but check journal style guide.

We will check when editing final version.

Have referred to e.g. F10, F11 satellites, suggest using full name (include DMSP) at the start of the paper for clarification.

Done (introduce DMSP acronym early in the text).

Specific comments: Some of the following are corrections of grammatical errors, and some are rewording suggestions to improve the readability of the paper.

Thank you very much for compiling all these suggestions!

Page 2 line 4: “allow” should be “allows” line 5: “are” should be “is” line 6: “to understand” should be “for understanding” line 11: “are” should be “is”, “have” should be “has” line 28: unclear what you mean by “possibly” in this context, if it’s the possibility that filtering can be applied needs rewording.

Implemented all suggestions. We reworded “possibly filtered” to “access to filtered as well as raw values”.

Page 3 line 17: remove “up-front” here, reads a bit strangely in this context. Also, “entering” should be “entered”

Done.

Page 4 line 3: “some” should be “a” line 4: “more” should be “most” line 6: give section number for Outlook. Line 20/21: “Such wavelength” should be “Such a wavelength” line 23: replace “needed for” with “used in” line 25: add “(Table 2)” after “channels” line 31: “diameters” should be “diameter”

Done.

Page 5 line 1: I think “One” should be “Two”, also change “swath” to “swaths” line 2: change “orbit” to “orbits”, “extent” to “extents” line 5: expand CM-SAF acronym line 7: “directly accessed directly” should be “accessed directly”, “Japan space agency” should be “Japan Aerospace Exploration Agency” line 15: “contribution” should be “contributions” line 18: “ERA-Interim” should be “ERA-Interim reanalysis” line 20: “ERA-Interim prior” should be “ERA-Interim data prior” (or similar), “early period with”

should be “earliest period of” line 24: “from” should be “of”, “for” should be “in” line 27: “operated to process” should be “for” line 32: “(L3) collects” should be “(L3) chain collects”

[Done.](#)

Page 6 line 3: “apply” should be “applies”, “format” should be “formats” line 5: “similarly” should be “similar” line 29: define OW (given above in context of algorithm but worth defining here again), same for CI line 30.

[Done.](#)

Page 7 line 1: “TB in point” should be “TB at point”, similarly “lines in point” should be “lines at point” line 2: “and geometric” should be “and a geometric” line 6: remove “originally”, “describes” should be “describe” line 20: “onto” should be “on” line 25: “cope for” should be “cope with”

[Done.](#)

Page 8 line 1: would read better as “Figure 4 (right panel) also shows that the optimum...” line 16: “space” should be “spaces” lines 19/20: replace arrows with “ “ line 26: “section so” should be “section has so” line 32: “by Eq. 1” should be “using Eq. 1”

[Done.](#)

Page 9 line 20: “was” should be “has been”, comma before “which” line 21: “varies” should be “vary”, “follows” should be “follow” line 25: “yield highest” should be “yield the highest” line 26: “yield departure” should be “yield a departure” line 27 and 28: “departure” should be “departures”

[Done.](#)

Page 10 line 3: add commas both before and after “the uncorrected SIC value” line 7: “re-analysis” should be “re-analyses” line 20: Add “For Tb_nwp” at the start of the line line 22: Add “For Tb_ref” at start of sentence before “Theta_instru” line 26: remove “for F10” (already mentioned in this sentence) line 29: “for being” should be “to be”

[Done.](#)

Page 11 line 3: “allows” should be “allowed” line 9: “ones” would read better as “datasets”. Also, having introduced the acronym WFs should use on this line instead of “Weather filters” (also on line 20). Line 14: no hyphen in unaffected line 18: suggest changing “so far did not adopt” to “have so far not adopted”, also “from” should be “in” line 19: change “by using adhoc status flags” to “on an adhoc basis by using status flags” (as the flags themselves are not adhoc) line 22: “re-used” should be “reuse” (or “have reused”) line 23: Suggest add “For example,” before Spreen et

al. Line 25: "to" should be "with" line 26: "with" should be "for", "for which" should be "where", suggest changing "threshold is 0.053" to "threshold is set to 0.053"

[Done.](#)

Page 12 line 2: "intersect" should be "intersects" line 6: missing close bracket after (AD), also "illustration how" should be "illustration of how" line 7: "into" should be "in" line 11: add "and" before "the varying effects" line 12: suggest replace "not remove" with "avoid removing" line 13: "show" should be "shown" lines 16,17: "T" should be in italics line 20: "naming" should be "name" line 22: change "is set to" to "will" as this is an unintended consequence line 23: suggest changing "we rather refer to such filters as 'Open Water Filter'" to "we refer to such a filter as an 'Open Water Filter'", also suggest "add" changed to "include" line 24: "are" should be "is" line 27: "Noticeably" should be "Notably" line 28: "attached a" should be "attached to a", also change "as to if the OWF detected it" to "corresponding to OWF detection"

[Done.](#)

Page 13 lines 1&2: "high concentration range" should be either "a high concentration range" or "high concentration ranges" line 5: remove "likewise" line 10: change "best appear" to "are best shown" line 11: "T" in $B_{CI}(T)$ should be bold lines 14&15: "constantly" should be "consistently" line 28: "Laptev and Kara Sea" should be "the Laptev and Kara Seas" line 29: would read better to remove "old" after "2 years", also "on right panel" should be "on the right panel"

[Done.](#)

Page 14 line 6: "north for Canadian" should be "north of Canadian" line 8: remove "that what" line 9: change "and" to "which" after "section 3.4.1," line 19: "data is assimilated" should be "data are assimilated" line 21: "those" should be "that" line 28: "algorithm to retrieve" should be "algorithm for retrieving"

[Done.](#)

Page 15 line 1: suggest change "relevant to discuss" to "relevant for discussion of" line 4: "Earth surface" should be "the Earth's surface" line 7: remove "that is" line 9: "cells" should be "cell" line 20: remove "shortly" line 21: suggest change "presenting less" to "have undergone little" line 28: "details" should be "detail" line 30: suggest change "among others" to "including" line 31: remove "is computed" line 32: change "the antenna pattern functions are approximated" to "the approximation of antenna pattern functions" line 33: "from central" should be "from the central"

[Done.](#)

Page 16 line 1: "for contribution" should be "for the contribution" line 4: "were" should be "have been" line 5: "where" should be "were" line 7: "as input" should be "as the input" line 13: "were" should be "was", suggest change "base" to "basis", "pixel"

should be “pixels” line 18: “in SH” should be “in the SH” line 19&20: change “where to select the Open Water training samples” to “where the Open Water training samples were selected” line 26: “conversely” should be “converse”, suggest “CDR of” should be “CDR method of”

Done.

Page 17 line 14: “of SICCI-25km” should be “of the SICCI-25km” line 22: “file” should be “files” line 27: “Bottom” should be “The bottom” line 29: “corresponds” should be “correspond” line 32: “by OWF” should be “by the OWF”

Done.

Page 18 line 6: “indicate” should be “indicates” line 14: replace “are covered by” with “cover” line 18: Suggest replace “several” with “three”, “One” with “The first” line 19: “its” should be “their” line 25: no hyphen in intermediate

Done.

Page 19 line 9: “albeit” should be “despite” line 12: “from” should be “for” line 15: “from” should be “for” line 16: “improve much” should be “much improve” line 18: “parametrization” should be “parametrizations” line 21: “from with” should be “for”, also “were” should be “where” line 25: “sensibly” - do you mean “ostensibly”?

Done.

Page 20 line 9: remove “at best” and add “ideally” before “preserving” line 19: reword “very little few jumps are” to “very little change is” (or similar) line 23: could remove “lowest” and “highest” as it’s already clear this is the range

Done.

Page 21 line 10: remove comma after “but” line 14: “details” should be “detail” line 21: “East Antarctic” should be “the East Antarctic” (or “East Antarctica”) line 23: remove “being”, suggest replace “by too” with “with” lines 29&30: suggest move “than for the other two CDRs” after “more” on line 29 line 30: “e.g.” should be “i.e.” line 31: add “for all three CDRs” after “2%”. lines 32&33: suggest change “less good than that” to “poorer than”

Done.

Page 22 lines 5&6: change “Arctic” to “the Arctic”

Done.

Page 23 line 3: Suggest reword “can be picked” to “may be selected” line 4: Suggest reword “and to the least at the location of the ground-truth estimates used in the section” to “where the ground-truth estimates used in the section are located” line 5:

Change "More developed" to "A more developed", "as wetter" to "as a wetter" line 6: Change "We finally" to "Finally, we" line 12: "in large extent" needs to be reworded, perhaps replace with "generally" or "to a large extent" line 13: Capitalisation of "Passive Microwave" varies, be consistent line 15: "on combination" should be "on a combination", also need to define acronym "PMR" line 19: "take" should be "pay" line 20: "in field" should be "in the field", also use "OWF" acronym for consistency line 21: "are pertaining" should be "pertain" line 25: Remove "distinguishing between" and add "to be distinguished" to end of sentence.

[Done.](#)

Page 24 line 1: "aims" should be "aim", also "from interested" should be "from the interested" line 6: replace "was" with "were" twice line 17: "is 'spilling'" should be "'spills'", also "appear" would be better than "look" line 19: "foot-print" sometimes has a hyphen, sometimes not, needs to be consistent line 20: "instrument" should be "instruments" line 29: "improvement" should be "improvements"

[Done.](#)

Page 25: line 7: "on March 1985" should be "in March 1985" line 8: add "dataset" before "only", also add "on" before "09 July" lines 9&10: change "achieving" to "to achieve" line 11: suggest reword "algorithms allowed e.g. to consistently process SIC" to "algorithms also allowed consistent processing of SIC" line 14: change "15 years record" to "15-year record" line 18: change "will" to "would" line 20: change "had met" to "would meet" line 33: add "the" before "coarsest"

[Done.](#)

Page 26 lines 3&4: Confusingly worded: "seasonal cycle of sea-ice and snow properties during summer". Should this be sea ice extent? (Also be consistent throughout about whether to use a hyphen in sea ice or not) line 15: "than" should be "as" line 17: Suggest remove "For all practical purposes" line 29: Remove "namely" line 33: remove "that"

[Done.](#)

Page 27 line 1: "impact of melting" should be "impact that melting" line 3: Suggest change "more efforts" to "further effort" line 4: Remove "same" and "that was" line 10: "if to selecting" should be "if selecting" line 12: "dimension" should be "dimensions" line 17: "the sea ice cover, sea ice area" should be "of sea ice cover, and sea ice area" line 27: "exploring" should be "exploration" line 28: "channels" should be "channel", "that" should be "than" line 30: Suggest change "could not be better embedded by SIC" to "could be better embedded in SIC" line 32: "Filter" should be "Filters"

Done.

Page 28: line 2: Suggest adding “still” after “can” line 24: Change “at best” to “to achieve” line 33: “passed” should be “past”

Done.

Page 29 line 5: Add “However,” before “Because” (as shouldn’t start a sentence with because) line 17: “product contains” should be “products contain” as there is more than one product. Line 19: Replace “on the hand a” with “ease of”, “product” should be “products” line 20: remove “of all products”, “is” should be “are”, “has” should be “have” line 25: “this provides” should be “this paper provides” (or similar)

Done.

Page 30 line 6: “making” should be “make”

Done.

=====

Version 2 of the EUMETSAT OSI SAF and ESA CCI Sea Ice Concentration Climate Data Records

Thomas Lavergne¹, Atle Macdonald Sørensen¹, Stefan Kern², Rasmus Tonboe³, Dirk Notz⁴, Signe Aaboe¹, Louisa Bell⁴, Gorm Dybkjær³, Steinar Eastwood¹, Carolina Gabarro⁵, Georg Heygster⁶, Mari Anne Killie¹, Matilde Brandt Kreiner³, John Lavelle³, Roberto Saldo⁷, Stein Sandven⁸, Leif Toudal Pedersen⁷

¹Research and Development Department, Norwegian Meteorological Institute, Oslo, Norway

²Integrated Climate Data Center, CEN, University of Hamburg, Hamburg, Germany

³Danish Meteorological Institute, Copenhagen, Denmark

⁴Max-Planck Institut für Meteorologie, Hamburg, Germany

⁵Barcelona Expert Center, ICM-CSIC, Spain

⁶Institute of Environmental Physics, University of Bremen, Bremen, Germany

⁷Danish Technical University-Space, Copenhagen, Denmark

⁸Nansen Environmental and Remote Sensing Center, Bergen, Norway

15

Correspondence to: Thomas Lavergne (thomas.lavergne@met.no)

Abstract. We introduce the OSI-450, the SICCI-25km and the SICCI-50km climate data records of gridded global sea-ice concentration. These three records are derived from passive microwave satellite data and offer three distinct advantages compared to existing records: First, all three records provide quantitative information on uncertainty and possibly applied filtering at every grid point and every time step. Second, they are based on dynamic tie points, which capture the time evolution of surface characteristics of the ice cover and accommodate potential calibration differences between satellite missions. Third, they are produced in the context of sustained services offering committed extension, documentation, traceability, and user support. The three records differ in the underlying satellite data (SMMR & SSM/I & SSMIS or AMSR-E & AMSR2), in the imaging frequency channels (37-GHz and either 6-GHz or 19-GHz), in their horizontal resolution (25-km or 50-km) and in the time period they cover. We introduce the underlying algorithms and provide an *initial* evaluation. We find that all three records compare well with independent estimates of sea-ice concentration both in regions with very high sea-ice concentration and in regions with very low sea-ice concentration. We hence trust that these records will prove helpful for a better understanding of the evolution of the Earth's sea-ice cover.

1 Introduction

30 Satellite-retrieved records of Arctic and Antarctic sea-ice concentration differ widely in their estimates of a specific sea-ice concentration on a given day in a given region (e.g., Ivanova et al., 2015; Comiso et al., 2017a). Integrated over the entire Arctic, these differences accumulate to an up to 20 % uncertainty in the long-term trends of sea-ice extent and sea-ice area (Comiso et al., 2017b), which hinders a robust evaluation and bias correction of climate models, and in particular hinders a robust estimate of the future evolution of the Arctic sea-ice cover. For example, Niederdrenk and Notz (2018) found that

observational uncertainty is the main source of uncertainty for estimating at which level of global warming the Arctic will lose its summer sea-ice cover. This is because both the bias correction of large-scale climate models and the extrapolation of observed relationships between forcing and sea-ice coverage can only be carried out robustly if observational uncertainty is sufficiently small. In this contribution, we introduce three new climate data records of gridded global sea-ice concentration

5 that address some of the shortcomings of existing records, and in particular provide additional information that allows users to judge the robustness of the sea-ice concentration estimates.

Our focus on sea-ice concentration is to a substantial degree driven by the fact that information on sea-ice concentration ~~are is key to the vast majority of approaches to understand for understanding~~ the changing sea-ice cover of our planet. This

10 importance of sea-ice concentration derives both from the availability of a long, continuous record of the underlying passive-microwave data, and from the central importance of sea-ice concentration for many physical processes connected to the sea-ice cover. For example, the albedo of the polar oceans is strongly influenced by sea-ice concentration~~For example, the albedo of the polar oceans directly depends on sea ice concentration~~ (e.g., Brooks, 1924; 1925), as does much of the heat and moisture transfer between the ocean and the atmosphere (e.g., Maykut, 1978).

15 Information on sea-ice concentration ~~are-is~~ also used to derive total sea-ice area or extent. The latter ~~have-has~~ in the Arctic been found to be linearly related to global-mean temperature (e.g., Gregory et al., 2002; Niederdrenk and Notz, 2018), atmospheric CO₂ concentration (e.g., Johannessen, 2008; Notz and Marotzke, 2012) and anthropogenic CO₂ emissions (Zickfeld et al., 2012; Herrington and Zickfeld, 2014; Notz and Stroeve, 2016). These linear relationships allow one to
20 estimate the future evolution of Arctic sea ice directly from the observational record (e.g., Notz and Stroeve, 2016; Niederdrenk and Notz, 2018), to evaluate the sea-ice evolution in coupled climate models, and to bias correct estimates from climate models for improved projections of the future sea-ice cover (e.g., Mahlstein and Knutti, 2012; Screen and Williamson, 2017; Sigmond et al., 2018). For any of these applications, the reliability of the underlying sea-ice concentration record is crucial.

25 This importance of a reliable sea-ice concentration record is also reflected in the definition of Sea Ice Essential Climate Variables (ECV) by the Global Climate Observing System (GCOS), a body of the World Meteorological Organisation (WMO). In their most recent update (GCOS-IP, 2016), they request that reliable observational records of sea-ice concentration must be made available to the climate research community. However, the reliability and long-term stability of
30 existing records is often not clear. This is for example reflected by substantial differences between existing estimates of sea-ice concentration from various algorithms (e.g., Ivanova et al., 2015; Comiso et al., 2017b).

With our three new climate data records of sea-ice concentration we aim at providing the users with new reference data sets that have three clear advantages over most existing records. First, all our three records provide quantitative information on

uncertainty and access to filtered as well as raw values~~possibly applied filtering~~—at every grid point and every time step. Second, they are based on dynamic tie points, which capture the time evolution of surface characteristics of the ice cover and help minimize the impact of sensor drift and change in satellite sensor. Third, they are produced in the context of sustained services offering committed extension, documentation, traceability, and user support.

5

The first of our three climate data records (CDR) is referred to as OSI-450. It is based on ~~eoarse-coarse~~-resolution (30-60 km) passive microwave (PMW) satellite data that are available from November 1978 onwards. This data is also at the heart of the two currently most widely used sea-ice concentration algorithms, namely the NASA Team algorithm (Cavalieri et al., [1996](#)[1984](#)) and the Bootstrap algorithm (Comiso et al., [2017a](#)[2017b](#)). OSI-450 has been released by the European Organisation for the Exploitation of Meteorological Satellites (EUMETSAT) Ocean and Sea Ice Satellite Application Facility (OSI SAF, <http://www.osi-saf.org/>) and is a fully revised version of its predecessor OSI-409 (Tonboe et al., 2016).

All three Sea Ice Concentration (SIC) CDRs share the same algorithms, processing chains, and data format. In particular, they were all developed with their primary application as climate-data records in mind, putting very narrow constraints on 15 the permissible long-term drift of the records. As such, the underlying algorithms are based on earlier work by the European sea-ice remote-sensing community (Anderson-Andersen et al., [1997](#)[2007](#); Tonboe et al., 2016) and provide sea-ice concentration estimates with a) low sensitivity to atmospheric noise including liquid water content and water vapour, b) low sensitivity to surface noise including wind roughening of the ocean surface, and variability of sea-ice emissivity and temperature, c) the capability to adjust to the climatological changes in the above-mentioned noise sources, and d) a 20 quantification of the remaining noise at each time step for each pixel.

In this contribution, we outline the underlying algorithms and the philosophy behind them. We also provide an initial evaluation of the resulting climate-data records. We start in section 2 by describing the satellite and ancillary data used as input. Section 3 describes the algorithms and processing steps implemented to process the data records. Afterwards, 25 section 4 is devoted to the resulting data records, their initial validation evaluation results, and known limitations. Discussion, outlook, and conclusions are covered in section 5.

2 Data

This section summarizes the satellite as well as the numerical weather prediction (NWP) data used in the climate data records. Each of these data sources are fully described in dedicated technical documentation, web resources, and scientific literature, so that we keep-provide here only the key information directly relevant to the discussion in this paper. Figure 1 shows the temporal coverage of the data sources entering the three SIC CDRs. Two ESA CCI data records (grey box marked “ESA CCI (2x)”) are based on the Advanced Microwave Scanning Radiometer - Earth Observing System (AMSR-E) and AMSR2 instruments (orange and dark orange horizontal bars), while the EUMETSAT OSI SAF data record (grey box

marked “OSI SAF (OSI-450)”) is based on the Scanning Multichannel Microwave Radiometer (SMMR, purple bar), Special Sensor Microwave/Imager (SSM/I, dark blue bars), and Special Sensor Microwave Imager / Sounder (SSMIS, light blue bars) instruments [on board the Defense Meteorological Satellite Program \(DMSP\) satellites](#). ERA-Interim reanalysis weather data from the European Centre for Medium-Range Weather Forecasts (ECMWF) are also used throughout the period (not shown).

- Overlap of satellite missions and the 9-months data gap between AMSR-E and AMSR2 operations are clearly visible from Figure-1. Although there always was at least one satellite mission carrying a relevant passive microwave instrument after October 1978, ~~some-a~~ few data gaps exist in the satellite data record that are too short to appear in Figure-1. The ~~more-most~~ prominent are documented in [the “comments” column of Table 2](#) [and extensive list of missing dates are in the Product User Guides \(PUGs\) of the CDRs. These PUGs are always accessible from the dataset landing pages \(see DOIs in Table 1\)](#). Figure-1 also shows other related satellite missions that do not enter the new CDRs, but might be relevant for their future extension in a compatible Interim Climate Data Record (grey box marked “OSI SAF ICDR”). They are discussed in our Outlooks [section 5.2](#).

2.1 Input satellite data

- More details about the satellite instruments and platforms are given in Table-2. It lists the satellite platforms, sensors, and time periods for brightness temperatures (T_B) used as input for the SIC CDRs. Some specific instrument characteristics like channel frequencies, spatial resolution, view angle and ~~width-area of covered by~~ the polar observation hole are also documented there. Table-2 documents that the instrument series might have quite different characteristics (e.g. channel frequencies or incidence angle). To build a consistent data record requires methodologies to carefully inter-calibrate and tune the algorithms to yield similar results when using all these sensors. This is the essence of the dynamic tuning approaches adopted in Tonboe et al. (2016) and further developed for the new CDRs (section-3).

- Building CDRs from this suite of satellite sensors is best achieved if the selected algorithms use only channels that are consistently available throughout the period. Slight changes of incidence angle or wavelengths between the sensor series can be compensated for by the algorithms, but it is harder or even impossible to achieve temporal consistency in the event of sudden loss of channels. In that respect, it is noteworthy that the 23.0-GHz channels of the SMMR instrument were highly unstable since launch, and eventually ceased to function on 11th March 1985 (Njoku et al., 1998). There is thus no continuous data record of brightness temperatures in the vicinity of the water vapour absorption line (22.235-GHz). Such a wavelength is typically ~~needed-used for-in~~ filtering weather effects in other SIC CDRs (e.g. Meier et al. 2017). Our algorithms do not rely on such a channel (section-3.4.2).

- Although not identical, the spatial resolution of the channels needed for the SIC algorithms is ~~somewhat~~-similar for the three coarse resolution sensor series (SMMR, SSM/I, and SSMIS) with about 70x45-km ~~(resp. 38x30 km)~~ instantaneous Field-of-View (iFoV) diameters for the 19-GHz [frequency channels, and 38x30 km for the \(resp. 37-GHz\) channels ones](#) (Table 2).

The two medium-resolution radiometers AMSR-E and AMSR2 have finer resolution at these channels (27x16-km and

Formatted: Superscript

14x9 km respectively), accompanied by increased sampling (10x10 km instead of 25x25 km for SSM/I). It is noteworthy that iFoV diameters, as reported in Table 2 and at several online resources such as the WMO OSCAR Space-based capabilities data base are not a measure of the true footprint of an individual measured pixel. This is because the iFoV neither takes into account the motion of the antenna (scan direction) nor of the spacecraft (along its orbit) during the integration time period

5 needed to acquire a single pixel. The effective Field-of-View (eFoV) diameter^s includes the two effects, and is a better measure of the true footprint of the instrument. For example, the eFoV of the SSM/I 19 GHz channels is closer to 70x75 km.

The dimensions of the iFoV and eFoV are referred to as the resolution of the channels. The sampling is how close in space the FoVs are acquired. Most channels are thus oversampled.

10 One-Two of the differences between the instrument series are the width of their observation swaths^s, and the inclination of their orbits^s. This translates into different extents^s of the polar observation hole, and no data are available for sea-ice monitoring north of 84° (SMMR), 87° (SSM/I), 89° (SSMIS) and 89.5° (AMSR-E and AMSR2).

For our data records, a newly reprocessed version of the SMMR, SSM/I, and SSMIS data into a Fundamental Climate Data

15 Record (FCDR, L1) was accessed from the EUMETSAT Climate Monitoring Satellite Application Facility (CM-SAF, Fennig et al. 2017). In the FCDR, the T_B are re-computed from Antenna Temperatures (T_A), screened and corrected for known artefacts like solar intrusion, and intercalibrated between missions. The AMSR-E data we use is the NSIDC FCDR AE_L2A V003 FCDR of Ashcroft and Wentz (2013), covering the full lifetime of the mission from 1st June 2002 to 10th October 2010. For AMSR2, we use re-calibrated (Version 2) L1R data that we directly accessed directly from the Japanese

20 Japan Aerospace space Exploration agency Agency (JAXA), covering 23rd July 2012 until 15th May 2017, that is the end of the SICCI-25km and SICCI-50km CDRs. For both AMSR-E and AMSR2, the T_B are available both at their nominal resolution (documented in Table 2), and post-processed at lower resolution matching those of other channels (e.g. the 36.5 GHz T_B at the resolution of the 6.9 GHz channel). We use the nominal resolution of the T_B channels is used, not the resolution-matched ones. It is noteworthy that the AMSR2 data is not from an FCDR, but rather from an archive of an 25 operational data stream. We use the data as they are provided by JAXA, without applying extra calibration towards AMSR-E (thus unlike Meier and Ivanoff, 2017) since our algorithms do not require such stringent calibration thanks to using dynamic tuning (section 3.3).

2.2 ERA-Interim data

The microwave radiation emitted by the ocean and sea ice travels through the Earth atmosphere before being recorded by the

30 satellite sensors. Scattering, reflection, and emission in the atmosphere add or subtract contributions^s to the radiated signal, and challenge our ability to accurately quantify sea-ice concentration. An initial step in our processing is thus the explicit correction of atmospheric contribution to the top-of-atmosphere radiation (see section 3.4.1). For this purpose, we accessed the global 3-hourly fields from ECMWF's ERA-Interim reanalysis (Dee et al., 2011). Fields of 10m wind-speed, 2m air

Formatted: Subscript

Formatted: Subscript

Formatted: Superscript

Formatted: Superscript

temperature, and total column water vapour are used. The ERA-Interim re-analysis starts in January 1979 and is available throughout the time period of our CDRs. Unavailability of ERA-Interim data prior to 1979 made it impractical to use the early-earliest period with-of SMMR data (October to December 1978).

3 Algorithms and processing details

- 5 This section introduces the algorithms and some processing elements that are used in the making of the SIC CDRs. In many cases, these algorithms are evolutions from-of those already applied for-in the previous version of the EUMETSAT OSI SAF CDR (OSI-409, Tonboe et al., 2016).

3.1 Overview of the processing chain

Figure 2 gives an overview of the processing chain operated-to-process-for the three CDRs. The red boxes are data (stored in 10 data files) and the blue boxes are processing elements that apply algorithms to the data. The whole process is structured into three chains, at Level_2 (left hand side), Level_3 (middle) and Level_4 (right hand side). The input Level_1 (L1) data files hold the fields observed by the satellite sensors at top-of-atmosphere, in satellite projection: the brightness temperatures (T_B) structured in swath files. The Level_2 (L2) chain transforms these into the environmental variables of interest, but still on 15 swath projection: the SIC, its associated uncertainties and flags. The L2 chain holds an iteration (marked by the “2nd iteration” grey box) similarly to the work-flow in Tonboe et al. (2016) and stemming from the developments of Andersen et al. (2006). This iteration implements two key correction schemes, the atmospheric correction algorithm at low concentration range (section -3.4.1) and a novel correction for systematic errors at high concentration range (section -3.4.3). The Level_3 (L3) chain collects the L2 data files and produces daily composited fields of SIC, uncertainties, and flags on regularly spaced polar grids. These fields can and will typically exhibit data gaps, e.g. in case of missing satellite data. The Level_4 (L4) 20 chain performs the necessary steps to fills the gaps, applies extra corrections, and formats the data files that will appear in the CDR.

The next sub-sections are devoted to giving some more details about the main features of the several algorithms involved.

Before that, we note that the L2 chain holds an iteration (marked by the “2nd iteration” grey box) similarly to the work-flow 25 in the (2016) and in the (2017) (the input data and the processing flow are identical to the one in the (2016) and in the (2017)).

3.2 A hybrid, self-tuning, self-optimizing sea-ice concentration algorithm

A new sea-ice concentration algorithm was developed during the ESA CCI Sea Ice projects and is used for the three CDRs. It is an evolution of the algorithms used in Tonboe et al. (2016). In this section, we describe both how the algorithm is trained to T_B training data sets, and how it is then applied to actual T_B measurements recorded by satellite sensors. The 30 process of selecting training T_B data is covered in section 3.3.

We call the SIC algorithm a “*hybrid*” algorithm because it combines two other SIC algorithms: one that is tuned to perform better over open water and low-concentration conditions (named B_{OW} for “Best Open Water”), and one that is tuned to perform better over closed-ice and the high-concentration conditions (named B_{CI} for “Best Closed Ice”). The combination equation is quite simply a linear weighted average of B_{OW} and B_{CI} results, where w_{ow} is the “open water” weight and SIC is

5 expressed as sea ice fraction [0;1]:

$$\left\{ \begin{array}{l} w_{ow} = 1; \text{for } B_{OW} < 0.7 \\ w_{ow} = 0; \text{for } B_{OW} > 0.9 \\ w_{ow} = 1 - \frac{B_{OW}-0.7}{0.2}; \text{for } B_{OW} \in [0.7; 0.9] \end{array} \right. ; \quad SIC_{hybrid} = w_{ow} \times B_{OW} + (1 - w_{ow}) \times B_{CI}, \quad (1)$$

OSI-409 already used such a hybrid method. It combined the Bootstrap Frequency Mode (BFM) algorithm (Comiso, 1986) as B_{OW} , and the Bristol (BRI) algorithm (Smith and Barrett, 1994; Smith, 1996) as B_{CI} . Andersen et al. (2007) and later Ivanova et al. (2015) confirmed that BFM (*resp* BRI) was so far the published algorithm (including NASA-Team and

10 Bootstrap) performing best at low (*resp* high) SIC conditions. and Notably that BRI is more accurate at high concentration than the Bootstrap Polarization Mode (BPM) algorithm. BFM and BPM are widely used for sea-ice monitoring in what is commonly known as the “Bootstrap” algorithm (Comiso and Nishio, 2008). Smith (1996) introduces the BRI algorithm as a generalization of the BFM and BPM algorithms. BFM computes SIC values in the (19V, 37V) T_B space and BPM in the (37V, 37H) T_B space. BRI uses the three-dimensional (19V, 37V, 37H) T_B space, where “19V”

15 (“19H”) is a notation for “the channel with a frequency near 19 GHz and with Vertical (Horizontal) polarization”.

Figure 3 illustrates the functioning of the BFM algorithm. Working with SMMR data for sea ice monitoring, Comiso (1986) recognized that the typical signature of Open Water (OW, SIC=0%, grey triangles) T_B data clusters around an averaged point location (the OW tie-point, H) in the (19V, 37V) T_B space. Conversely, the Closed Ice (CI, SIC=100%, grey discs) T_B data mostly clusters along a line (the consolidated ice line A-D). Comiso (1986) thus designed a SIC algorithm where isolines of constant SIC are parallel to the A-D line and pass through the measured T_B in-at point P. A geometric algorithm using the intersection of the (H,P) and (A,D) lines in-at point I returns the SIC value (in our example SIC=68%). In the same study, similar aggregation of typical T_B signatures and a geometric algorithm were also used in the (37V, 37H) T_B space (BPM algorithm). For easing later discussion, we note here that in winter Arctic conditions, the typical multiyear

25 sea-ice signature is to the “left” of the ice line -close to AD- while first-year sea ice and young sea ice is to the right -closer to DA- (Comiso et al. 2012). The AMSR-E T_B samples on Figure 3 are from Pedersen et al. (2018), the ESA CCI Sea Ice Round Robin Data Package (RRDP).

The left-hand panel of Figure 4 is originally adapted from Smith (1996) and modified with colors to describes how BFM (Frequency scheme”), BPM (“Polarisation scheme”) and BRI (Bristol algorithm) view the open water (scatter around H) and closed ice (scatter along the D – A line) data in the three-dimensional (19V, 37V, 37H) T_B space. The view direction of

BRI is equivalent to projecting the T_B data onto a “data plane”, which Smith (1996) chooses as the plane containing both the closed ice line ($D - A$) and the open water point H . Because this particular plane offers the largest dynamic range between the closed-ice and open water signatures, Smith (1996) states it to be an optimum projection plane. This however fails to recognize that the scatter of the closed-ice points around the line, and that of open water T_B samples around the point H are 5 anisotropic in the (19V, 37V, 37H) T_B space. The open water scatter has increased variance along the directions resulting from weather effects (including wind speed, cloud liquid water, water vapour, etc...) on the emissivity of water. The closed-ice scatter also has increased variance directions, e.g. due to ice type and snow characteristics. Because of these anisotropies, the optimal projection plan will generally not be that of BRI.

10 Our new algorithm is a generalization of BRI. Its principle is also introduced on Figure 4 (left panel). Like in BRI we seek an optimum “data plane” on which to project the T_B data, and we impose that this plane holds the closed-ice line (the $D - A$ line, supported by unit vector u). Vector u is computed by Principal Component Analysis (PCA), and is the direction with highest variance in the CI T_B samples. Conversely to BRI, we do not impose that H is onto the projection plane. We rather rotate the plane around u , and seek the optimum rotation angle θ that yields best SIC accuracy. On Figure 4 (left panel), we 15 mark three unit vectors v , corresponding to three different rotation angles and thus projection planes. By convention, we define that $\theta = 0^\circ$ defines the BFM (19V, 37V) plane, and $\theta = +90^\circ$ defines the BPM (37V, 37H) plane. The BRI plane typical has values around $\theta = +30^\circ$. By varying θ the optimization process samples several planes and eventually returns the optimal angles θ_{OW} and θ_{CI} that define respectively the Bow and B_{CI} algorithms. This optimization step allows us to cope for with the anisotropy of the OW and CI T_B samples in the (19V, 37V, 37H) T_B space. The right-hand side panel of Figure 4 20 shows the process of such an optimization in a case using AMSR2 data from the Northern Hemisphere. The solid lines plot the variation of the accuracy (measured as standard deviation of SIC, on the y-axis) of the SIC algorithms defined by the rotation angle (x-axis) against the OW (blue) and CI (red) training T_B data. The minimum of the blue and red curves are not achieved at the same angle. This is a clear illustration that there cannot be a single SIC algorithm that performs best both on low-concentration and high-concentration conditions and confirms the strategy already adopted by Comiso (1986), Andersen 25 et al. (2007) and Tonboe et al. (2016) to construct hybrid algorithms.

Still on Figure 4 (right panel), we can see also shows that the optimum rotation angle for OW cases is generally not exactly at $\theta = 0^\circ$ (BFM). Likewise, the optimum rotation angle for CI cases is generally not the same as that corresponding to the BRI plane. θ_{OW} (blue disc) and θ_{CI} (red disc) thus indeed define more accurate algorithms than BFM and BRI. In that 30 particular example, the improvement is mostly for OW conditions and limited for CI conditions. The value of θ_{OW} and θ_{CI} will vary with the exact frequencies, calibration, or viewing angle of the instrument (Table 2), as well as with the OW and CI signatures that exhibit regional, seasonal and inter-annual variations. The new hybrid, self-optimizing algorithms

described in this section can always be tuned to available training data (see section 3.3) and deliver optimum and time-consistent performance.

We can draw some additional information from the right-hand side panel of Figure 4. First, we seem to confirm the findings 5 of Smith (1996) that BRI performs better than BPM (that corresponds to $\theta = +90^\circ$). Indeed, the red curve increases all the way to $\theta = +90^\circ$ and shows poor algorithm accuracy for the (37V, 37H) projection plane. Second, we observe that both the blue and red curves hit a maximum standard-deviation (minimum accuracy) somewhere around $\theta = -60^\circ$ (the peak value is outside the y-range of the plot). This quite simply corresponds to the worst possible choice of projection plane, for which the OW T_B data are projected onto the CI ice line, resulting in the smallest dynamic range between OW and CI signatures.

10

The geometric descriptions above were all carried out in a (19V, 37V, 37H) space. The same reasoning can however be carried within other 3D T_B spaces, as long as such spaces offer a clustering of the CI conditions along an ice line, and sufficient dynamic range between the OW signature and the CI line. In the new CDRs, we use two different T_B spaces: The OSI-450 and SICCI-25km CDRs use the (19V, 37V, 37H) space, while the SICCI-50km CDR uses the (6V, 37V, 37H) 15 space. Both T_B spaces feature two «higher frequency» channels with same wavelength but alternate polarization (37-GHz in both cases), and a «lower frequency» vertically polarized channel (19V or 6V). The role of the “higher” frequencies is to ensure a significant spread of the CI T_B samples along the ice line, and thus offer a good base for computing vector u with PCA. They also bring higher spatial resolution to the retrieved SIC, since higher frequency channels achieve higher spatial 20 resolution (Table 2). The role of the “lower” vertically polarized channel is to ensure sufficient dynamic range between OW and CI signatures, and thus aim at reducing retrieval noise. This is at the cost of bringing coarser spatial resolution into the algorithm.

25

This section has so far covered how the new algorithms are designed and tuned to training data. At the end of the tuning process, the unit vector u defining the closed-ice line, the two angles θ_{OW} and θ_{CI} , and the T_B coordinates of the OW and CI 30 mean tie-points are recorded and stored to disk for later use. These values are the tuned parameters needed to apply the algorithms. To apply the algorithm to a set of new T_B data (e.g. a new swath of instrument data) is then straightforward. Each T_B triplet - (19V, 37V, 37H) or (6V, 37V, 37H) - is projected onto the two optimal planes (defined by u and each of the θ angles), and a BFM-like geometric SIC algorithm is applied in both planes (like in Figure 3 but the x-axis and y-axis are now along directions in the projection plane), yielding two values : SIC_{BOW} and SIC_{BCI} . The two SIC values are combined by using Eq. 1 to yield the final SIC estimate.

3.3 Dynamical tuning of the SIC algorithm

As described in the previous section, tuning the algorithms requires two sets of training data, one from OW areas ($SIC=0\%$), and one from areas we assume have fully CI cover ($SIC=100\%$). As in Tonboe et al. (2016), the training of the algorithms is

performed separately for each instrument, and for each hemisphere. In addition, the training is updated for every day of the data record, and is based on a [-7;+7-days] sliding window worth of daily samples (where Tonboe et al. 2016 used a [-15;+15-days] sliding window). Our sliding window is made shorter so that tie-points react more rapidly to seasonal cycles, e.g. onset of melting.

5

The dynamic training of our algorithms allows us to a) adapt to inter-season and inter-annual variations of the sea-ice and open water emissivity, b) cope with different calibration of different instruments in a series, or between different FCDRs, c) cope with slightly different frequencies between different instruments (e.g. SMMR, SSM/I, and AMSR-E all have a different frequency around 19 and 37-GHz, see Table 2), d) mitigate sensor drift (if not already mitigated in the FCDR), e) 10 compensate for trends potentially arising from use of NWP re-analysed data to correct the T_B (see section 3.4.1).

As in Tonboe et al. (2016), the CI training sample is based on the results of the NASA Team (NT) algorithm (Cavalieri et al., 1984): locations for which the NT value is greater than 95% are used as a representation of 100 % ice (Kwok, 2002). Recent investigations, e.g. during the ESA CCI Sea Ice projects confirmed that NT was an acceptable choice for the purpose of

15 selecting closed-ice samples. As in Tonboe et al. (2016), the CI training sample is based on the results of the NASA Team (NT) algorithm (Cavalieri et al., 1984). It is assumed that locations for which the NT value is greater than 95% are in fact mostly a representation of 100 % ice (Kwok, 2002). The tie-points for applying the NT algorithm to SMMR, SSM/I, and SSMIS are taken from Appendix A in Ivanova et al. (2015). The same tie-points are used for AMSR2 (not covered by Ivanova et al., 2015) than as for AMSR-E. Recent investigations, e.g. during the ESA CCI Sea Ice projects documented that

20 NT is an acceptable choice for the purpose of selecting closed ice samples all year round, even in the summer melt season (Kern et al. 2016). To ensure temporal consistency between the SMMR and later instruments, the closed-ice samples for NH are only used for algorithm tuning if their latitude is less than 84°N, which is the limit of the SMMR polar observation hole (Table 2).

25 The selection of the OW tie-point samples was has been revised since Tonboe et al. (2016), which used fixed ocean areas at mid-high latitudes. The training areas now varies vary on a monthly basis, and follows sea-ice cover more closely. In practice, the OW locations are those falling in a 150 km wide belt just outside the monthly varying maximum ice extent climatology (which is itself described in section 3.6).

3.4 Strategies to further reduce systematic errors and random noise

30 The algorithms described in section 3.2-3.2 are self-optimizing to yield the highest accuracy at high and low concentration ranges. Nevertheless, all T_B triplets with a departure from the mean CI or OW signatures will yield a departure from 0% and 100% sea-ice concentration. Random departures s that do not have apparent spatial or temporal structures are often referred to as *random noise*, while departures that are somewhat stable (correlated) in space and time are referred to as *systematic errors*.

Analysis of time-series of sea-ice concentration maps retrieved from the algorithm from section 3.2 reveal that the departure at low concentration range (open water) is typically a random noise, while more systematic errors are observed at high concentration range (closed ice). This is explained by the different nature of the error sources playing a role at these two ends of the sea-ice concentration range: weather-related effects at synoptic scales over open water, and surface emissivity variability (due to ice type, temperature of the emission layer, snow depth, etc...) over closed ice. In this section, we describe strategies implemented in the processing chain to further reduce random noise over open water, and systematic errors over closed ice. Both correction steps are applied during the second iteration of the L2 chain (Figure 2) and we note SIC_{ucorr} (uncorrected), the uncorrected SIC value before the start of the second iteration.

3.4.1 Radiative Transfer Modelling for correcting atmosphere influence on brightness temperatures

As described in Andersen et al. (2006) and confirmed in Ivanova et al. (2015), the accuracy of retrieved sea-ice concentration can be greatly improved when the brightness temperatures are corrected for atmospheric contribution by using a Radiative Transfer Model (RTM) combined with surface and atmosphere fields from NWP re-analyses. The correction using NWP data is only possible in combination with a dynamical tuning of the tie-points, so that trends from the NWP model are not introduced into the sea-ice concentration dataset. The correction scheme implemented in the new CDRs is based on a “double-difference” scheme, similar (but not identical) to that described in Andersen et al. (2006) or Tonboe et al. (2016).

The scheme evaluates the correction offsets δT_B (one per channel), the difference between two runs of the RTM: T_{Bnwp} uses estimates from NWP fields (in our case ERA-Interim), while T_{Bref} uses a reference atmospheric state with the same air temperature as T_{Bnwp} , but zero wind, zero water vapour, and zero cloud liquid water. δT_B is thus an estimate of the atmospheric contribution at the time and location of the observation.

$$\begin{aligned} Tb_{nwp} &= F(W_{nwp}, V_{nwp}, L_{nwp} = 0; T_s, SIC_{ucorr}, \theta_0) \\ Tb_{ref} &= F(0, 0, 0; T_s, SIC_{ucorr}, \theta_{instr}) \\ 25 \quad \delta Tb &= Tb_{nwp} - Tb_{ref} \\ Tb_{corr} &= Tb - \delta Tb, \end{aligned} \tag{2}$$

For T_{Bnwp} , the RTM function F simulates the brightness temperature emitted at view angle θ_0 by a partially ice-covered scene with sea-ice concentration SIC , and with surface and atmospheric states described by W_{nwp} (10 m wind-speed, $m.s^{-1}$), V_{nwp} (total columnar water vapour, mm), L_{nwp} (total columnar liquid water content, mm), and T_s (2 m air temperature). For T_{Bref} , θ_{instr} is the nominal incidence angle of the instrument series (see Table 2). Our double-difference scheme is thus both a correction for the atmosphere influence on the T_B (as predicted by the NWP fields) and a correction to a nominal incidence angle. The latter is required for stabilizing the DMSP SSM/I F10 signal, whose view angle varied significantly: the peak-to-

Formatted: Subscript

peak daily average incidence angle variation due to the platform's orbital drift was 52.6° – 53.7° ~~for F10~~ according to Colton and Poe (1999). The typical values of δT_B range from about 10 K over open water to few tenths of a Kelvin over consolidated sea-ice. The liquid water content (L) fields from global NWP fields (and ERA-Interim in particular) were found to not be accurate enough ~~for being to be~~ used in our atmospheric correction scheme (Lu et al. 2018). The T_B are thus not corrected for L ($L=0$) in both $T_{B_{\text{NWP}}}$ and $T_{B_{\text{Ref}}}$), and the induced remaining noise transfers into uncertainty in SIC.

We use the Remote Sensing Systems (RSS) RTM, ~~whose tuning to different instruments is~~ documented in Wentz (1983) for SMMR, Wentz (1997) for SSM/I and SSMIS, and Wentz and Meissner (2000) for AMSR-E and AMSR2. It is a parametrized, fast RTM optimized for the frequencies and view angles covered by the passive microwave sensors at hand. It originally ~~allows–allowed~~ ocean and atmosphere simulations, and was later extended to cover sea ice surface conditions (Andersen et al. 2006). Since the RTM is used in the double-difference scheme described above, accurate calibration of the RTM simulation with the measured brightness temperatures is not critical since such offsets cancel out. ~~The atmospheric correction step has more impact over open water and low concentration values than over closed ice conditions. This is because 1) a generally dryer atmosphere above the consolidated ice pack, 2) of the effect of wind speed on ocean (and not sea-ice) emissivity, and 3) of the low emissivity and high reflectivity of water at the frequencies we use in SIC algorithms (Andersen et al. 2006).~~

3.4.2 Open Water Filtering

The Weather Filters (WFs) of Cavalieri et al. (1992) have been used in basically all available SIC CDRs except the earlier EUMETSAT OSI SAF ~~ones–datasets~~ (Andersen et al. 2007, Tonboe et al. 2016). ~~Weather filter~~ WFs are algorithms that combine T_B channels to detect when rather large SIC values ~~(sometimes up to 50% SIC)~~ are in fact noise due to atmospheric influence (mainly wind, water vapour, cloud liquid water effects), and should be reported as open water (SIC=0%). The concept of WFs is very different from the atmospheric correction of T_B described in the previous section: the atmospheric correction reduces noise in the resulting SIC fields (but does not yield exactly SIC=0% over open water) while the WF is a binary test to decide if a pixel should be set to exactly SIC=0% or left un-affected. In the new CDRs, we combine both approaches as we apply the WFs after the atmospheric correction.

While WFs are effective at removing false sea ice in open water regions, they will always falsely remove (detect as open water) some amount of low concentration (and/or thin) sea ice, especially along the ice edge (Ivanova et al. 2015). This is why the OSI SAF SIC CDRs ~~has~~ so far ~~did not adopt~~ WFs and why the effect of WFs can be fully reverted ~~from~~ ~~in~~ our new SIC CDRs by using ~~on an ad-hoc basis by~~ status flags in the product files (see section 4.1).

The ~~Weather Filter~~ WF by Cavalieri et al. (1992) detects as open water (and consequently forces SIC to 0%) all observations with either $GR3719v > 0.050$ and/or $GR2219v > 0.045$. The GR notation stands for Gradient Ratio and this quantity is

computed as e.g. $GR3719v = (T_B37v - T_B19v) / (T_B37v + T_B19v)$. Many investigators have re-used these thresholds unchanged, while they should really be adapted to the different wavelengths and calibration of the different instruments. For example, Spreen et al. (2008) adapted the GR3719v threshold to 0.045 and GR2219v to 0.040 when processing sea-ice concentration with AMSR-E data. The NOAA/NSIDC Sea Ice Concentration CDR uses the Cavalieri et al. (1992) thresholds, to-with the exception of Southern Hemisphere processing with-for SSMIS F17 for whichwhere the GR3719v threshold is set to 0.053 (Algorithm Theoretical Basis Document for Meier et al. 2017).

Following Lu et al. (2018), we use a WF computed from T_B that have been corrected for atmospheric influence, and features a test on GR3719v only. There are two reasons for not using GR2219v: 1) a near 22 GHz channel is not available throughout the satellite time-series (section 2.1); and 2) the correction of water vapour using ERA-Interim data is effective enough in polar regions so that very limited additional screening is triggered by GR2219v when applied after T_B correction. Indeed, GR2219v is mostly effective at detecting water vapour effects, while GR3719v is effective at screening cloud liquid water and wind roughening effects (Cavalieri et al, 1995).

The functioning of the WF is illustrated on Figure 3. In the (19V, 37V) diagram of Figure 3, the GR3719v= T isolines are steeper than the consolidated ice line (A-D). For selected values of T , the isoline intersects the regions of typical open water and low concentration ice (the solid blue isoline GR3719v=0.058 is plotted as an illustration). All T_B data falling below the GR3719v isoline will result in $GR3719v > T$ and will thus be flagged as OW (SIC=0%) by the GR3719v test. Most of the OW T_B data (grey triangle symbols) are thus flagged as OW, as expected. Some low-concentration T_B data (not shown, but falling between H and (A-D), closer to H will also be detected as OW by the GR3719v test. This is an illustration of how WFs based on this gradient ratio will not only successfully detect false sea ice as open water, but also wrongly result into ice-free conditions where some true sea ice should have been observed. The greediness of the GR3719v filter is controlled by the threshold T , whose tuning is of paramount importance for the temporal consistency of the climate data record. The varying signature of sea-ice and ocean emissivity with time and hemisphere, the different frequencies of the 19 and 37-GHz channels for different instruments, and the varying effects of atmospheric correction all prevent the adoption of fixed thresholds. Instead, we adopt a dynamic approach to tune the threshold. Our WF is tuned to anot-void remove-removing true ice with concentration larger than 10%, on average, as The tuning is shown on Figure 3. First, the coordinates for the point J are computed: J falls where the SIC=10% isoline (thick blue line) crosses the (blue, dotted) line between the OW signature point H and a point at the right-most end of the line A-D. Then, the GR3719v value corresponding to J is computed, and used as a threshold T . Since the exact location of H, A, and D vary for each instrument, hemisphere, and day in the data record, our threshold T will change (although slightly so) during the whole data record, without the need for prescribed values (such as $T=0.05$ for the Cavalieri 1992 WF). The value of 10% SIC is chosen to be below the threshold commonly used for defining sea-ice extent (15% SIC), to ensure that the Weather Filter does not interfere when computing sea-ice extent.

Formatted: Font: Italic

Formatted: Font: Italic

We note finally that the ~~name~~ “Weather Filter” can be mis-leading as the non-expert could understand that it is meant for filtering out weather effects (false sea ice) from “calm” open water and low ice concentration conditions. As seen in Figure 3, this is not how the GR3719v filter works, as it ~~is set to will~~ remove true sea ice as well, even in “calm” weather
 5 conditions (OW samples below J). In addition, GR3719v contains information on sea-ice type (Cavalieri et al. 1984) and it is desirable the filter should work equally for first-year and multiyear sea ice. For this these reasons, we ~~rather~~ refer to such a filters as an “Open Water Filter” (OWF) and add include a test on the SIC value. The OWF implemented in the new CDRs are is thus defined by the following two tests (corresponding to the thick solid blue line in Figure 3):

$$\begin{cases} \text{GR3719v} \geq T \\ \text{or SIC} \leq 10\% \end{cases}, \quad (3)$$

10 NoticeablyNotably, we compute OWFs in swath projection, in the Level-2 chain (Figure 2). As a result, each FoV observation at Level-2 is attached to a binary flag as to if the corresponding to OWF detected detection it as “probably” open water or not. This binary flag is combined during gridding and daily averaging to yield Level-3 fields of OWFs. This is a better approach than computing WFs from daily averaged gridded T_B data which will smooth and smear the sea-ice edge region, as well as rapidly changing weather effects such as cloud liquid water content or wind roughening. To compute
 15 OWFs at Level 2 can also help mitigate the potential impacts of changes in satellite crossing time between different missions. The impact of the dynamic tuning of the OWF is evaluated in section 4.2.1.

3.4.3 Reducing systematic errors at high concentration range

Winter-time, monthly averaged maps of SIC_{corr} exhibit systematic errors at high concentration ranges, especially visible in the central Arctic Ocean. A novel correction scheme is implemented as part of the second algorithm iteration (Figure-2) that
 20 effectively mitigates most of these systematic errors over the basin.

By construction, SIC algorithms BFM, BPM, BRI, and our new dynamic algorithms likewise, consider that the SIC is exactly 100% when the input T_B fall on the consolidated ice line (Figure-3). The concept of an ice line has sustained the development of SIC algorithms for decades, since it allows algorithms to return SICs close to 100% for all consolidated ice
 25 conditions, whatever the type of sea ice (multiyear ice, first-year ice, mixture of types). However, careful analysis of the spread of consolidated ice samples along the ice line reveals that systematic deviations exist and are stable with time. These systematic deviations draw a consolidated sea-ice curve, as illustrated with the solid black curve around the 100% SIC samples. These deviations best appear are best shown in a coordinate system whose abscissae are computed as $u \cdot T$ (dot product of u the unit vector sustaining the consolidated ice line, and T a 3D T_B triplet in T_{Cl} , Figure 4) and the ordinate as
 30 $B_{Cl}(T)$ (the result of the “best ice” SIC algorithm for a given T_B triplet). We refer to the quantity $u \cdot T$ as the Distance Along the ice Line (DAL). Since u points from multiyear ice to first-year sea ice (section 3.2, and Figure 4), older ice have lower DAL values than younger ice. In winter Arctic conditions, it is typical to observe that $B_{Cl}(T)$ values are

~~constantly~~consistently lower than 100% (down to 85-90%) for old ice (low values of DAL), and ~~constantly~~consistently higher than 100% (up to 105-110%) for new and first-year ice (high values of DAL). In between these two extremes, the $B_{CI}(T)$ values oscillate between being below and over the SIC=100% line. Our novel correction scheme moves the concept of an ice line to an ice curve, that more closely follow the $B_{CI}(T)$ samples along the u axis. A new ice curve is tabulated for each day in the record

- 5 by binning the $B_{CI}(T)$ values by their DAL values. This consolidated ice curve defines the SIC 100% isoline during the second iteration of Level 2~~s~~, and ~~–conversely to the atmospheric correction described in section 3.4.1-~~ has most effect over ~~consolidated ice regions. It is noteworthy that the sea-ice curve shown on Figure 3 is for illustration purpose. As part of the processing, the consolidated ice curve is not used in the two-dimensional BFM space, but in the three-dimensional data plane of the dynamic SIC algorithm (see section 3.2).~~ The amplitude of the sea-ice curve around the sea-ice line can be different in
10 ~~shape in the SIC algorithm plane. In addition, the ice curve on Figure 3 is fitted through the consolidated ice points from the ESA CCI Sea Ice RRDP (Pedersen et al., 2018) that spans several years and winter months and thus illustrate an average sea-ice curve. The consolidated sea-ice samples we extract dynamically for [-7:+7 days] sliding windows (section 3.3) will typically exhibit more variability due to shorter term changes in sea-ice signatures.~~

- 15 Figure 5 (left and middle panels) shows the spatial distribution of the ~~average total~~ correction for January 2015 (SIC minus SIC_{ucorr}), ~~thus including both the effect of the correction based on the consolidated ice curve, and the effect of the RTM-based correction of the T_B .~~ Black solid lines show the mean sea-ice edge region (at 15% and 70% SIC values) during the same period. Left panel shows the average total correction (daily maps of SIC minus SIC_{ucorr} , averaged over the month of January 2015), while center panel shows the effect of the total correction on SIC variability (variability -standard deviation-
20 of daily SIC_{ucorr} maps throughout the month, minus the same variability of daily SIC maps after correction).

Formatted: Not Superscript/ Subscript

- 25 Over closed-ice conditions (inside the 70% SIC isoline), ~~The~~ regional patterns of the correction are clearly visible and seem to match variations in sea-ice age: large positive correction (increase SIC) north of the Canadian Arctic Archipelago and Ellesmere island (intense red color) where the ice is oldest in the Arctic, moderate negative correction over a large part of the central basin (extending from the central Beaufort Sea, over to North Pole, and to Northern Greenland, light blue color, second year ice) and a slightly positive correction again over large parts of the Siberian Arctic (light red color, first year ice). The mean January 2015 DAL is shown on Figure 5 (right) (blue-green-yellow color shade).

- On Figure 5 (right) we observe an overall increase of the DAL value from the Canadian Arctic Archipelago (multiyear ice)
30 across the pole and towards ~~the~~ Laptev and Kara Seas (first-year ice). To confirm the link between DAL and sea-ice age, we overlay contours ≥ 1 year, ≥ 2 years-old, and ≥ 3 years old sea ice ~~for January 2015~~ from Korosov et al. (2018) on ~~the~~ right panel. Korosov et al. (2018) developed an improved Lagrangian-based sea-ice age tracking algorithm using the sea-ice drift product of the EUMETSAT OSI SAF (Lavergne et al., 2010). The correspondence in the transitions of DAL values with the contour lines of sea-ice age is very good, indicating that a combination of DAL (right panel) and ice curve

correction (left panel) could be used for sea-ice type (if not age) classification studies. This is outside the scope of our study which is focused on SIC algorithms and the new data records.

Figure 5 (center) shows the result of the ice curve correction ~~on SIC variability averaged for January 2015. It plots the difference between the variability (standard deviation) of the un-corrected SIC values (SIC_{uncorr}) and that of the SIC after correction. Black solid lines show the mean sea-ice edge region (at 15% and 70% SIC values).~~ In the regions covered with sea-ice ($\geq 70\%$ SIC), the shades of light blue indicate that the variability at high concentration is rather consistently reduced by about 1-2% SIC by the ice curve correction~~–: the SIC after correction is a more accurate description of a nearly 100% ice cover.~~ A limited number of regions show no improvement (white color) or slight degradation. This reduction of the variability comes in addition to the correction for the systematic errors (e.g. underestimation north ~~for of~~ Canadian Arctic Archipelago, see [panel a\)](#)[left panel](#) for which the ice curve correction was designed. [The analysis of the closed-ice \(\$\geq 70\%\$ SIC\) region in Figure 5, thus confirms that the ice curve correction works as expected at high concentration range, and is potentially linked to the age of sea ice.](#)

In the open water regions [of Figure 5 \(<=outside the 15% SIC contour\)](#), the reduction of variability [\(center panel\)](#) is even larger (3-4% SIC) [than over closed-ice regions](#). This reduction is the result of the atmospheric correction step, ~~that what~~ described in section 3.4.1 ~~and has most impact over open water (Andersen et al. 2006). From left panel, it appears that the atmospheric correction step in average increases SIC (shades of red) over open water regions close to the sea-ice edge, e.g. in East-Greenland Sea, Barents Sea, and in Labrador Sea. These regions generally present negative SICs before correction, and are brought closer to 0% SIC by the process of atmospheric correction. This is due to selecting the training OW samples in lower latitude conditions (ocean surface, atmosphere conditions) than prevailing closer to the ice edge, and is also discussed in section 4.2.3 when evaluating uncertainties.~~

Formatted: Font color: Red

[Still on Figure 5 \(center panel\). The the increased variability \(red tones\) between the 15% and 70% isolines follows logically from the two above mentioned reductions: the corrections enable more accurate retrievals of SICs, thus the ice edge is more sharply defined in the daily SIC fields, and this results in higher variability on a monthly basis.](#)

In this section, we described the strategies we implemented to improve the accuracy of the SIC algorithms. In the next section, we discuss how the remaining noise is quantified and reported to the users of the data records in the form of uncertainties.

3.5 Uncertainties

Spatially and temporally varying uncertainty estimates for each and every SIC value are required of state-of-the-art CDRs (GCOS-IP, 2016). Uncertainties are needed as soon as the data are compared to other sources (e.g. other similar data

records), or when data ~~is-are~~ assimilated into numerical models. However, there is no unique way to derive nor to present uncertainties in EO data (Merchant et al., 2017).

The approach to derive and present uncertainties in the new SIC CDRs is mostly similar to ~~those-that~~ of Tonboe et al.

5 (2016): we make the assumption that the total uncertainty σ_{tot} is given by two uncertainty components, i.e.:

$$\sigma_{\text{tot}}^2 = \sigma_{\text{algo}}^2 + \sigma_{\text{smear}}^2, \quad (4)$$

where σ_{algo} is the inherent uncertainty of the SIC algorithm (algorithm uncertainty) including sensor noise and the residual geophysical noise quantified as variability around the OW and CI mean signatures, and σ_{smear} is the representativeness uncertainty due to resampling from satellite swath to a grid (smearing uncertainty) and ~~the mismatch between footprints at different channels mismatch~~.

10 The derivation of σ_{algo} is to a large extent similar to that described in Tonboe et al. (2016). This term is derived from the accuracy (estimated as statistical variance) of the algorithm ~~to-for retrieve-retrieving~~ 0% (*resp* 100%) when applied onto the OW (*resp* CI) training data samples (section ~~-~~3.3). This uncertainty term is computed at Level 2 (Figure 2). Each Level 2 SIC
15 estimate in the data record has an associated σ_{algo} value.

15 The uncertainty term σ_{smear} is a representativeness uncertainty. It measures the increase of uncertainty due to mismatching spatial dimensions such as when a) the satellite sensor footprint potentially covers a larger area than that of a target grid cell, or when b) the imaging channels used by the SIC algorithms do not have the same FoV diameter. Table 2 lists the
20 dimensions relevant ~~to-for~~ discussion of these two effects. Effect a) : the size of the ~~3-dB~~-footprint of the 19-GHz channels of the SMMR, SSM/I, and SSMIS instruments is larger than the resolution of the grid used to present the SIC field (25x25-km, see Table 1). Effect b) : the ~~3-dB~~-footprint of the 37-GHz channels is smaller than that of the 19-GHz ones, so that the two frequencies entering the SIC algorithms do not cover the same area of Earth's surface. Intuitively, both effects should have no or limited impact where the sea ice cover is homogeneous (fully consolidated sea ice, or open water). It
25 should be at a maximum where sharp spatial gradients occur, typically at the sea-ice edge. The smearing contribution σ_{smear} is difficult to derive analytically and we carry on the approach of Tonboe et al. (2016) ~~that is~~ to parametrize σ_{smear} as a function of a proxy. For the three new CDRs we parametrize σ_{smear} as a function of the $(\text{MAX}-\text{MIN})_{3\times 3}$ value, that is the difference between the highest and lowest SIC value in a 3×3 grid cell~~s~~ neighbourhood around each location in the grid. Specifically:

$$\sigma_{\text{smear}} = K \times (\text{MAX} - \text{MIN})_{3\times 3}, \quad (5)$$

30 where K is a scalar whose value depends on the FoV diameter of the instrument channels used for the SIC computation, and the spatial spacing of the target grid. Several other proxies for the local variability of the SIC field (among others the 3×3 standard deviation, the Laplacian, power-to-mean-ratio...) were tested and this one was selected for its simplicity and robustness. Values of K were tuned using a foot-print simulator and selected cloud-free scenes of the marginal ice zone imaged by the Moderate-Resolution Imaging Spectroradiometer (MODIS) as described in Tonboe et al. (2016). The MODIS

images are first classified as water/ice at full resolution. Two sets of coarser resolution SIC fields are then prepared: 1) the footprint simulator is applied to prepare a synthetic sea-ice concentration field at the resolution of the frequency channels, and 2) the high-resolution classified pixels are binned into regular grid cells, e.g. at the target resolution of the CDR (e.g. 25x25 km). The mismatch between the two fields is what we call the smearing uncertainty, and is parametrized against

5 proxies such as (MAX-MIN)_{3x3}. A value of $K=1$ was found to yield good results for all three CDRs. The value for σ_{smear} is computed as part of the Level-3 chain (Figure-2), after gridding and daily averaging. The total uncertainty σ_{tot} is finally computed using Eq.-4. In the data files, both the total, the algorithm, and the smearing uncertainty fields are made available.

3.6 Other relevant algorithms and processing steps

This section shortly introduces some other algorithms and processing steps that are important to the generation of the data 10 records, but are either less critical for prospective users of the data, or presenting have undergone less little evolution since Tonboe et al. (2016).

Due to the coarse resolution of the sensors used, especially SMMR, SSM/I, and SSMIS (Table-2), the T_B data are influenced by land emissivity several tens of km away from the coastline. The emissivity of land is comparable to sea-ice emissivity and

15 much higher than water emissivity. This means that sea-ice concentration will be consistently overestimated in coastal regions. In Tonboe et al. (2016), a statistical method similar to Cavalieri et al. (1999) was implemented as a post-processing to the daily-gridded sea-ice concentration maps. Such a method showed limitation and the new SIC CDRs now introduce explicit land spill-over correction of the T_B at all used channels, and on swath projection. The correction algorithm is described in details in Maass and Kaleschke (2010). The basic principle is that a fine-resolution land mask is used together

20 with the antenna viewing geometry to estimate (and correct for) the simulated contribution of land emissivity to the observed T_B . The algorithm of Maass and Kaleschke (2010) was adopted with some modification and tuning, among others including:

a) the computation of the fraction of land in each FoV is-computed in the view geometry of the antenna (not after projection to a map), b) the antenna-pattern-functions-are-approximatedapproximation of the antenna pattern functions as Gaussian (Normal distribution) shapes indexed on the aperture angle from the central view direction, instead of distance on a 25 projection plane. At the end of this step, T_B of FoV that overlap land and ocean are corrected for the contribution by land, and can enter the Level-2 sea-ice concentration algorithms. Note that although this swath-based correction step is quite efficient at reducing land spill-over contamination, a statistical method similar to that of Cavalieri et al. (1999) still had to be applied at Level-3-this is further discussed in section 5.2.

30 The land masks and climatology for the new SIC CDRs were-have been revised since Tonboe et al. (2016). New land masks for the target 25x25 km grids (one for NH and one for SH) where computed based on the Operational Sea Surface Temperature and Sea Ice Analysis (OSTIA) 0.05x0.05° land mask (Donlon et al., 20112012). This mask was re-used in the ESA CCI Sea Surface Temperature (SST) L4 data records and was selected as the input mask for the new SIC CDRs to

increase cross-ECV consistency. The masks are tuned to closely match that of the NSIDC SIC CDR (the NSIDC “SSM/I” 25 km Polar Stereographic mask). On average, in the NH, this corresponds to setting all 25x25 km grid cells with a fraction of land lower than 30% to water (and these cells can thus potentially be covered with sea ice). There is no right or wrong

binary land masks at such coarse resolution, and the choice of tuning to the NSIDC SIC CDR land mask is to help 5 intercomparison of data records. By the same token, the monthly varying maximum sea-ice extent climatology implemented in Meier et al. (2017) ~~were-was~~ used as a ~~base-basis~~ for our own climatology. The modifications included manual editing of some single pixels based on US National Ice Center, Canadian Ice Service, and Norwegian Ice Service ice charts (e.g. along the coast of Northern Norway, for some summer months in the vicinity of ~~New-Scotia~~Nova Scotia, etc...). The climatology of peripheral seas and large fresh water bodies (e.g. Bohai and Northern Yellow Seas, Great Lakes, Caspian Sea,

10 Sea of Azov, etc...) was also revisited. The cleaned climatologies were then expanded with a buffer zone of 150 km in the NH and 250 km in the SH. The larger expansion in SH is to cope with the positive trends in ~~the~~ SH sea-ice extent (Hobbs et al., 2016). The expanded monthly sea-ice climatology is used both for masking of the final product and for defining the monthly varying area ~~where the Open Water training samples were selected~~where to select the Open Water training samples (section 3.3).

15

As described in the sections above, all the geophysical processing is performed on swath projection (Level-2 processing). Gridding (using Gaussian weighting of distance) and daily averaging (equal weights) of the swath data is tackled as an initial step of the Level-3 chain (Figure-2). The methodology is mostly similar to that of Tonboe et al. (2016) as swath data from all available instruments of similar spatial resolution are combined into daily maps of the NH and SH polar regions. It is

20 noteworthy that full advantage of the overlap of satellite missions (see Figure-1 and Table-2) was taken in order to reduce as much as possible the occurrence of missing data areas in the daily composited fields. This ~~is conversely to contrasts with~~ the SIC CDR method of Meier et al. (2017) that uses one SSM/I or SSMIS sensor at a time.

Despite using all the sensors, some data gaps still appear in the daily SIC maps, especially in the early part of the data record 25 (late 1970s to mid-1990s). These data gaps are filled by interpolation (both spatially and temporally) to yield a more user-friendly data record. The polar observation gap (largest for SMMR and SSM/I, see Table-2) is filled by interpolation as well. All interpolation of missing data is performed with basic isotropic schemes using Gaussian weighting in the space domain, and equal weighting in temporal domain~~schemes, and nNo~~ model data, nor advanced methods (among others Strong and Golden, 2016) were implemented. All interpolated data are clearly marked in the product files using status flags. Days with 30 fully missing input data (e.g. every other day in the SMMR period) are not created by interpolation, and the files are missing.

4 The resulting data records and their initial evaluation

4.1 The data records and selected examples

The SIC CDR released by the EUMETSAT OSI SAF (OSI-450) extends from January 1979 throughout December 2015. It uses data from SMMR, all SSM/I (F08, F10, F11, F13, F14, F15), and three SSMIS (F16, F17, and F18). It is delivered on two Equal Area Scalable Earth_2 (EASE2) grids with 25x25_km spacing (Brodzick et al. 2012 and 2014), one for the Northern and one for the Southern Hemisphere. SMMR data for the period October to December 1978 are not included in the CDR because of the unavailability of ERA-Interim data for correction of the atmospheric influence on T_b (section 2.2). OSI-450 has the following Digital Object Identifier (DOI): [10.15770/EUM_SAF_OSI_0008](https://doi.org/10.15770/EUM_SAF_OSI_0008) and data is freely available to any users from the EUMETSAT OSI SAF web pages (<http://www.osi-saf.org/>).

Formatted: Subscript

10 The two SIC CDRs released by the ESA CCI Sea Ice project (SICCI-25km and SICCI-50km) extend over two disjointed periods and process data from AMSR-E (June 2002 to October 2011) and AMSR2 (July 2012 to May 2017). SICCI-25km (DOI: [10.5285/f17f146a31b14dfd960cde0874236ee5](https://doi.org/10.5285/f17f146a31b14dfd960cde0874236ee5)) is delivered on the same EASE2 25x25_km grids as the OSI SAF CDR. SICCI-50km (DOI: [10.5285/f5f75fcbb0c58740d99b07953797bc041e](https://doi.org/10.5285/f5f75fcbb0c58740d99b07953797bc041e)) is delivered on an EASE2 50x50_km grid, whose 15 cells exactly cover four 25x25_km cells of the SICCI-25km and OSI-450 grids. Both SICCI-25km and SICCI-50km are freely available to any user from the ESA CCI Data Portal (<http://cci.esa.int/data/>). Figure 6 shows the OSI-450 (top left panel), SICCI-25km (top right) and SICCI-50km (bottom left) SIC fields over the Weddell Sea region on 25th September 2015. The two SIC fields on the top row are rather similar except in the Marginal Ice Zone where the better resolution of the 20 AMSR2 instrument (SICCI-25km) with respect to that of the SSMIS (OSI-450) leads to resolving finer details. The SICCI-50km SIC has increased granularity due to the lower resolution of the 6_GHz channels wrt to 19 GHz.

All three data records share the same data format, which is Network Common Data Format (NetCDF) version 4 (classic format). Files abide by the Climate and Forecast (CF) convention (CF-1.6) and the Attribute Convention for Data Discovery (ACDD-1.3). The variables inside the files enable a flexible use of the data. The main variable is named ice_conc and holds a SIC field where all the filters (among others the Open Water Filter, section_3.4.2) and correction steps (among others the statistical coastal correction scheme, section_3.6) are applied. This is the entry point for most prospective users of these new SIC CDRs and is the variable plotted in the top row and bottom left panel of Figure_6. In addition, a variable named raw_ice_conc_values gives access to the original (“raw”) values of sea-ice concentration, before filtering is applied.

30 The Bottom-bottom right panel in Figure_6 shows the content of variable raw_ice_conc_values that holds values as nominally returned by the SIC algorithm from the OSI-450 CDR on the same date and location as the three other panels. A blue-yellow-red color scale is used for the low-range of SIC values. Both negative (blue) and positive (red) values appear that corresponds to the intrinsic retrieval noise level of the SIC algorithm before the OWF is applied. All these values are

indeed set to exactly 0% by the OWF in variable `ice_conc`. Note how the belt of low SIC values is bordered by a dark red region. This is very probably true low-concentration or thin sea ice that is removed by the OWF at the marginal ice zone. Removal of true sea ice by the OWF was discussed in section [3.4.2](#). Still on the bottom right panel, a yellow-green color scale is used to plot large off-range SIC>100% values, as nominally returned by the SIC algorithm. These raw values are

5 non-physical (like the blue-shaded SIC<0% values) and are set to exactly 100% in variable `ice_conc`. They might be interesting for advanced users interested in accessing the full Probability Distribution Function (PDF) of retrieved SIC values, for example for Data Assimilation (DA) applications. The off-range SIC values are also needed to compute temporal averages (e.g. monthly means) to avoid introducing biases if only SIC>=0% or SIC=<100% values enter the averaging.

10 Example fields of uncertainties from the OSI-450 CDR are shown in Figure [7](#). The two uncertainty components σ_{algo} (left panel), and the smearing uncertainty σ_{smear} (center), as well as the total uncertainty σ_{tot} (right) are shown. The algorithm uncertainty is typically between 2% and 3% SIC. It is lower for sea ice than for open water because the global variability of closed sea ice is lower than the SIC variability over open water. It is noted that this variability is not due to real SIC variability but rather to ice and open water signature variability reflected in the estimated SIC, thus an uncertainty. The
15 smearing uncertainty is largest, up to 40% SIC, at the ice edge and low, near 0% SIC, in areas where all contributing satellite footprints are covered by cover the same SIC (e.g. open water). The total uncertainty, which is the sum (in variance) of σ_{algo} and σ_{smear} (section [3.5](#)) is dominated by σ_{smear} . The patterns seen in Figure [7](#) are representative of the uncertainties of all three CDRs, for both hemispheres, during winter. During summer, σ_{algo} is larger by few percents, and the increased variability inside the ice pack yields higher σ_{smear} , leading to larger σ_{tot}

Formatted: Not Superscript/ Subscript

Formatted: Not Superscript/ Subscript

20 [4.2 Initial-eEvaluation results](#)

The evaluation of a CDR needs to cover several three aspects. One-The first is to demonstrate consistency of the methods used to derive the CDR. Key elements of our new suite of algorithms are i) its-their application to different sensors (various SSM/I, AMSR-E and AMSR2), ii) a self-optimizing algorithm which dynamically tunes tie points to minimize SIC errors at 0% and 100%, and iii) a dynamic open-water filtering (OWF) to mitigate spurious SIC values caused by residual weather
25 influences while keeping actual low SIC. For the three SIC CDRs published here we investigate time-series plots of the optimized skills of the SIC algorithms, and the temporal stability of the OWF (section [4.2.1](#)).

4.2.1 Monitoring stability and internal consistency

Many time-series plots can be produced to illustrate the stability and internal consistency of the three CDRs. As an example, Figure [8](#) shows the time-series of the algorithm training statistics at the Open Water target. As described in sections [3.2-3.2](#)
30 and [3.3](#), the algorithms implemented in the three CDRs dynamically tune their parameters to yield zero bias and minimum standard deviation of the computed SICs (*aka* best accuracy) over the Open Water (OW) and Closed Ice (CI) training targets. Figure [8](#) shows the Northern Hemisphere (NH, top) and Southern Hemisphere (SH, bottom) temporal evolution of the

standard deviation (solid lines) and bias (dotted lines) of the SIC algorithms over OW target areas. Prior to further describing Figure 8, it is important to note that the biases and standard deviations discussed here are internal to the processing chains, not an evaluation of the CDRs against independent observations of SICs. An ~~initial~~-evaluation of the CDRs against independent ground-truth observations is the topic of section 4.2.2.

5

From Figure 8, it is easy to see that the algorithms implemented in the three CDRs achieve zero bias (dotted lines along the y=0 axis) for all instruments and both hemispheres, on a daily basis. To achieve zero bias ~~albeit despite~~ the changes in central wavelengths and calibrations from one satellite to the next is one of the key advantages of using dynamically-tuned algorithms (section 3.3).

10

The impact of the explicit correction of brightness temperature ~~from for~~ atmospheric noise effects is also clearly visible on Figure 8, since the standard deviations resulting from un-corrected T_B data (thin solid lines) are consistently above those ~~from-for~~ corrected data (thick solid lines) by about 3% to 4% on average, depending on the season and hemisphere. The seasonal variability is also larger from the un-corrected data, especially in the NH. It is noteworthy that the atmospheric

15 noise reduction step does not ~~much~~ improve ~~much~~ the OW standard deviation in the SH at the beginning of the OSI-450 period, for the SMMR instrument (1979-1987). As noted at the end of section 3.4.1, OSI-450 uses the Wentz (1983) RTM for SMMR, and the Wentz (1997) RTM for SSM/I and SSMIS. The parametrizations ~~s~~ implemented in the SMMR RTM are probably less developed than in the SSM/I and SSMIS RTM, which might explain why the impact on our standard deviation is more limited for SMMR. ~~Another plausible explanation is that the re-analysed fields for wind speed and water vapour from ERA-Interim are less accurate in the SMMR era than in the SSM/I and SSMIS era. We note that clear-sky radiances from SSM/I and SSMIS were directly assimilated in ERA-Interim over the ocean (Dee et al. 2011), but not SMMR radiances (Paul Poli, personal communication, 28/09/2018). This can especially have an impact in the SH, where other sources of conventional ~~data~~ data have available only ERA-Interim and SMMR radiances. For this reason, this might have had a significant impact on the accuracy of OW SICs during the SMMR era.~~

20

The SICCI-25km and SICCI-50km standard deviations are also plotted on Figure 8 (only those after atmospheric correction so as not to clutter the plot area). SICCI-25km (reds) achieves ~~sensibly roughly~~ the same OW standard deviation as OSI-450. Since SICCI-25km uses very similar frequency channels to those of OSI-450 (Table 1), it is not surprising they achieve similar accuracy. The central frequency of the AMSR-E and AMSR2 channels (18.7 GHz) is slightly further away from the 25 water vapour absorption line (~22 GHz) than the SSM/I and SSMIS channels (19.3 GHz). This difference in frequency yields better accuracy for SICCI-25km than OSI-450 when using un-corrected T_B data (not shown) but this effect is mostly cancelled after atmospheric correction (though not fully in SH, bottom panel). ~~The same effect is observed for the standard deviations resulting from un-corrected SMMR T_B data (purple thin line), which is consistent with a central frequency of 18.0 GHz (Table 2).~~

SICCI-50km (greens) is more accurate than both SICCI-25km and OSI-450, by nearly 1% in NH, and 0.5% in SH. This is expected from the choice of frequency channels, since SICCI-50km uses a C-band (6.9 GHz) channel, while SICCI-25km and OSI-450 use Ku-band (~19 GHz). Three effects lead to better accuracies of SIC retrievals at low-frequencies: 1) the atmosphere is more transparent, yielding better accuracy over OW, 2) the noise sources such as sea-ice type, snow depth, snow scattering, etc... have less impact at low frequencies, and 3) the permittivity (and hence T_B) of sea ice and water are more different, resulting in a larger dynamic range for sea-ice concentration retrievals. SICCI-50km is designed to be the most accurate of the three SIC CDRs. However, it achieves a coarser spatial resolution (50-km) due to the limited size of the AMSR-E and AMSR2 antenna. The time-series in Figure 8 illustrate that the algorithms ~~are internally consistent~~, behave as expected across instruments, and are effectively tuned to achieve zero bias and ~~a small~~smallest possible retrieval noise for each instrument in the time series.

The role of Open Water Filters (OWF) is to detect and remove weather-induced false sea ice over open water, while ideally preserving the true low concentration values (typically at the ice edge)~~-at best~~. As introduced in section 3.4.2, the threshold 15 of the OWF is tuned dynamically against the daily updated training data samples (thus by instrument, and by hemisphere) to preserve true SIC values down to 10%. A water/ice separation limit at 10% SIC is an ambitious goal, but is necessary to ensure that time-series of Sea Ice Extent (SIE, usually defined with a threshold of 15% SIC) are not influenced by the OWF and only by the evolution of true SIC. Figure 9 shows time-series of NH (solid lines) and SH (dashed lines, almost coinciding with NH lines) of the 1%-percentile value of all ice conc values (thus after all filters including the OWF is applied) that are strictly positive and below 30% SIC for the OSI-450 (blue), SICCI-25km (red), and SICCI-50km (green) CDRs. These are thus time-series of the typical minimum detected SIC that are preserved by the OWFs. A solid horizontal line is drawn at 15% SIC value, the threshold commonly chosen for SIE computations. The OSI-450 curves are very stable with time and increase only slightly from around 9% SIC at the beginning of the period to around 10.5% SIC at the end. 20 Seasonal variations are visible especially at the beginning of the time-series for NH cases, when typical winter values are around 7.5% SIC and peak to 10% SIC in summer. They are in any case well below the 15% threshold throughout the data record and very little few jumps change are is observed when transitioning between sensors. The seasonal cycles are limited to few tens of a percent at the end of the period (few percent at the beginning). The SICCI-25km curves are close to the OSI-450 ones, but at a slightly larger value of 11%, with a seasonal variation range of about 2%. The SICCI-25km curves are also well below 15%. The SICCI-50km curves are those showing the largest variation. The average value for SICCI-50km is at 25 about 10%, but the seasonal variations are much larger, ranging from ~~lowest~~ 5% to ~~highest~~ 15%. The temporal stability of the time-series on Figure 9 document that the tuning of the OWFs at values close to 10% SIC is successful for the two data records that rely on the 19-GHz and 37-GHz for computing their SICs (OSI-450 and SICCI-25km) and not as good for SICCI-50km that uses the 6-GHz and 37-GHz channels to compute the SIC values. Although SICCI-50km does not compute SICs from 19-GHz and 37-GHz channels, its OWF is still based on the GR3719v threshold (section 3.4.2). The 30

mismatch in frequency and resolution between the channels used to compute the OWF and those used to compute SIC explains the larger variability of the SICCI-50km time-series in Figure 9.

We note in addition that both the OSI-450 and SICCI-25km CDRs dynamically tune their optimal data plane for low concentration range θ_{OW} in the (19V, 37V, 37H) 3D T_B space, while the OWF is only tuned in the (19V, 37V) T_B plane. The departure of the optimal SIC data plane from the (19V, 37V) OWF plane (by convention at $\theta=0^\circ$, see right-hand side panel in Figure 4) could be the causes for the slight increase of the 1%-percentile curves of OSI-450 during the time period (via an improvement of the re-analysis data entering the atmosphere correction step over time), and the different value obtained with SICCI-25km. Ideally, the OWF should be tuned in the same 3D T_B space as used for the SIC algorithms. Such 3D-based filters do not exist at present and additional research is needed in that field this is addressed as future work in section 5.2. All in all, we note that all three CDRs achieve a rather stable detection of true SIC mostly below the 15% SIC threshold commonly used to define SIE. To the best of our knowledge the temporal consistency of the minimum detected SIC has not been documented for other available CDRs, although all use OWFs.

4.2.2 Evaluation against ground truth

- For the evaluation of the SIC CDRs, we used a temporal extension of the Round Robin Data Package (RRDP) used by Ivanova et al. (2015) to study the strengths and weaknesses of more than 30 published SIC algorithms. Among other datasets, the RRDP v2 holds ground-truth locations for Open Water cases (OW, 0% SIC) for the period 2002-2015, as well as ground-truth locations for Closed Ice (CI, 100% SIC) for the period 2007-2016. The OW locations are situated just outside the climatological mask delineating maximum sea-ice extent but, well inside the buffer zone added to it in section 3.6. They are distributed as evenly as possible in longitude. The CI locations are selected in areas of high sea-ice concentration and after 24 h of convergent sea ice motion, as computed from a highly accurate SAR-based sea-ice drift product from the Copernicus Marine Environment Monitoring Service (CMEMS, <http://marine.copernicus.eu>). The OW and CI datasets of RRDP are described in more details in Ivanova et al. (2015).
- For the evaluation of the SIC CDRs over open water, we extracted OSI-450, SICCI-25km and SICCI-50km CDR SIC (variable `raw_ice_conc_values`) and total uncertainty σ_{tot} data at the grid cell closest to the OW locations in the RRDP v2 from two months in summer: August and September in the Arctic and January and February in the Antarctic, and from three months in winter: January through March in the Arctic and July through September in the Antarctic. For the evaluation at 100% SIC conditions, we collocated the SIC CDRs with the SAR-based CI locations in the RRDP v2 for months November through March (Arctic) and May through September (Antarctic) in the same way as we did for open water; no spatial or temporal interpolations are performed. We note that CI ground-truth data from East Antarctica are missing completely, however, because of a lack of enough SAR image acquisitions. Using the `status_flag` variable, any SIC being contaminated by land spill-over effects or by too with high air temperatures were discarded.

For open water, we find quite similar SIC distributions around 0% for all three CDRs for both hemispheres (Figure 10). During winter (blue curves) OSI-450 and SICCI-25km are skewed a bit towards negative SIC in the Arctic but not in the Antarctic. During summer (red curves) we find SIC distribution to be skewed to negative SIC for all CDRs except OSI-450

- 5 in the Antarctic. Distributions are generally more narrow for SICCI-50km than for the other two CDRs. Figure 10-12 (a) and b), black crosses) illustrates the very similar accuracies for OSI-450 and SICCI-25km with a mean SIC of 0% or -0.2% during summer and of ~-0.5% during winter in both hemispheres. For SICCI-50km, the accuracy varies more than for the other two CDRs: summer: ~ -0.5% and winter: 0.2% to 0.5%, than for the other two CDRs. The standard deviation of the mean SIC (black bars), ei. ge., the precision, ranges between 1% and 2% for all three CDRs. Without exception the precision
10 is better (smaller) in summer than winter. For both hemispheres, we find that the precision of OSI-450 and SICCI-25km SIC CDRs is similar to each other and less good than that poorer than for SICCI-50km, which is in line with the findings in Figure 8.

For sea ice, we find almost identical SIC distributions around 100% for OSI-450 and SICCI-25km for both hemispheres (Figure 11, a), b), and d), e)). Distributions for SICCI-50km are considerably narrower (Figure 11, c), f)) and, in comparison
15 to OSI-450 and SICCI-25km, have a modal value closer to 100%. All three CDRs exhibit a negative bias, i.e. a modal SIC < 100%. Figure 11-12 c), d) further illustrates that SICCI-50km provides the smallest bias (best accuracy) in both hemispheres with a mean SIC of 99.5% and 99.3% for the Arctic and Antarctic, respectively. In addition, SICCI-50km also offers the smallest SIC standard deviation of the mean (black bars), i.e. the best precision, of ~2% and ~3% for the Arctic and Antarctic, respectively. OSI-450 and SICCI-25km provide a less good accuracy slightly larger bias with a mean SIC of ~98%
20 in the Arctic and ~98.5% in the Antarctic, which comes also with a higher SIC standard deviation of the mean: 3.5% to 4.0%. Accuracy and precision are quite similar for OSI-450 and SICCI-25km.

4.2.3 Evaluation of the uncertainties

We computed the mean SIC total uncertainty σ_{tot} for OSI-450, SICCI-25km and SICCI-50km for exactly the same set of grid cells as used in section 4.2.2 (Figure 12, blue bars).

- 25 For open water, SIC = 0% (Figure 12, a), b)), we find that mean SIC total uncertainties differ by less than 0.3% between OSI-450 and SICCI-25km and take values of ~2% during summer and of ~2.5% during winter. For SICCI-50km, the mean SIC total uncertainty is smaller than for the other two CDRs – particularly during summer in the Northern Hemisphere: ~1.5% compared to ~2% in winter. Without exception mean SIC total uncertainties exceed one standard deviation of the
30 retrieval errors (compare black and blue bars in Figure 12 a), b)). Also without exception, mean SIC total uncertainties are smaller than two standard deviations of the retrieval errors (not shown).

For sea ice, SIC = 100% (Figure -12 c), d)), we find that mean SIC total uncertainties for OSI-450: ~3% are smaller than those for SICCI-25km: ~3.5%, in both hemispheres. For SICCI-50km mean SIC total uncertainties are smaller than for the other two CDRs – particularly in the Northern Hemisphere: ~2% (Figure -12, c)). For OSI-450 and SICCI-25km, mean SIC total uncertainties are smaller than one standard deviation of the retrieval errors. For SICCI-50km, mean SIC total

5 uncertainties are comparable to (Figure -12, c)) or larger than (Figure -12, d)) one standard deviation of the retrieval errors. These results are in agreement with those introduced in section 4.2.1 and are mainly explained but the frequency channels used in the three CDRs: 18.7 GHz for SICCI-25km, instead of 19.3 GHz for OSI-450 (less noise contribution from atmospheric water vapour content), and 6.9 GHz for SICCI-50km (smaller sensitivity to atmosphere and surface snow and sea-ice property variations).

10

Thus, the results summarized in Figure -12 indicate that the uncertainty σ_{tot} provided with the three CDRs are slightly underestimated, especially for OSI-450, for the high sea-ice concentration range (SIC = 100%), and are slightly overestimated on average at an appropriate level for the high sea-ice concentration range (SIC = 100%) but are (slightly) overestimated for the low sea-ice concentration range (SIC = 0%). The SIC total uncertainty σ_{tot} has contributions from the

15 algorithm uncertainty σ_{algo} and the smearing uncertainty σ_{smear} . Because the locations for ground truth estimates generally are not at the ice edge, the smearing uncertainty term is close to zero and σ_{algo} dominates the evaluation results summarized in Figure -12. As introduced in section -3.5, the algorithm uncertainty is computed as the standard deviation of the retrieval error at the dynamically selected training data samples. For SIC = 100% cases, the dynamically selected training samples are spread mostly all over the high sea-ice concentration regions, and there are thus good odds that the training samples are

20 representative of the geophysical conditions in the ground-truth dataset, and that in turn the reported uncertainties are in agreement with the retrieval errors for SIC=100% cases. For SIC = 0% however, the training data samples are selected at the outskirts of an expanded maximum ice climatology, while the ground truth locations are just outside the same climatology. For SIC = 0%, the ground-truth open water locations are selected just outside the maximum sea-ice climatology, while we used an expanded version of this climatology for the selection of the open water training data samples (sections 3.3 and 3.6).

25 The OW The training samples thus generally correspond to lower latitude conditions (ocean surface, and atmosphere conditions) than the ground-truth locations. For example, training samples can be pickedmay be selected in regions of more frequent synoptic low-pressure paths than the conditions really prevailing at the ice edge, and where the ground-truth estimates used in the section are locatedto the least at the location of the ground truth estimates used in this section. A More more developed sea state as well as a wetter atmosphere contribute to the overestimation of σ_{algo} (hence σ_{tot}) by at maximum

30 1% SIC (one standard deviation) in SIC = 0% conditions. We finally, we note that the results from Figure -12 cover the end of the time period (the AMSR-E and AMSR2 years) while the maximum ice extent climatology driving the selection of training samples is computed for the whole almost 40 years of sea-ice data record. Trends in sea-ice decline (in the NH,

(especially summer) might thus have an amplification effect on the overestimation of the uncertainties, as the location for selecting training samples is increasingly further away from sea-ice edge as decades pass.

4.3 Caveats and known limitations

Known limitations of the SIC CDR are listed in this section. All the aspects listed below apply ~~in large extent generally~~ to the other existing SIC data records based on ~~Passive Microwave sensor~~^{PMW satellite} data. Not all of these limitations are reflected in the uncertainty fields of the CDR, as presented below.

The Open Water Filter (aka Weather Filter) implemented in the new SIC CDR is based on ~~a~~ combination of the ~~PMR frequency~~ channels around 19-GHz and 37-GHz (section 3.4.2). Although the filter is efficient at detecting and removing weather-induced noise (false ice) over open water, ~~it also has the effect of removing it is also designed to remove~~ some amount of true low-concentration ice, especially in the marginal ice zone. Although dynamic tuning strategies were developed for these new CDRs, users are explicitly warned to ~~take pay~~ close attention to filtered conditions, especially close to the ice edge. The un-filtered (“raw”) SIC values can always be accessed in ~~the~~ field raw_ice_conc_values (section 4.1, Figure 6). The effect of the ~~open water filter~~^{OWF} is not included in the uncertainty variables, which ~~are pertaining~~^{pertain} to the un-filtered (raw) ice concentration values. See also the discussion on the temporal consistency of the OWF for the three CDRs in section 4.2.1.

All SIC algorithms based on the passive microwave data are very sensitive to melt-pond water on top of the ice (Kern et al. 2016). The radiation emitted at ~~the wavelengths of the frequency channels~~^{these wavelengths} comes from a very thin layer at the surface of the ~~ice~~^{melt-pond}, which does not enable ~~distinguishing between~~ ocean water (in leads and openings) and melt water (in ponds) ~~to be distinguished~~. The ice_conc variable of the SIC CDRs, thus should hold an estimate of 1 minus the open water fraction in each grid cell, irrespective if this water is from lead and openings or ponds. The mis-interpretation of melt water on top of sea ice as open water is not included in the uncertainty variables (Yang K. et al., 2016). The uncertainties embedded in the files are those for “1 minus the open water fraction”.

Due to many factors (including smooth surface, absence of snow, brine content) concentration of thin sea-ice (< 30 cm) is underestimated by most of the ~~PMR-PMW~~ SIC algorithms (Cavalieri 1994). A complete, 100% cover of thin sea ice will be retrieved with a lower concentration, depending on the thickness (Ivanova et al. 2015). The effect of thin sea ice is not included in the uncertainty fields of the SIC CDRs.

The SIC data records aims at addressing needs from a wide range of users, from ~~the~~ interested general public to climate modellers and climate services. It was decided to provide interpolated sea-ice concentration values in places where original input satellite data was missing, ~~aiming to produce the most complete daily maps possible aiming at most complete daily~~

~~maps~~. Both temporal and spatial interpolation is used (section_3.6). The locations where interpolation is used are clearly identified in the status_flag layer. These interpolated sea-ice concentration values should generally be used with caution for scientific applications, especially the values obtained from spatial interpolation. The uncertainty variables are not interpolated where data ~~was-were~~ missing. Days where no satellite data was available, e.g. every other day in the SMMR time period, are not

5 interpolated and corresponding files are missing from the data records.

OSI-450 is presented at 25_km grid spacing. However, a spatial sampling of 25_km does not fully represent the true spatial resolution of the product since the footprint of the SMMR, SSM/I, and SSMIS channels used by the algorithms is coarser (Table_2). The mismatch of grid spacing to the true resolution of the instrument footprint is taken into account in the
10 uncertainty model of the OSI SAF CDR and is a key contribution to the *smearing* uncertainty (section_3.5). The footprint of the AMSR-E and AMSR2 channels used in the ESA CCI CDRs (SICCI-25km and SICCI-50km) are much more compatible with the 25x25_km (SICCI-25km) and 50x50_km (SICCI-50km) target grids, so that their grid spacing is closer to the true resolution. The true resolution of the SICCI-25km CDR might be slightly better than 25x25 km, but this grid spacing was retained to ease uptake by users, and comparison with OSI-450.

15

The radiometric signature of land is similar to that of sea ice at the wavelengths used for estimating the SIC. Because of the large foot-prints and the relatively high brightness temperatures of land and ice compared to water, the land signature ~~is~~ “~~spilling~~spills” into the coastal zone open water and it will falsely ~~look-appear~~ as intermediate concentration ice. This land-spill-over effect is corrected for as described in section_3.6. However, coastal correction procedures are not perfect, and
20 some false sea-ice remains along some coastlines, especially for OSI-450 and SICCI-50km because of the larger foot-print of the instruments. By the same token, some true coastal sea ice might be removed by the coastal correction scheme. Users are advised to check the values in the raw_ice_conc_values variable where the SIC estimates before the final coastal correction step are available. The uncertainty variables have larger values in the coastal regions where land spill-over effects are detected. See also section 5.2.

25

Ice resulting from freezing of fresh and brackish waters does not have the same emissivity as that from sea water. The retrieval of ice area fraction in these conditions would call for dedicated tie-points (e.g. Ghaffari et al. 2011), which we did not implement here. In addition to the difficulty of computing dynamic tie-points over such small areas, it is unclear if such dedicated tie-points would make a large difference in the end, because of the combination of many error sources in these close water bodies (land spill-over, thin sea-ice, larger atmospheric influence, etc...). A layer in the status_flag variable indicates fresh and brackish water bodies.

5 Discussion, Outlook and Conclusions

5.1 Discussion

This paper documents three new Sea Ice Concentration (SIC) Climate Data Records (CDR). One from EUMETSAT OSI SAF (OSI-450), and two from ESA CCI (SICCI-25km and SICCI-50km). All three share the same algorithm baseline, which

- 5 is both a continuation of the EUMETSAT OSI SAF SIC approach (Andersen et al. 2006, Tonboe et al. 2016) and a series of innovations contributed mostly by the ESA CCI activities. The three CDRs are a family of data records that aim at addressing the GCOS Requirements for the Sea Ice Essential Climate Variable (ECV) (GCOS-IP, 2016). The improvements with respect to earlier versions of the CDRs include 1) using high-quality Fundamental Climate Data Records (FCDR) as input data (section 2.1), 2) a new family of self-tuning, self-optimizing SIC algorithms that dynamically adjust to the input
10 T_B data (sections 3.2, and 3.3), 3) novel noise reduction and filtering approaches (section 3.4), and per-pixel uncertainty estimates (section 3.5). The product data files are designed so that interested users can revert some of the filtering steps and access the “raw” output of the SIC algorithms (section 4.1).

The three CDRs are designed to ensure temporal continuity throughout the almost 40-years of passive microwave data records. The OSI-450 dataset currently covers 1979 throughout 2015 with a consistent set of frequencies at 19-GHz and 37-GHz. Conversely to other CDRs (e.g. Meier et al. 2017 and its two algorithm components Bootstrap and NasaTeam), the channels around 22-GHz are not used for filtering water vapour contamination. The 23.0-GHz channels of the SMMR instrument were highly unstable since launch, and eventually ceased to function in March 1985. This is one of the reasons why the Meier et al. (2017) dataset only starts with SSM/I F08 on 09 July 1987 as a fully-qualified CDR (according to
20 <https://nsidc.org/data/g02202>). A key asset of the algorithms we adopted is that they are self-tuning and self-optimizing to the data, which greatly helps achieving temporal consistency between different satellite missions, both in the past and future (discussed later as outlook section 5.2).

The self-tuning and self-optimizing algorithms also allowed e.g. to consistently process consistent processing of SIC CDRs
25 from the AMSR-E and AMSR2 instruments. The SICCI-25km is an attempt at closing the gap in spatial resolution between what can be achieved from coarse resolution sensors like SMMR, SSM/I and SSMIS and the requirements of GCOS for 10-15-km spatial resolution (GCOS-IP, 2016). The almost 15-years record of brightness temperature observations from these two instruments is a key complement to OSI-450.
30 The decision to produce distinct CDRs, one with SMMR, SSM/I, and SSMIS and the other two with AMSR-E and AMSR2 data is mainly based on the difference in spatial resolution. To mix the two types of sensors (coarse resolution with medium resolution) into a single CDR will would require careful consideration of the mismatch of spatial resolution, and possibly advanced enhanced resolution methods (e.g. Long and Daum, 1998; Long and Brodzik, 2016) which are not used here. It is

in any case doubtful if the resulting single CDR ~~had~~would meet the temporal consistency requirements of many climate applications.

An initial validation~~evaluation~~ of the three CDRs and their uncertainties is reported upon in section [4.2](#). Time-series plots document that the dynamic tuning of the SIC algorithms and of the OWF perform as expected, and that temporal consistency is mostly achieved despite the changes of ~~channel~~ frequencies and calibration between sensors. Based on similar frequency channels at 19 -GHz and 37 -GHz , the OSI-450 and SICCI-25km CDRs achieve similar accuracies, both in the time-series plots of internal tuning parameters (section [4.2.1](#)) and when validated against ground-truth (section [4.2.2](#)). Over open water, the retrieval accuracy of these two CDRs is as good as 1.5% to 2% SIC (one standard deviation) and without biases. Over [consolidated](#) sea ice, the retrieval accuracy is somewhat poorer (3.5% to 4% SIC) and with a limited low bias (2% SIC in NH, 1% in SH). The SICCI-50km uses a 6 -GHz frequency channel instead of 19 -GHz . Theoretically 6 -GHz is a better channel for estimating sea-ice concentration since the atmosphere is more transparent, the influence of error sources like sea-ice age or snow processes have less influence, and the contrast between ocean and ice is larger. This is confirmed in our validation~~evaluation~~ results. Over open water, the retrieval accuracy of SICCI-50km is as good as 1% to 1.5% SIC (one standard deviation). Over [consolidated](#) sea ice, the accuracy is better than 2.5% SIC and the bias limited to below 1%. The SICCI-50km is thus the most accurate of our three new CDRs but is also that with the coarsest spatial resolution due to the large footprint of the 6 -GHz channels.

Our evaluation results reveal very similar accuracies in the Northern and Southern hemispheres, even though the sea-ice conditions can be very different. Regarding algorithm performance, the Arctic is more challenging at first glance. At least two radiometrically different ice types, multiyear ice and first-year ice, and a pronounced seasonal cycle of sea-ice and snow properties during summer with regular wide-spread occurrence of melt ponds on the ice surface need to be accommodated by the algorithm. Antarctic multiyear ice has a less well studied and different radiometric signature ~~than as~~ Arctic multiyear ice, resulting from other summer melt processes, e.g. melt ponds occur rarely; one could say it differs less from that of first-year ice on the one hand. On the other hand, direct and indirect weather influences, causing an unwanted variation in the retrieved sea-ice concentration, have been quite regional in extent in the Arctic Ocean (largely encompassed by land masses) while these have been a common, wide-spread phenomenon on Antarctic sea ice (bordered by oceans and at lower latitudes). Therefore, a very similar algorithm performance in both hemispheres is not a surprise and agrees with earlier findings (e.g. Ivanova et al. 2015). We note that because they automatically tune their coefficients (tie-points, plane angle θ , etc...) to the training data specific for each hemisphere, our new algorithms can best adapt to radiometric properties of sea ice being different in both hemispheres.

An analysis of the temporal consistency of the Open Water Filter (section [4.2.1](#)) also revealed that our dynamic tuning of the OWF does not perform as optimally on the SICCI-50km CDR than on SICCI-25km and OSI-450. This is explained by

the larger mismatch in frequency and resolution between the channels entering the SIC algorithms, and those used in computing the OFW (19.5-GHz and 37.5-GHz only). ~~For all practical purposes we~~ We note that the dynamic tuning of the OFW as implemented here secures a ~~rather quite~~ stable level for the minimum detectable true SIC, ~~in on~~ on the order of 10% SIC, ~~on average~~ well below the 15% SIC threshold commonly used for defining Sea Ice Extent.

5

An evaluation of the uncertainties, a key element of the CDRs, is reported upon in section 4.2.3. We compare the uncertainty values reported in the product files with the retrieval error of the SIC field in conditions of known 0% and 100% SIC. Over 100% SIC, there is a close correspondence between the reported uncertainty and the observed retrieval noise, for both hemispheres. In open water conditions, the uncertainties provided in the CDR product files overestimate ~~(by maximum 4% SIC in terms of standard deviation)~~ the observed retrieval noise by a couple of SIC percent (in terms of standard deviation). This slight overestimation is probably due to the use of a buffer zone outside of the monthly maximum ice climatology extent to dynamically select the data samples used to train the algorithms (section 3.3) and derive uncertainties (section 3.5).

5.2 Outlook

The Climate Data Records presented in this manuscript will be further developed and extended in the context of the EUMETSAT OSI SAF. A full-reprocessing of the OSI-450, SICCI-25km, and SICCI-50km CDRs is ~~namely~~ committed to by OSI SAF (version 3 of the CDRs) and should happen in 2021. It will use updated versions of the FCDRs –if available– and the new ERA5 atmosphere re-analysis from the EU C3S ([Hersbach and Dee, 2016](#)). At time of writing, no radical change of algorithms and processing steps is foreseen, but our paper identifies several improvements and evolutions that would be beneficial for these upcoming versions, and ~~that~~ these are briefly described below.

Although the ESA Climate Change Initiative Sea Ice projects went far in the characterization of the impact ~~of that~~ melting, and melt-ponds have on sea-ice concentration retrievals from passive microwave data (Kern et al. 2016), the question on how to limit and best convey the increased uncertainty to users will benefit from ~~more futher~~ efforts. Results of an inter-comparison between the ~~same~~ data set of melt-pond fraction, sea-ice concentration and net sea-ice surface fraction ~~that was~~ used in Kern et al. (2016) and the three CDRs presented in this paper as well as other available sea-ice concentration products, including those based on NASA-Team and Bootstrap algorithms, will be reported in a forthcoming article.

The uncertainty model presented here is already a significant improvement over that used in the previous version of the SIC CDR (Tonboe et al. 2016). Nonetheless, additional research is needed to better quantify the uncertainties and validate that they are fit-for-purpose. Since the way we derive uncertainties is directly linked to the way we select training data samples, it could be investigated if ~~to~~ selecting training samples closer to the ice edge ~~could would~~ improve the uncertainty values, and for example reduce the slight overestimation of uncertainties at SIC = 0% conditions documented in section 4.2.3. Another

challenging topic is the quantification of cross-correlation scales (both in the temporal and spatial dimensions) necessary to fully aggregate such CDRs at the scales relevant for evaluation of models or higher-level climate indicators (Bellprat et al. 2017).

- 5 Despite being from all seasons and in both hemispheres, the validation results presented in this paper cover 0% and 100% SIC conditions, but not the intermediate range found in the marginal ice zone due to the lack of high quality validation data. Results of the evaluation of the three CDRs with independent data, i.e. ship-based visual observations ~~the-of~~ sea-ice cover, and sea-ice area fraction derived from high-resolution optical satellite imagery, have been reported in the Product Validation and Intercomparison Report PViR (available from <http://cci.esa.int>) and will also be published in forthcoming articles. These
10 will also include an inter-comparison of time-series of the sea-ice area (SIA) and ~~extent~~ (SIE) as derived from the three CDRs and from other sea-ice concentration products.

Already from the early assessment of the new CDRs presented here, we can outline a number of algorithm developments that have the potential to further improve the accuracy of future SIC estimates based on passive microwave data, both in climate
15 and operational applications. The new self-tuning, self-optimizing algorithms introduced in this paper are currently limited to 3D T_B spaces. This is because the optimization of the projection plane is handled via a rotation angle along a 3D axis, a geometrical concept that is difficult to upscale to more dimensions. The generalization of this optimization to nD (where n could be any subset of the channels available on a given passive microwave imager) would open for ~~exploring-assessing~~ all possible T_B channels combinations in a systematic manner, and maybe unveil algorithms ~~to achieving~~ even better accuracy
20 ~~that-than~~ the 3D ones used here. By the same token, it should be investigated if the concept of a consolidated ice curve (as opposed to an ice line) could ~~not~~ be better embedded ~~by-in~~ SIC algorithms in the future, instead of being a correction step applied a-posteriori as is the case in our CDRs. A third algorithm development to be investigated is the generalization of the concept of Open Water Filters (*aka* Weather Filters) to 3D or even nD , so that the OWFs are always tuned and computed using the same T_B channels as the SIC. This development has the potential to improve the temporal consistency of the OFW
25 at low SIC values, across changes of wavelengths and calibration, or when using other T_B channels than 19-GHz and 37-GHz. ~~Finally, research is needed to assign a true spatial resolution to SIC fields computed from combinations of n T_B channels, themselves at different spatial resolutions. Some knowledge is embedded in our parametrization of σ_{smear} , but it is currently not enough to e.g. choose and fully justify a grid spacing for SIC data records.~~ In any case and even after almost 40-years of routinely available passive microwave observations of the polar regions, the underlying algorithms can ~~still~~ be
30 improved to yield improved accuracy and there is scope for continued research and development in the field.

~~Other steps in the processing chain can further be improved upon, e.g. the land spill-over correction schemes. In section 3.6 we described how land spill-over was corrected in two steps, first through a physically-based algorithm on swath T_B data (adapted from Maass and Kaleschke, 2010), followed by a statistically-based correction of gridded SICs (adapted from~~

Formatted: Font: Italic

Formatted: Subscript

Formatted: Font: Symbol

Formatted: Subscript

Formatted: Subscript

Cavalieri et al. 1999). Several reasons can have led to the swath-based correction to not be enough. For example, the method relies heavily on accurate geolocation of the T_b measurements, however its uncertainty for the SSM/I and SSMIS instrument is known to be large (Poe et al. 2008), and is not corrected for in the current version of the FCDR (R3) we used (Fennig et al. 2017). We used approximated iFoVs weighting functions instead of eFoVs (see section 2.1) when convolving antenna pattern with the land mask, thus neglecting the effect of the measurements integration period. Finally, strategies to avoid gridding land-contaminated FoVs when building Level 3 maps might help in the future. It will also be beneficial to use objective high-resolution SIC maps from coastal regions to tune the various thresholds embedded in the statistically-based correction. To improve further on the land spill-over correction will be an objective for upcoming versions of the CDRs.

Formatted: Subscript

5 Another development for using such SIC CDRs to evaluate models and perform Data Assimilation would be the definition and uptake of observation operators (aka satellite simulators, e.g. Kaminski and Mathieu, 2017). Once the remaining systematic errors (such as underestimation of very thin ice, impact of melt-pond water...) have been described and quantified, the next step is for the Earth Observation EO science community to define observation operators. These operators are typically parametric formulations that express the quantity retrieved from Earth Observation EO techniques (in our case the

15 sea-ice concentration values in the CDR) as a combination of physical variables in the model world (e.g. sea-ice area fraction, thickness of sea ice categories, area coverage of melt-pond...). We advocate these operators are built in a step-wise, pragmatic manner (Lavergne, 2017). This development should happen in complement to building more “end-to-end” satellite simulators that aim at linking the physical variables in the model world directly to satellite radiances.

20 Thanks to using the C-band channels (4-8-GHz) the SICCI-50km CDR exhibits outstanding sea-ice concentration retrieval accuracy, both at low and high concentration range. The usability of this CDR can however be challenged by its rather coarse resolution (the 6-GHz channels of AMSR-E have a iFoV of 75x43-km (Table-2) and the CDR is presented on a 50-km grid), which is a direct consequence of the limited antenna diameter of the AMSR-E (2.0-m) and AMSR2 (2.1-m) instruments. Our results fully support that a passive microwave mission measuring at the C-band frequency, and carrying a

25 large-enough antenna to enable ground resolutions better than 15-km (at C-band) would be a clear asset for all-weather, global, daily-covering sea-ice concentration mapping for operational applications. At time of writing, such a satellite mission is under study as a High Priority Candidate Mission for the European Union’s Copernicus Space Component Expansion: the Copernicus Imaging Microwave Radiometer (CIMR, <https://cimr.eu>).

30 A key requirement of GCOS for addressing the needs of the climate modelling community as well as the Climate Information Services such as the EU Copernicus Marine Environment Monitoring Service (CMEMS, <http://matinemarine.copernicus.eu>) and Copernicus Climate Change Service (C3S, <http://climate.copernicus.eu>) is the seamless extension of the CDRs in the context of operational services. These operational services aim at-to have the best temporal consistency with the CDRs, but still may have to rely on different data streams. They are referred to as Interim

Climate Data Records (ICDR) because they are meant as a temporary extension until a full-reprocessing of the CDRs is performed (Yang_W_ et al., 2016). For the SIC variable, both the EUMETSAT OSI SAF CDR of Tonboe et al. (2016) and the NOAA/NSIDC CDR (since late 2017, Version 3) are extended daily by such ICDR. We are naturally working towards starting an operational ICDR for our new CDRs, tentatively by late 2018, with a 16-days latency. [The algorithm developments will also be introduced to the operational stream of sea-ice products from the EUMETSAT OSI SAF.](#)

Aside from the technical aspects of reliably running the CDR processing chains on a daily basis, a major challenge that all SIC CDR data producers now face is the end of life for the U.S. Defense Meteorological Satellite Program (DMSP), that has been the work-horse for virtually all Sea Ice CDRs since SSM/I F08 in 1987 (Table 2 and Figure 1). At time of writing, the Japanese AMSR2 instrument is already ~~passed past~~ its design lifetime (5-years, launched mid 2012), with no committed successor. For the continuation of the new OSI SAF SIC CDR, we are investigating the quality of the Micro-Wave Radiation Imager (MWRI) on board China's Feng-Yun 3 (FY3) satellites. Preliminary results are encouraging and, when consolidated, will be presented in a follow-up paper. The first satellite of the European Polar System Second Generation (EPS-SG), ~~that series to will~~ carry a Microwave Imager (MWI) ~~will beis scheduled for~~ launched in 2023. It can be used to further extend the SIC CDR up-until the late 2040s. It is noticeable that EPS-SG MWI implements quite a different ~~channel~~ frequency for Ka-band (26.5–40-GHz): 31.4-GHz instead of 36 - 37-GHz for SSM/IS and AMSRs (Table 2). ~~However, Beeause because~~ our algorithms are self-adapting to the data and their calibration, the implementation with MWI should be possible. The impact of using 31.4-GHz instead of 36 - 37-GHz for sea-ice concentration mapping still needs to be addressed.

5.3 Conclusions

Long-term consistency, traceability and an evaluation and documentation of uncertainties are arguably the three major properties of any climate-data record. In this contribution, we have described how these requirements are reflected by the algorithm underlying the three new sea-ice concentration climate-data records OSI-450, SICCI-25km and SICCI-50km.

Long-term consistency is achieved by developing an algorithm that dynamically adjusts to changing environmental conditions and changing satellite sensors. In particular, applying the same algorithm to microwave products based on different frequencies and satellites allows users to combine the advantages of the length of the record of the OSI-450 product with the high true spatial resolution of the SICCI-25km product and/or the low-noise product SICCI-50km.

Traceability of the algorithm and the resulting climate-data records is achieved by a combination of two approaches. First, the final products ~~contains~~ substantial information on the impact of the various processing steps. For example, they include at every time step per-pixel information on the impact of possible filtering. Second, the algorithm and the products are embedded into an operational context. This guarantees ~~on the handease of~~ a long-term maintenance of these products, but in

particular establishes clear rules on version-tagging, documentation and availability of the underlying code, which allows other researchers to easily build on our work and to develop it further.

Uncertainties ~~of all products is are~~ systematically documented in the final products and ~~has have~~ carefully been evaluated. All 5 products contain at every time step per-pixel information on uncertainties arising from the algorithm itself (e.g., sensor noise or residual geophysical noise) and the smearing uncertainty from spatial remapping. This information is in particular helpful for data-assimilation purposes. The evaluation of uncertainties carried out in this [paper](#) provides some initial information on the remaining random per-pixel uncertainty which can be used as an estimate of observational uncertainty for example during model evaluation or data assimilation. We find in particular that our product has a long-term stable zero bias arising 10 from the dynamical re-tuning of the tie points.

We hope that by explicitly addressing the three requirements of a climate-data record, our three new sea-ice concentration records and the underlying algorithm will be a helpful resource for the climate-research community.

Competing Interests

15 The authors declare that they have no conflict of interest.

Acknowledgements

The authors are grateful to Prof Edward Hanna and Dr Doug Smith for sharing insights and software for the dynamic tuning of the Bristol SIC algorithm. Our gratitude goes to the open-source community at large, and especially the maintainers of the Python language and its modules (numpy, scipy, matplotlib, pytroll,...).

20 The SMMR, SSM/I, and SSMIS FCDR (R3) was accessed from the EUMETSAT CM SAF (www.cmsaf.eu). Karsten Fennig and Marc Schröder, both at DWD, helped ~~making make~~ best use of this data. The AMSR-E FCDR was accessed from NSIDC, and the AMSR2 data from JAXA. ECMWF ERA-Interim was accessed from the MARS archive.

25 This study and the development of the three new SIC CDRs was funded by EUMETSAT (through the 2nd Continuous Developments and Operation Phase of OSI SAF) and ESA (through the Climate Change Initiative Sealce_cci project).

References

[Andersen, S., Tonboe, R., Kern, S., and Schyberg, H.: Improved retrieval of sea ice total concentration from spaceborne passive microwave observations using Numerical Weather Prediction model fields: An intercomparison of nine algorithms, Remote Sensing of Environment, 104, 374-392, 2006](#)

5

[Andersen, S., Toudal Pedersen, L., Heygster, G., Tonboe, R., and Kaleschke, L.: Intercomparison of passive microwave sea ice concentration retrievals over the high concentration Arctic sea ice. J. Geophys. Res., 112, C08004, doi:10.1029/2006JC003543, 2007](#)

10 [Bellprat, O., Massonet, F., Siegert, S., Prodhomme, C., Macias-Gómez, D., Guemas, V., and Doblas-Reyes, F.: Uncertainty propagation in observational references to climate model scales. Remote Sensing of Environment, Volume 203, doi:10.1016/j.rse.2017.06.034, 2017](#)

15 [Brodzik, M. J., Billingsley, B., Haran, T., Raup, B., and Savoie, M. H.: EASE-Grid 2.0: Incremental but Significant Improvements for Earth-Gridded Data Sets. ISPRS International Journal of Geo-Information, 1\(1\):32-45, doi:10.3390/ijgi1010032, 2012](#)

20 [Brodzik, M. J., Billingsley, B., Haran, T., Raup, B., and Savoie, M. H.: Correction: Brodzik, M. J. et al. EASE-Grid 2.0:](#)

[Incremental but Significant Improvements for Earth-Gridded Data Sets. ISPRS International Journal of Geo-Information](#)

25 [2012, 1, 32-45. ISPRS International Journal of Geo-Information, 3\(3\):1154-1156, doi:10.3390/ijgi3031154, 2014](#)

[Brooks, C. E. P.: The Problem of Warm Polar Climates. Q. J. R. Meteorol. Soc. 51, 83–91, 1925](#)

25 [Cavalieri D. J., Gloersen, P., and Campbell, W. J.: Determination of Sea Ice Parameters With the NIMBUS 7 SMMR, Journal of Geophysical Research, vol. 89, no. D4, pp. 5355-5369, 1984](#)

30 [Cavalieri, D. J., Crawford, J., Drinkwater, M., Emery, W. J., Eppler, D. T., Farmer, L. D., Goodberlet, M., Jentz, R., Milman, A., Morris, C., Onstott, R., Schweiger, A., Shuchman, R., Steffen, K., Swift, C. T., Wackerman, C., and Weaver, R. L.: NASA sea ice validation program for the DMSP SSM/I: final report. NASA Technical Memorandum 104559. National Aeronautics and Space Administration, Washington, D.C. 126 pages, 1992](#)

[Cavalieri, D. J.: A microwave technique for mapping thin sea ice. J. Geophys. Res., 99:12561–12572, 1994](#)

Formatted: Font: Not Italic

Formatted: Font: Italic

Formatted: No underline

Formatted: No underline

Cavalieri, D. J., St. Germain, K. M., and Swift, C. T.: Reduction of weather effects in the calculation of sea ice concentration with the DMSP SSM/I. Journal of Glaciology 41(139): 455-464, 1995

Formatted: Font: Not Bold

5 Cavalieri, D. J., Parkinson, C. L., Gloersen, P., Comiso, J. C., and Zwally, H. J.: Deriving long-term time series of sea ice cover from satellite passive-microwave multisensor data sets. J. Geophys. Res., 104(C7), 15803–15814, doi:10.1029/1999JC900081, 1999

Formatted: No underline

10 Colton, M. C., and Poe, G. A.: Intersensor calibration of DMSP SSM/Is: F-8 to F-14, 1987-1997. IEEE Trans. Geosci. Remote Sens., 37, 418–439, 1999

Comiso, J. C.: Characteristics of arctic winter sea ice from satellite multispectral microwave observations. Journal of Geophysical Research 91(C1), 975-994, 1986

15 Comiso, J. C., and Nishio, F.: Trends in the sea ice cover using enhanced and compatible AMSR-E, SSM/I, and SMMR data. J. Geophys. Res., 113, C02S07, doi:10.1029/2007JC004257, 2008

Formatted: No underline

20 Comiso, J. C., Gersten, R.A., Stock, L.V., Turner, J., Perez, G.J., and Cho, K.: Positive Trend in the Antarctic Sea Ice Cover and Associated Changes in Surface Temperature. J. Climate, 30, 2251–2267, doi:10.1175/JCLI-D-16-0408.1, 2017

Formatted: No underline

25 Comiso, J. C.: Large Decadal Decline of the Arctic Multiyear Ice Cover. J. Climate, 25, 1176–1193, doi:10.1175/JCLI-D-11-00113.1, 2012

Comiso, J. C., Meier, W. N., and Gersten, R.: Variability and trends in the Arctic Sea ice cover: Results from different techniques. J. Geophys. Res. Oceans, 122, 6883–6900, 2017

30 Dee, D. P., Uppala, S. M., Simmons, A. J., Berrisford, P., Poli, P., Kobayashi, S., Andrae, U., Balmaseda, M. A., Balsamo, G., Bauer, P., Bechtold, P., Beljaars, A. C. M., van de Berg, L., Bidlot, J., Bormann, N., Delsol, C., Dragani, R., Fuentes, M., Geer, A. J., Haimberger, L., Healy, S. B., Hersbach, H., Hólm, E. V., Isaksen, L., Källberg, P., Köhler, M., Matricardi, M., McNally, A. P., Monge-Sanz, B. M., Morcrette, J.-J., Park, B.-K., Peubey, C., de Rosnay, P., Tavolato, C., Thépaut, J.-N., and Vitart, F.: The ERA-Interim reanalysis: configuration and performance of the data assimilation system. Q.J.R. Meteorol. Soc., 137: 553–597, 2011

Formatted: No underline

Donlon, C. J., Martin, M., Stark, J. D., Roberts-Jones, J., Fiedler, E. and Wimmer, W.: The Operational Sea Surface Temperature and Sea Ice analysis (OSTIA). Remote Sensing of the Environment. doi:10.1016/j.rse.2010.10.017, 2012

- Fennig, K., Schröder, M., Hollmann, R.: Fundamental Climate Data Record of Microwave Imager Radiances, Edition 3, Satellite Application Facility on Climate Monitoring, doi:10.5676/EUM_SAF_CM/FCDR_MWI/V003, 2017
- 5 GCOS-IP: GCOS Implementation Plan 2016. GCOS-200. Available at https://library.wmo.int/opac/doc_num.php?explnum_id=3417, 2016
- Ghaffari, P., Pedersen, L., Eastwood, S., Lavergne, T.: Sea Ice in the Caspian Sea, Technical Report OSI_AS11_P04, available at <https://osisaf.met.no>, 2011
- 10 Gregory, J. M., Stott, P. A., Cresswell, D. J., Rayner, N. A., Gordon, C., and Sexton, D. M. H.: Recent and Future Changes in Arctic Sea Ice Simulated by the HadCM3 AOGCM, *Geophys. Res. Lett.* 29, no. 24, 2175, doi:10.1029/2001GL014575, 2002
- 15 Herrington, T., and Zickfeld, K.: Path independence of climate and carbon cycle response over a broad range of cumulative carbon emissions, *Earth Syst. Dyn.* 5, 409–422, doi:10.5194/esd-5-409-2014, 2014
- Hersbach, H. and Dee, D.: ERA5 reanalysis is in production, *ECMWF Newsletter*, Number 147 - Spring 2016 <https://www.ecmwf.int/en/newsletter/147/news/era5-reanalysis-production>, 2016
- 20 Hobbs, W., Massom, R., Stammerjohn, S., Reid, P., Williams, G., and Meier, W.: A review of recent changes in Southern Ocean sea ice, their drivers and forcings, *Global and Planetary Change*, Volume 143, doi:10.1016/j.gloplacha.2016.06.008, 2016
- 25 Ivanova, N., Pedersen, L. T., Tonboe, R. T., Kern, S., Heygster, G., Lavergne, T., Sørensen, A., Saldo, R., Dybkjær, G., Brucker, L., and Shokr, M.: Inter-comparison and evaluation of sea ice algorithms: towards further identification of challenges and optimal approach using passive microwave observations, *The Cryosphere*, 9, 1797-1817, doi:10.5194/tc-9-1797-2015, 2015
- 30 Johannessen, O. M.: Decreasing Arctic Sea Ice Mirrors Increasing CO₂ on Decadal Time Scale, *Atmospheric and Oceanic Science Letters* 1, no. 1, 51–56. doi:10.1080/16742834.2008.11446766, 2008

Formatted: No underline

Formatted: No underline

Kaminski, T. and Mathieu, P.-P.: Reviews and syntheses: Flying the satellite into your model: on the role of observation operators in constraining models of the Earth system and the carbon cycle, Biogeosciences, 14, 2343-2357, doi:10.5194/bg-14-2343-2017, 2017

5 Kern, S., Rösel, A., Pedersen, L. T., Ivanova, N., Saldo, R., and Tonboe, R. T.: The impact of melt ponds on summertime microwave brightness temperatures and sea-ice concentrations, The Cryosphere, 10, 2217-2239, doi:10.5194/tc-10-2217-2016, 2016

10 Korosov, A. A., Rampal, P., Pedersen, L. T., Saldo, R., Ye, Y., Heygster, G., Lavergne, T., Aaboe, S., and Girard-Ardhuin, F.: A new tracking algorithm for sea ice age distribution estimation, The Cryosphere, 12, 2073-2085, doi:10.5194/tc-12-2073-2018, 2018

15 Kwok, R.: Sea ice concentration estimates from satellite passive microwave radiometry and openings from SAR ice motion, Geophys. Res. Lett., 29(9), 1311, doi:10.1029/2002GL014787, 2002

Lavergne, T., Eastwood, S., Teffah, Z., Schyberg, H., and Breivik, L.-A.: Sea ice motion from low-resolution satellite sensors: An alternative method and its validation in the Arctic, J. Geophys. Res., 115, C10032, doi:10.1029/2009JC005958, 2010

20 Lavergne, T.: A step back is a move forward, figshare, 16-Oct-2017, doi:10.6084/m9.figshare.5501536.v1, 2017

Formatted: No underline

Long, D. G. and Daum, D. L.: Spatial resolution enhancement of SSM/I data, IEEE Trans. Geosci. Remote Sens., vol. 36, no. 2, pp. 407–417, 1998

25 Long, D. G., and Brodzik, M. J.: Optimum Image Formation for Spaceborne Microwave Radiometer Products, IEEE Transactions on Geoscience and Remote Sensing 54(5): 2,763-2,779, doi:10.1109/TGRS.2015.2505677, 2016

Formatted: Font: Not Bold

Formatted: No underline

Lu, J., Heygster, G. and Spreen, G.: Atmospheric Correction of Sea Ice Concentration Retrieval for 89 GHz AMSR-E Observations, IEEE J-STARS., 11(5), 1442–1457, doi:10.1109/JSTARS.2018.2805193, 2018

30 Maass, N., & Kaleschke, L. Improving passive microwave sea ice concentration algorithms for coastal areas: applications to the Baltic Sea, Tellus Series A-Dynamic Meteorology and Oceanography, 62(4), 393-410, doi:10.1111/j.1600-0870.2010.00452.x, 2010

Formatted: No underline

Mahlstein, I. and Knutti, R.: September Arctic sea ice predicted to disappear near 2°C global warming above present. J. Geophys. Res. 117, D06104, doi:10.1029/2011JD016709, 2012

Maykut, G. A.: Energy Exchange over Young Sea Ice in the Central Arctic, J. of Geophysical Research: Oceans 83, no. C7, 3646–3658, doi:10.1029/JC083iC07p03646, 1978

Meier, W., Fetterer, F., Savoie, M., Mallory, S., Duerr, R., and Stroeve, J.: NOAA/NSIDC Climate Data Record of Passive Microwave Sea Ice Concentration, Version 3. Boulder, Colorado USA. NSIDC: National Snow and Ice Data Center, doi:10.7265/N59P2ZTG, 2017

Formatted: No underline

Meier, W. N. and Ivanoff, A.: Intercalibration of AMSR2 NASA Team 2 Algorithm Sea Ice Concentrations With AMSR-E Slow Rotation Data, in IEEE Journal of Selected Topics in Applied Earth Observations and Remote Sensing , vol.PP, no.99, pp.1-11, doi: 10.1109/JSTARS.2017.2719624, 2017

Merchant, C. J., Paul, F., Popp, T., Ablain, M., Bontemps, S., Defourny, P., Hollmann, R., Lavergne, T., Laeng, A., de Leeuw, G., Mittaz, J., Poulsen, C., Povey, A. C., Reuter, M., Sathyendranath, S., Sandven, S., Sofieva, V. F., and Wagner, W.: Uncertainty information in climate data records from Earth observation, Earth Syst. Sci. Data, 9, 511-527, https://doi.org/10.5194/essd-9-511-2017, 2017

Niederdrenk, A.-L., and Notz, D.: Arctic Sea Ice in a 1.5°C Warmer World, Geophysical Research Letters 45, no. 4, 1963–71, doi:10.1002/2017GL076159, 2018

Njoku, E. G., Rague B. and Fleming K.: The Nimbus-7 SMMR Pathfinder Brightness Temperature Data Set, Jet Propulsion Laboratory Publication 98-4, 1998

Notz, D., and Marotzke, J.: Observations reveal external driver for Arctic sea-ice retreat, Geophys. Res. Lett. 39, L08502, doi: 10.1029/2012GL051094, 2012

Notz, D., and Stroeve, J.: Observed Arctic Sea-Ice Loss Directly Follows Anthropogenic CO₂ Emission, Science, aag2345, doi:10.1126/science.aag2345, 2016

Pedersen, L. T., Saldo, R., Ivanova, N., Kern, S., Heygster, G., Tonboe, R., Huntemann, M., Ozsoy, B., Arduuin, F. and Kaleschke, L.: Reference dataset for sea ice concentration, doi:10.6084/m9.figshare.6626549.v3, 2018

Poe, G. A., Uliana, E. A., Gardiner, B. A., vonRentzell, T. E. and Kunkee, D. B. : Geolocation Error Analysis of the Special Sensor Microwave Imager/Sounder, in IEEE Transactions on Geoscience and Remote Sensing, vol. 46, no. 4, pp. 913-922, doi:10.1109/TGRS.2008.917981, 2008

5 Sigmond, M., Fyfe, J. C., and Swart, N. C.: Ice-Free Arctic Projections under the Paris Agreement, Nature Climate Change, doi:10.1038/s41558-018-0124-y, 2018

Screen, J. A., and Williamson, D: Ice-Free Arctic at 1.5 °C?, Nature Climate Change 7, no. 4, 230–31, doi:10.1038/nclimate3248, 2017

10

Smith D. M., and Barrett, E. C.: Satellite mapping and monitoring of sea ice, CB/RAE/9/2/4/2034/113/ARE, RSU, University of Bristol, 1994

15 Smith, D. M.: Extraction of winter total sea ice concentration in the Greenland and Barents Seas from SSM/I data, International Journal of Remote Sensing 17(13), 2625-2646, 1996

Spreen, G., Kaleschke, L., and Heygster, G.: Sea ice remote sensing using AMSR-E 89-GHz channels, J. Geophys. Res., 113, C02S03, doi:10.1029/2005JC003384, 2008

Formatted: No underline

20 Strong, C., Golden, K.M.: Filling the Polar Data Gap in Sea Ice Concentration Fields Using Partial Differential Equations, Remote Sens, 8, 442, 2016

Tonboe, R. T., Eastwood, S., Lavergne, T., Sørensen, A. M., Rathmann, N., Dybkjær, G., Pedersen, L. T., Høyer, J. L., and Kern, S.: The EUMETSAT sea ice concentration climate data record, The Cryosphere, 10, 2275-2290, 25 https://doi.org/10.5194/tc-10-2275-2016, 2016

Wentz, F. J.: A model function for ocean microwave brightness temperatures, J. Geophys. Res., 88(C3), 1892–1908, doi:10.1029/JC088iC03p01892, 1983

Formatted: No underline

30 Wentz, F. J.: A well-calibrated ocean algorithm for SSM/I. Journal of Geophysical Research 102(C4), 8703-8718, 1997

Wentz, F. J., Meissner, T.: AMSR ocean algorithm version 2, RSS Tech. Proposal 121599A-1, Remote Sensing Systems, Santa Rosa, California, 2000

Yang, Q., Losch, M., Losa, S. N., Jung, T., Nerger, L., and Lavergne, T.: Brief communication: The challenge and benefit of using sea ice concentration satellite data products with uncertainty estimates in summer sea ice data assimilation. The Cryosphere, 10, 761-774, doi:10.5194/tc-10-761-2016, 2016

5 Yang, W., John, V. O., Zhao, X., Lu, H., and Knapp, K.R.: Satellite Climate Data Records: Development, Applications, and Societal Benefits. *Remote Sens.* 8, 331, 2016

Zickfeld, K., Arora, V. K., Gillett, N. P.: Is the climate response to CO₂ emissions path dependent? *Geophys. Res. Lett.* 39, L05703, doi:10.1029/2011GL050205, 2012

10 Andersen, S., R. Tonboe, S. Kern, and H. Schyberg. Improved retrieval of sea ice total concentration from spaceborne passive microwave observations using Numerical Weather Prediction model fields: An intercomparison of nine algorithms. *Remote Sensing of Environment*, 104, 374-392, 2006.

Figures

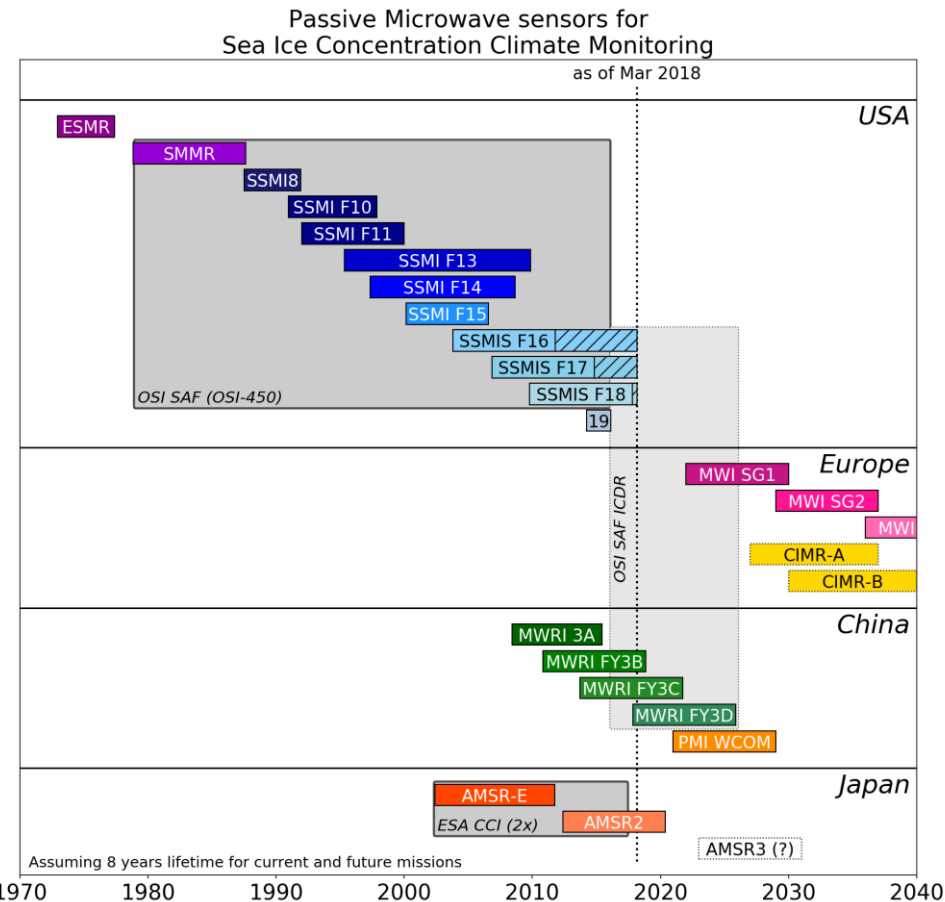


Figure 1: Time-coverage diagram for the new ESA CCI and EUMETSAT OSISAF SIC CDRs. The ESA CCI CDR is based on medium resolution AMSR-E and AMSR2 sensors, while the EUMETSAT OSISAF CDR uses the coarse resolution SMMR, SSM/I, and SSMIS instruments. Other current and future passive microwave instruments, as well as the OSI SAF ICDRs are discussed in our Outlook [section 5.2](#).

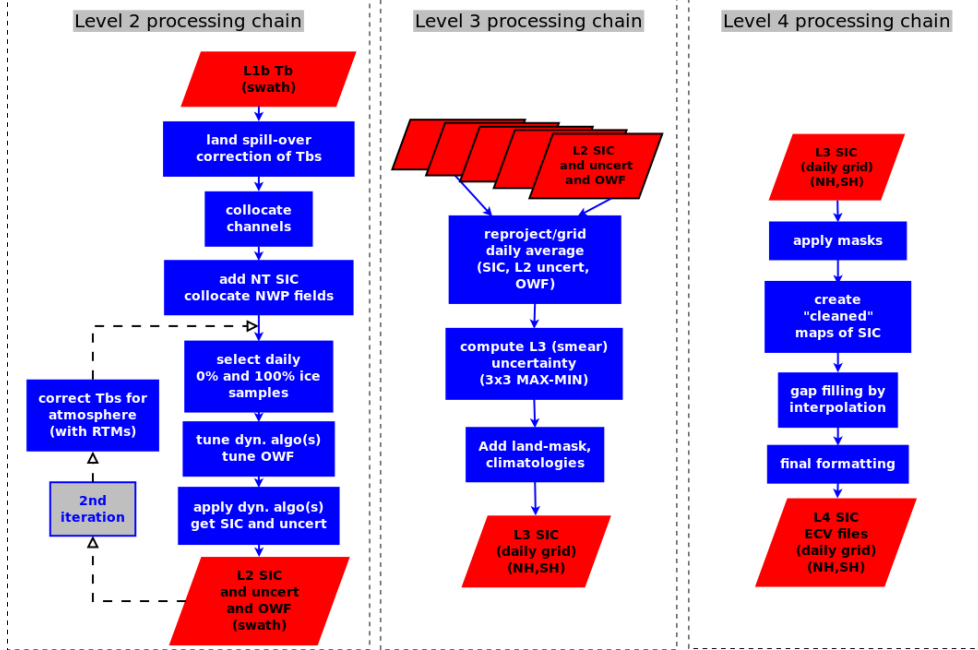
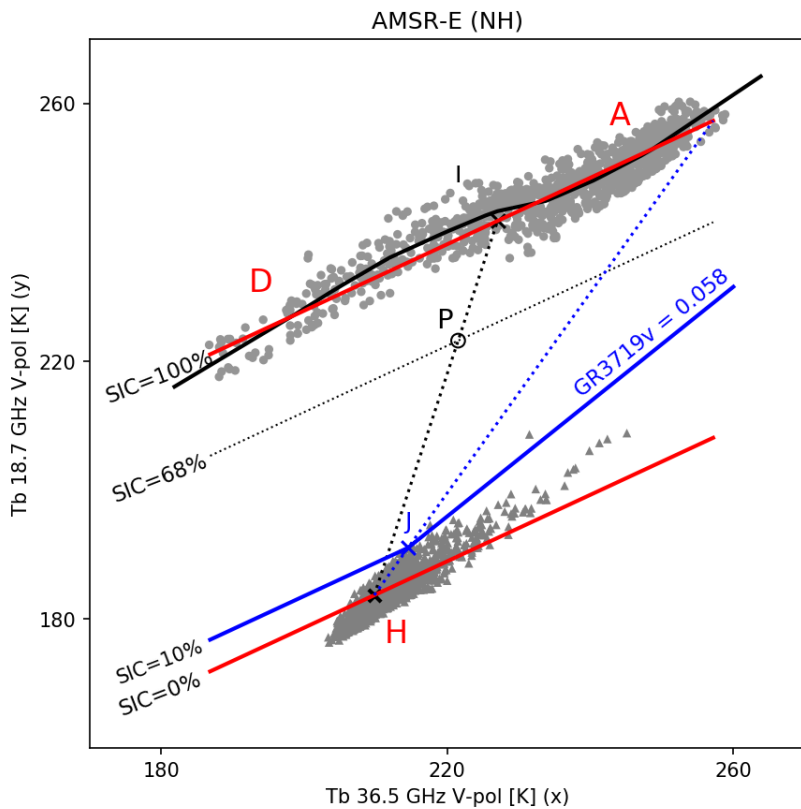


Figure 2: From left to right, the three main elements (Level 2, Level 3, and Level 4) in the sea ice concentration (**SIC**) processing work-flow. The red boxes depict data files, the blue boxes correspond to individual steps (aka algorithms) in the processing. The files that exit a processing chain (e.g. the “L2 SIC and uncert and OWF” at the bottom of the Level 2 processing chain) are the input for the next level of processing. Acronyms: NT is the Nasa Team algorithm, OWF is Open Water Filter, RTM is Radiative Transfer Model, uncert stands for uncertainty, L2 is Level 2, L3 is Level 3, L4 and is Level 4.



Formatted: Centered

Figure 3: Illustration of the Bootstrap Frequency Mode (BFM, [section 3.2](#)) and Open Water Filter (OWF, [section 3.4.2](#)) algorithms in a 36.5V (x-axis) and 18.7GHz (y-axis) Tb space of AMSR-E (Winter NH conditions). The grey symbols are actual [AMSR-E](#) Tb measurements over SIC=0% (triangles) and SIC=100% (disks) conditions, [from Pedersen et al. \(2018\)](#). The SIC=100% measurements fall [generally](#) along a line (the consolidated ice line) while the mean [open](#) water signature is point H. An example measurement P (black circle) falling on the SIC=68% isoline illustrates the functioning of BFM. The blue solid and dotted lines illustrate the tuning and functioning of the OWF (as described in section 3.4.2). [The black solid curve fitting SIC=100% conditions illustrates the ice curve correction \(as described in section 3.4.3\).](#)

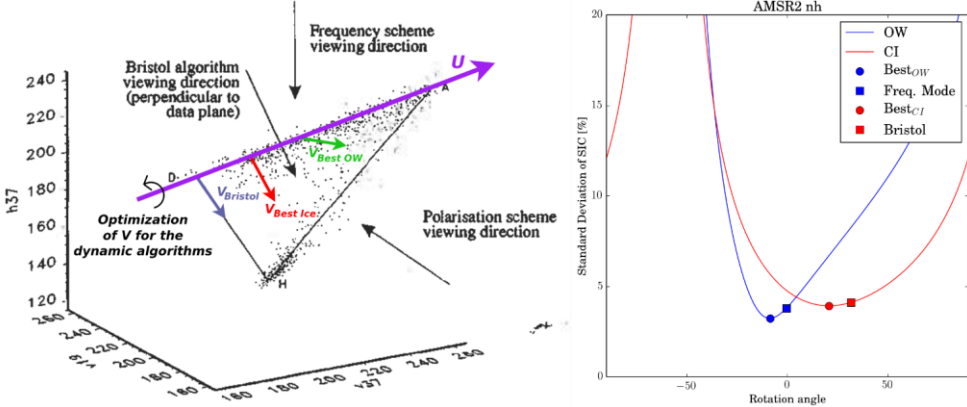


Figure 4: Left: three dimensional diagram of open water (H), and closed ice (ice line between D and A) brightness temperatures in a 19V, 37V, 37H space (black dots). The original figure is from Smith et al. (1996). The direction U (violet, sustained by unit vectors u defined in violet section 3.4.3) is shown, and vectors vBristol (blue), vBest-ice (red), and vBest-OW (green) are added, as well as an illustration of the optimization of the direction of V for the “dynamic” (self-optimizing) algorithms. Right: Evolution of the SIC algorithm accuracy for Open Water (blue) and Closed Ice (red) training samples as function of the rotation angle θ in the range [-90°, 90°]. Square symbols are used for the BFM (Freq. Mode) and BRI (Bristol) algorithms. Disk symbols locate the new, self-optimizing algorithms.

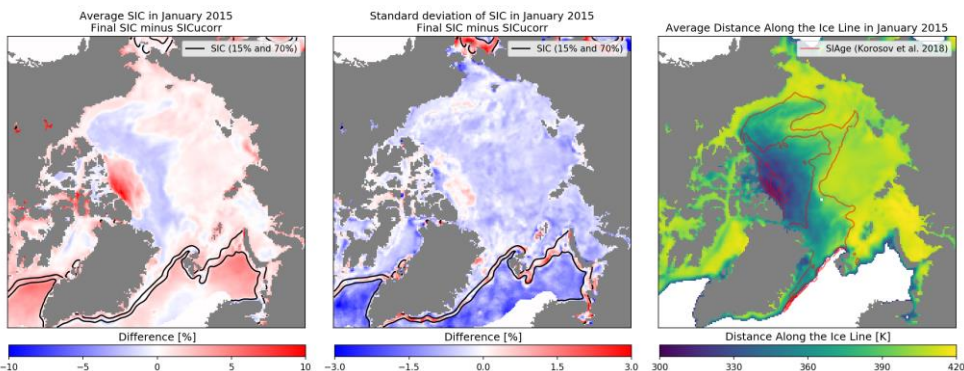


Figure 5: Left and center panels: difference maps between the January 2015 mean (left) and temporal variability (center) of the final SIC and the uncorrected SIC (SIC_{uncorr}) in the Arctic Ocean. Black solid lines are at the 15% and 70% SIC levels (marginal ice zone). Right panel: January 2015 mean Distance Along the Ice Line (DAL) values, red lines are transitions between 1st year sea ice, 2nd year sea ice, and older sea ice from Korosov et al. (2018).

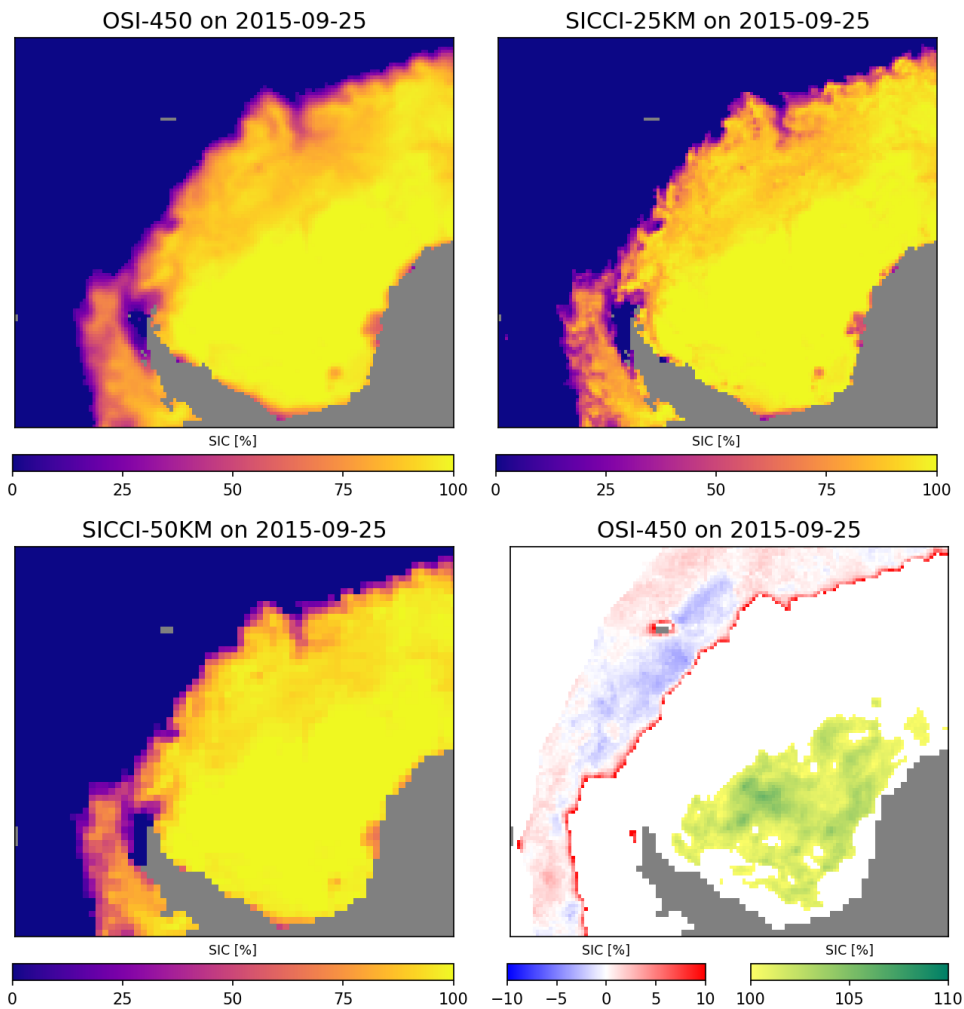


Figure 6: Example SIC fields on 25th September 2015 from the three CDRs (top left: OSI-450, top right: SICCI-25km, bottom left: SICCI-50km) over the Weddell Sea. Bottom right panel shows the content of variable `raw_ice_conc_values` from the OSI-450 file for the same date and area. Note the two discontinuous color scales for the bottom right panel.

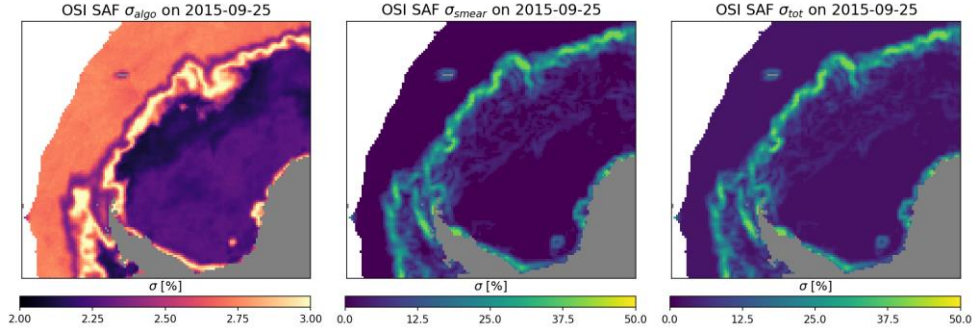


Figure 7: Example fields of uncertainties on 25th September 2015 from the EUMETSAT OSI SAF CDR over the Weddell Sea. The component σ_{algo} (left), σ_{smear} (center), and the total uncertainty σ_{tot} (right) are shown. σ_{tot} is dominated by the σ_{smear} contribution.

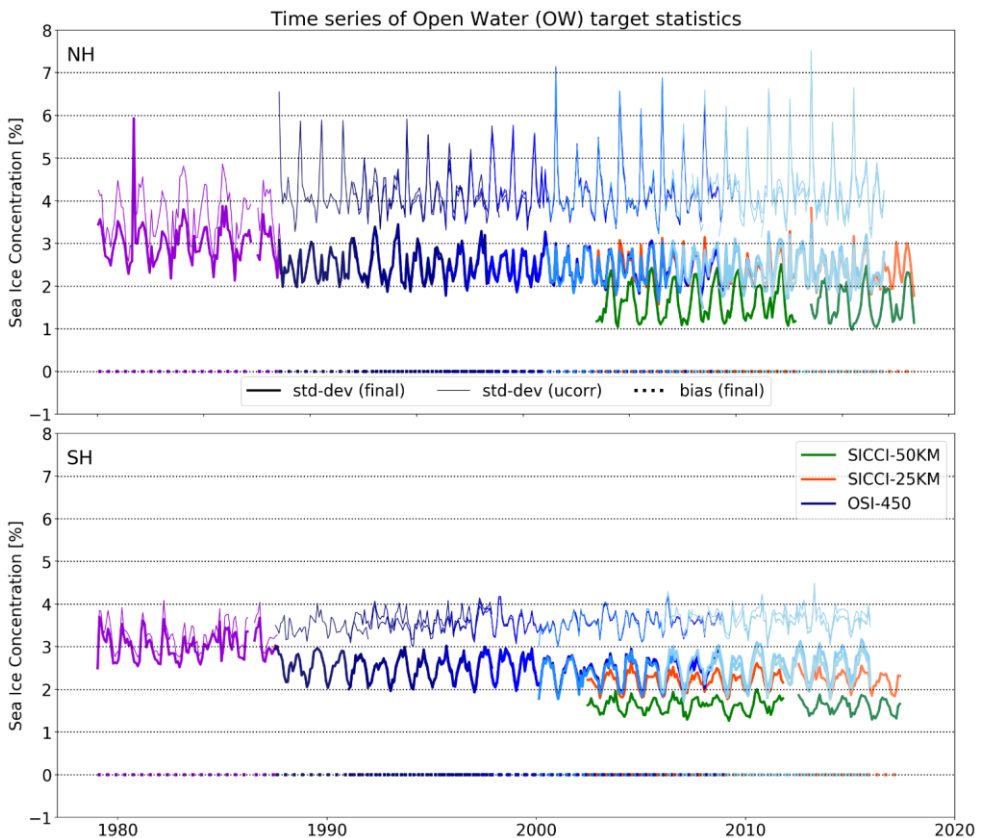


Figure 8: Time series of performance statistics for the three CDRs (blues: OSI-450, reds: SICCI-25km, greens: SICCI-50km) over the Open Water target for the Northern Hemisphere (top) and Southern Hemisphere (bottom). For OSI-450 and SICCI-25km, the color of the lines is for individual satellites, as used in Figure 1. For OSI-450, the thick (*resp* thin) solid lines plot the OW standard deviation of SIC (*resp* SIC_{ucorr}). The thin solid lines are only plotted for OSI-450 so as not to clutter the plot area. The bias of SIC is plotted with a dotted line.

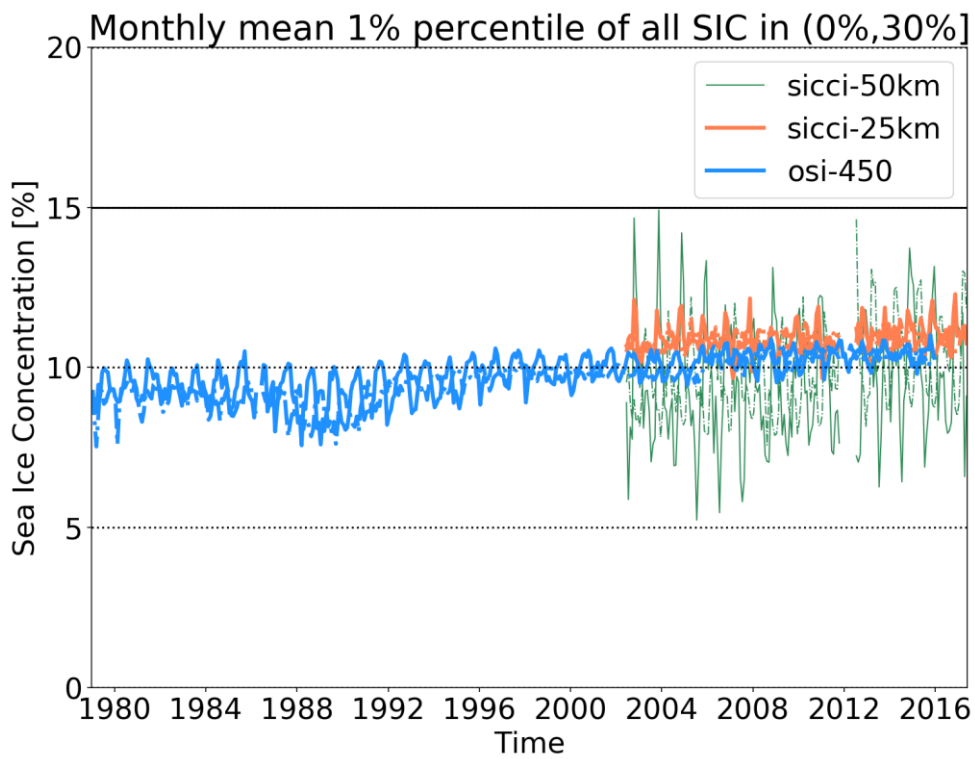


Figure 9: Time-series of the monthly mean 1%-percentile value of all strictly positive SICs that are below 30% (variable `ice_conc`) for the three CDRs (blues: OSI-450, reds: SICCI-25km, greens: SICCI-50km). Solid lines are for NH, dashed lines for SH. This time-series plot investigates if the dynamic tuning of the Open Water Filters results in temporal consistency of the minimum detected true SIC across all satellites.

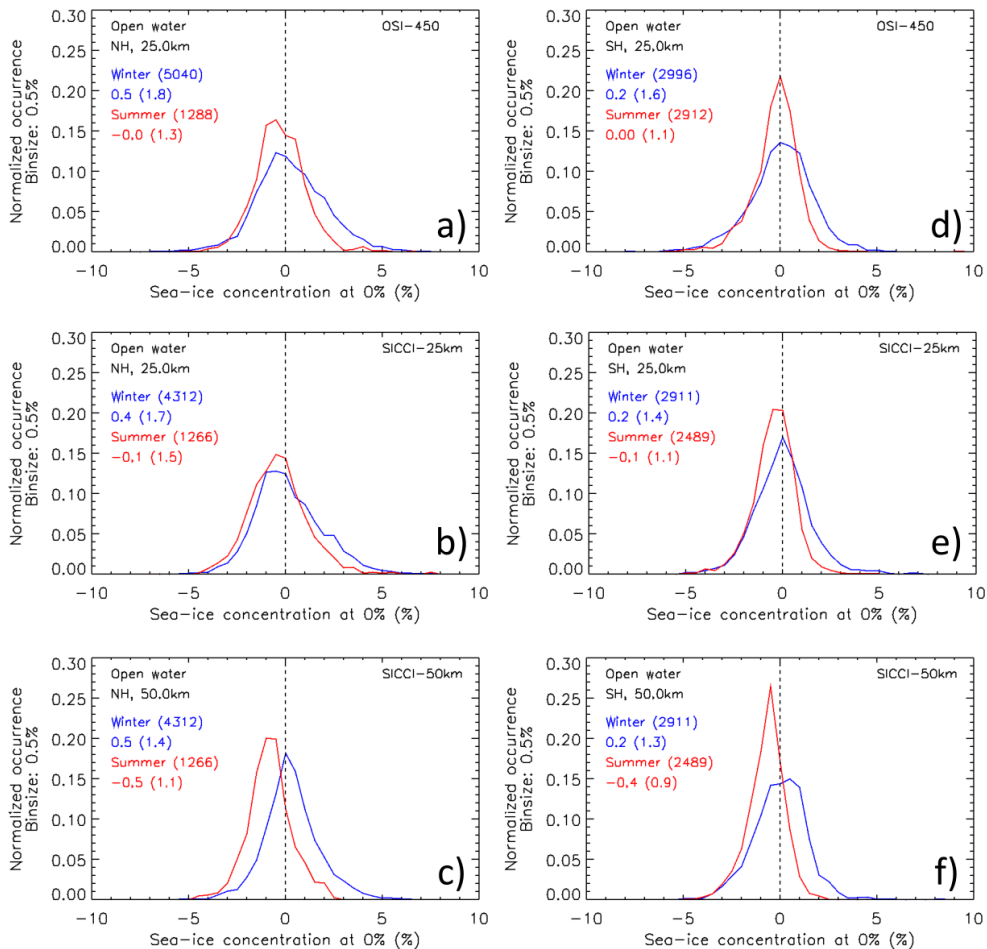


Figure 10: SIC distribution around $SIC = 0\%$ at the selected open ocean locations for, from top to bottom, OSI-450, SICCI-25km and SICCI-50km in the Arctic (images a) to c)) and the Antarctic (images d) to f)). The unfiltered distribution is shown (no OWF by combining ice_conc and raw_ice_conc_values variables. Blue (red) curves and numbers refer to results from winter (summer); the numbers in parenthesis behind the season denote the count of cases used. Numbers below the season denote the mean SIC plus/minus one standard deviation of the mean (in parenthesis) in percent SIC. Binsize is 0.5%. Distributions are normalized to give a total of 1.

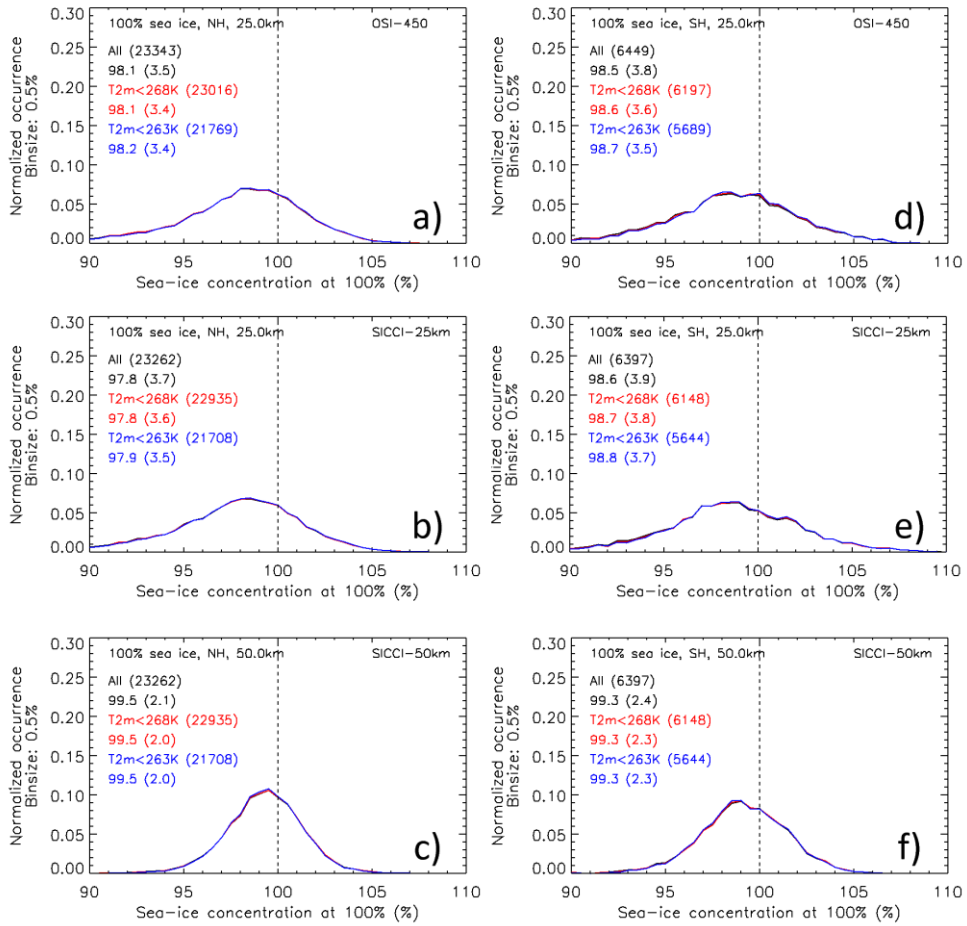


Figure 11: SIC distribution around SIC = 100% from the RRDP-2 data set for, from top to bottom, OSI-450, SICCI-25km and SICCI-50km in the Arctic (images a) to c) and the Antarctic (images d) to f). The unfiltered distribution is shown (no threshold at 100% SIC) by combining ice conc and raw ice conc values variables. Black, red and blue curves and numbers refer to all data and data limited to ERA-Interim 2m-air temperatures < -5°C and < -10°C, respectively. The numbers behind the limitation text (e.g. “all”) denote the count of data used; the numbers below denote the mean SIC plus/minus one standard deviation (in parenthesis) in percent SIC. Binsize is 0.5%. Distributions are normalized to give a total of 1.

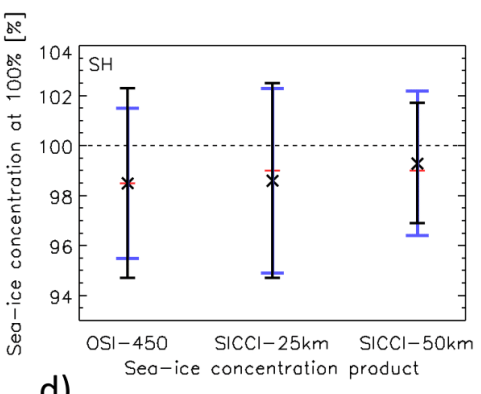
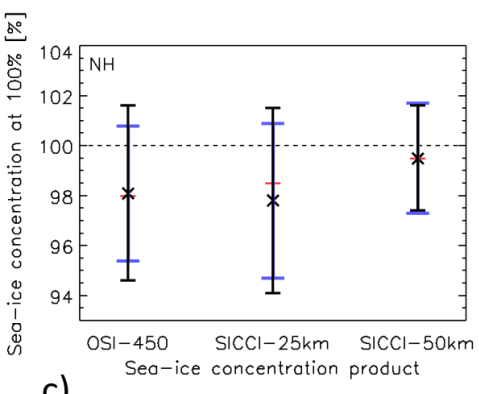
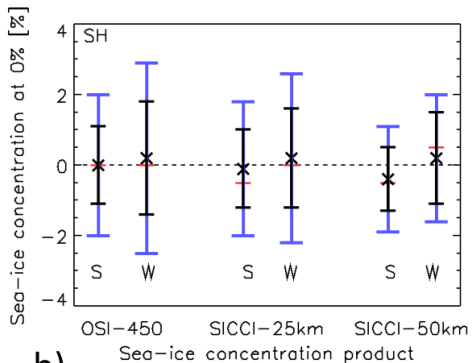
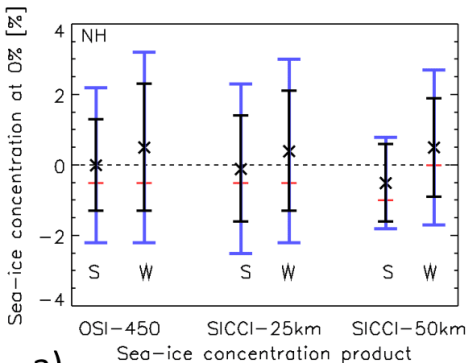


Figure 12: Summary of histogram statistics from Figures 10 and 11 for SIC = 0% (images a) and b)) and SIC = 100% (images c) and d)) for the Arctic (left) and the Antarctic (right). Crosses and black bars denote the mean SIC plus/minus one standard deviation of the standard error. Red horizontal bars denote the modal SIC. Blue bars denote the range covered by the mean SIC plus/minus one standard deviation of the total uncertainty/total standard error. Letters "S" and "W" in images a) and b) refer to summer and winter, respectively.

	Instruments & [Channels]	Time Period	Grid Spacing	Originator	DOI
OSI-450	SMMR, SSM/I, SSMIS [19V, 37V, 37H]	<u>01/1979-</u> <u>12/2015</u>	25x25km	OSI SAF	10.15770/EUM SAF_OSI_000 8
SICCI-25km	AMSR-E, AMSR2 [19V, 37V, 37H]	<u>06/2002-</u> <u>10/2011,</u> <u>07/2012-</u> <u>05/2017</u>	25x25km	ESA CCI	10.5285/f17f14 6a31b14df960 cde0874236ee5
SICCI-50km	AMSR-E, AMSR2 [6V, 37V, 37H]	<u>06/2002-</u> <u>10/2011,</u> <u>07/2012-</u> <u>05/2017</u> <u>2002-2011,</u> <u>2012-2017</u>	50x50km	ESA CCI	10.5285/5f75fc b0c58740d99b0 7953797bc041e

Table 1: Summary of the three SIC CDRs presented in this paper. The values entered in the table are all described in the course of the paper.

Platform and Instrument	Start date	Stop date	Frequency, in GHz, (footprint resolution in km) of channels	Width of polar observation hole <u>(north- and southward of)</u>	View angle	Comment
Nimbus-7 SMMR	01/01/1979	20/08/1987	18.0 (54x35), 37.0 (28x18)	84°	50.2°	Operates every other day. Two long periods with missing data are 29/03-23/06 1986, and 03/01-15/01 1987.
DMSP F08 SSM/I	09/07/1987	18/12/1991	19.3 (70x45), 37.0 (38x30)	87°	53.1°	A long period with missing data is 03/12-31/12 1987.
DMSP F10 SSM/I	07/01/1991	13/11/1997	19.3 (70x45), 37.0 (38x30)	87°	53.1°	Significant variation (slow oscillation) of the incidence angle during its life time.
DMSP F11 SSM/I	01/01/1992	31/12/1999	19.3 (70x45), 37.0 (38x30)	87°	53.1°	
DMSP F13 SSM/I	03/05/1995	31/12/2008	19.3 (70x45), 37.0 (38x30)	87°	53.1°	F13 operated longer but 31/12/2008 is the end of coverage in CM-SAF FCDR R3
DMSP F14 SSM/I	07/05/1997	23/08/2008	19.3 (70x45), 37.0 (38x30)	87°	53.1°	
DMSP F15 SSM/I	28/02/2000	31/07/2006	19.3 (70x45), 37.0 (38x30)	87°	53.1°	F15 operated longer but 31/07/2006 is the end of coverage in CM-SAF FCDR R3
DMSP F16 SSMIS	01/11/2005	31/12/2015	19.3 (70x45), 37.0 (38x30)	89°	53.1°	
DMSP F17 SSMIS	14/12/2006	31/12/2015	19.3 (70x45), 37.0 (38x30)	89°	53.1°	F17 operated longer but 31/12/2015 is the end of coverage in CM-SAF FCDR R3
DMSP F18 SSMIS	08/03/2010	31/12/2015	19.3 (70x45), 37.0 (38x30)	89°	53.1°	F18 operated longer but 31/12/2015 is the end of coverage in CM-SAF FCDR R3
EOS Aqua AMSR-E	01/06/2002	03/10/2010	6.9 (75x43), 18.7 (27x16), 36.5 (14x9)	89.5°	55°	
GCOM W1 AMSR2	23/07/2012	31/05/2017	6.9 (62x35), 18.7 (22x14), 36.5 (12x7)	89.5°	55°	AMSR2 operated longer but 31/05/2017 is the last date we fetched from JAXA for the CDRs.

Table 2: Platform, instrument, time period for input brightness temperatures used in the sea ice data records. All frequencies listed have both horizontal and vertical polarization channels

